SORBONNE UNIVERSITÉ
CRÉATEURS DE FUTURS DEPUIS 1257

SORBONNE UNIVERSITÉ
LJLL

Doctoral School **École Doctorale Sciences Mathématiques de Paris Centre**

University Department **Laboratoire Jacques-Louis Lions**

Thesis defended by **LU LIUDI**

Defended on **29th September, 2021**

In order to become Doctor from Sorbonne Université

Academic Field **Mathématiques appliquées**

Speciality **Analyse numérique**

Approches Lagrangiennes pour la modélisation et l'optimisation du couplage hydrodynamique-photosynthèse

Thesis supervised by

Julien SALOMON	Supervisor
Olivier BERNARD	Co-Supervisor

Committee members

Referees	Benoît CHACHUAT	Professor at Imperial College London
	Yannick PRIVAT	Professor at Université de Strasbourg
Examiners	Céline GRANDMONT	Senior Researcher at INRIA Paris
	Florence HUBERT	Professor at Aix-Marseille Université
	Camille POUCHOL	Associate Professor at Université de Paris
	Magali RIBOT	Professor at Université d'Orléans
	Jacques SAINTE-MARIE	Senior Researcher at INRIA Paris
Supervisors	Julien SALOMON	Senior Researcher at INRIA Paris
	Olivier BERNARD	Senior Researcher at INRIA Sophia Antipolis

Colophon

Doctoral dissertation entitled "Approches Lagrangiennes pour la modélisation et l'optimisation du couplage hydrodynamique-photosynthèse ", written by LU Liudi, completed on 7th September, 2021, typeset with the document preparation system LaTeX and the yathesis class dedicated to theses prepared in France.

Keywords: optimization, mathematical modeling, hydrodynamics, dynamical system, resource allocation, periodic control, nonlinear problem, saint-venant equations, han model, microalgae

Mots clés : optimisation, modélisation, hydrodynamique, système dynamique, allocation des ressources, contrôle périodique, problème nonlinéaire, équations de saint-venant, modèle de han, microalgues

This thesis has been prepared at

Laboratoire Jacques-Louis Lions
Sorbonne Université
Campus Pierre et Marie Curie
4 place Jussieu
75005 Paris
France

☎ +33 1 44 27 42 98
Web Site `https://ljll.math.upmc.fr/`

Approches Lagrangiennes pour la modélisation et l'optimisation du couplage hydrodynamique-photosynthèse

Abstract

Microalgae are photosynthetic micro-organisms whose potential has been highlighted in the last decade. Applications can be found from to renewable energy production and wastewater treatment to some high added value commercial products e.g., food, pharmaceutical, cosmetics. Nevertheless, finding optimal growth conditions for full-scale cultivation of microalgae remains challenging in practice. Mathematical models are therefore of great help to better manage this complex, nonlinear dynamical system. The aim of this thesis is to better understand how different factors affect microalgal growth.

In a first part, we study the influence of the light attenuation and the optimal condition to maximize the productivity. In this way, we introduce an optical productivity which enables us to determine the optimal condition for general light extinction function. A global optimal optical depth is found which consists in canceling the algal net growth rate at the bottom of the reactors to maximize the optical productivity. It can be used to characterize the optimization of the areal productivity in some specific cases, whereas an asymptotic behaviour has been observed in more general case.

We then limit ourselves to a specific reactor - the raceway pond, which is an outdoor circuit basin combining with a paddle wheel. We start by investigating a resource allocation problem issuing from the re-distribution of the light resource to the algae by the paddle wheel. A generic mixing device is considered to assign at each lap the light resource to the algae layers in the raceway. We determine the optimal allocation strategies to maximize the algal growth.

In a third part, we show how the shape of the topography affects (or not) the algal growth in raceway ponds. In this way, we consider a hydrodynamical-biological coupled model and introduce an optimization problem associated with the topography to maximize the algal growth. We also combine the optimization of the topographies with the previous allocation strategies to investigate their influence on algal production. Non-trivial topographies are obtained numerically to enhance the algal growth.

The mathematical study of these optimization problems leads to new interesting working directions, improves and clarifies the understanding of influence by different factors on algal growth. We conclude with some discussions and perspectives of this work.

Keywords: optimization, mathematical modeling, hydrodynamics, dynamical system, resource allocation, periodic control, nonlinear problem, saint-venant equations, han model, microalgae

Laboratoire Jacques-Louis Lions
Sorbonne Université – Campus Pierre et Marie Curie – 4 place Jussieu – 75005 Paris – France

Résumé

Les microalgues sont des micro-organismes photosynthétiques dont le potentiel a été mis en évidence au cours de la dernière décennie. Des applications peuvent être trouvées dans la production d'énergie renouvelable ou dans le traitement des eaux usées par exemple. Elles peuvent être utilisées dans beaucoup de produits commerciaux à haute valeur ajoutée comme par exemple dans l'alimentation, la pharmacie ou les cosmétiques. Néanmoins, trouver des conditions optimales pour la production des microalgues à grande échelle reste un défi en pratique. Les modèles mathématiques sont donc d'une grande aide pour mieux gérer ce système dynamique complexe et non linéaire. L'objectif de cette thèse est de mieux comprendre comment différents facteurs affectent la croissance des microalgues.

Dans un premier temps, nous étudions l'influence de l'atténuation lumineuse et obtenons une condition d'optimalité pour maximiser la productivité. De cette façon, nous introduisons une productivité optique qui nous permet de caractériser la fonction d'extinction de la lumière optimale dans un cadre général. On trouve une profondeur optique optimale globale qui consiste à annuler le taux de croissance net des algues au fond des réacteurs pour maximiser la productivité optique. Cette étude nous permet de caractériser la productivité surfacique optimale dans certains cas particuliers, et de décrire le comportement asymptotique des autres cas dans certains régimes.

On se limite ensuite à un réacteur spécifique, le raceway pond, qui est un bassin de circuit extérieur associé à une roue à aubes. Nous commençons par étudier un problème d'allocation de ressources issu de la redistribution de la ressource lumineuse aux algues par la roue à aubes. Un dispositif de mélange générique est envisagé pour affecter à chaque tour la ressource lumineuse aux algues qui se situent sur differentes couches dans le raceway. Nous déterminons les stratégies d'allocation optimales pour maximiser la croissance des algues.

Dans une troisième partie, nous montrons comment la forme de la topographie affecte (ou non) la croissance des algues dans le raceway. De cette façon, nous considérons un modèle hydrodynamique-biologique couplé et introduisons un problème d'optimisation associé à la topographie pour maximiser la croissance des algues. Nous combinons également l'optimisation des topographies avec les stratégies d'allocation précédentes pour étudier leur influence sur la production d'algues. Des topographies non triviales sont obtenues numériquement pour améliorer la croissance des algues.

L'étude mathématique de ces problèmes d'optimisation conduit à de nouvelles directions de travail, améliore et clarifie la compréhension de l'influence de différents facteurs sur la croissance des algues. Nous concluons par quelques discussions et perspectives de ce travail.

Mots clés : optimisation, modélisation, hydrodynamique, système dynamique, allocation des ressources, contrôle périodique, problème nonlinéaire, équations de saint-venant, modèle de han, microalgues

Contents

Remerciements

Je tiens tout d'abord à remercier mes directeurs de thèse, Julien Salomon, Olivier Bernard et Jacques Sainte-Marie, de m'avoir proposé un sujet d'étude interdisciplinaire, passionnant et aussi riche. Ils m'ont fait découvrir le monde de la recherche et l'univers des mathématiques appliquées sous différents angles. Je n'oublie pas que, tout d'abord, Jacques m'avait amené dans le monde hydrodynamiques et m'avait fait connaître Julien et Olivier pour débuter ce magnifique trajet de trois ans. Je remercie Olivier de m'avoir accueilli sous le soleil de Sophia Antipolis, et de m'avoir appris les connaissances sur les algues durant la moitié de temps de ma thèse. J'ai beaucoup apprécié les discussions régulières avec Julien depuis le stage de master, il répond toujours avec patience à toutes mes questions naïves et me transmet le goût et la curiosité, et m'avoir fait connaître le monde de la recherche. J'ai eu la chance et l'honneur d'être encadré par eux, je tiens à leur adresser mon profond sentiment de gratitude.

Je tiens à remercier ensuite Benoît Chachuat et Yannick Privat qui ont accompli l'ardu travail de rapporteurs. Leurs commentaires et remarques, grâce auxquelles j'ai pu améliorer cette thèse, m'ont été précieux. Je voudrais également remercier Florence Hubert, Céline Grandmont, Camille Pouchol, Magali Ribot qui me font l'honneur de faire partie de mon jury.

Je tiens à remercier sincèrement Martin Gander pour m'avoir offert un post-doc à l'Université de Genève, je poursuivrai ainsi ma carrière en mathématiques appliquées à Genève l'automne prochain. Je voudrais aussi exprimer ma reconnaissance envers Nina Augillon d'avoir acceptée de collaborer avec moi. J'aimerais remercier Jean-Luc Gouzé pour m'avoir accueilli chez l'équipe BIOCORE et m'avoir donné l'accès au labo pendant les confinements. Durant ma thèse, j'ai eu la chance de profiter des nombreuses idées et conseils des membres de l'équipe ANGE et de l'équipe BIOCORE, en particulier, je tiens à remercier Edwige Godlewski pour la discussion sur l'équation de Burgers, Emmanuel Audusse pour les conseils sur l'étude des topographies, et Frédéric Grognard pour la discussion sur le problème des resources d'allocation.

J'ai eu la chance de passer une partie de ma thèse au LJLL, à l'Inria Paris et à l'Inria Sophia Antipolis pendant ces trois ans, pour cette raison, j'ai pu rencontrer et travailler avec différents collègues. En tant qu'étranger, les procédures administratives pouvaient des fois être très compliquées, heureusement je n'ai jamais eu de problème grâce à tous les personnes administratives que j'ai rencontré. J'aimerais remercier l'équipe administrative du LJLL, Nolwenn Garimé, Malika Larcher, Salima Lounici, et en particulier Catherine Drouet qui m'avait beaucoup aidé au début de ma thèse pour pouvoir signer mon contrat et obtenir mon titre de séjour. Je tiens aussi à remercier Maryse Desnous, Julien Guieu de l'Inria Paris et Florence Beautier, Marie-Line Meirinho de l'Inria Sophia Antipolis de m'avoir facilité toutes les démarches administratives à l'Inria.

Si je peux garder un beau souvenir de ma thèse, c'est essentiellement grâce aux personnes que j'ai côtoyées. Ce faisant, je remercie les doctorantes/doctorants du LJLL Elise, Gabriela, Jules, Lise, Olivier (le basketteur), ainsi que mes co-bureau Charles, Giorgia, Katia, Lucas, Pierre et toutes les autres personnes croisées dans les couloirs ou la salle de café. Un grand merci

à Alexandre P. pour toutes les discussions et aussi les conseils sur le manuscrit. Je souhaite également remercier les personnes de l'Inria Paris Antoine, Apolline, Bao, Bilal, Chourouk, Fabien R., Fabien S., Frédéric, Janelle, Juliette, Léa, Martin, Mathieu M. (coach du crawl), Mathieu R., Matthias, Nelly, Thibault, Van Thanh (kung-fu man), Vincent pour les discussions, les sorties sports et afterwork. Je n'oublie surtout pas la belle équipe du sud qui rend mes séjours à Sophia très heureux et brillants, je voudrais remercier Agustín (j'ai des nouvelles lunettes maintenant), Alésia, Azouaou, Bruno, Carlos (prof d'algues), Clotilde (la vraie Youtubeuse), Jan-Luka, Juan Carlos, Francesca, Ignacio (thanks for continuing my work), Lamberto, Lucie, Marielle, Nicolas, Odile, Walid, Yan (the real biologist).

During my nine years' journey in France, it is not always simple to find someone speaking Chinese, let alone talking about math in Chinese. For this reason, I would like to thank my friends Allen (not really an ABC), Hong-Wei (amazing journey since Chambéry), Jingrui, Long, Po-Yi, Rui, Shengquan, Shijie, Siyuan, Yangyang for exploring the good Chinese restaurants in Paris. Je tiens aussi à remercier mes amis de Lyon Dijun, Nicolas, Emile pour les moments de détente et Jinzhe (村长) pour les jours que l'on a passés sur Onmyoji. Un grand merci à mon cher ami Damien d'avoir passé vingt heures de trajets pour me rendre visiter à Sophia, ces jours restent inoubliables pour moi.

Je remercie plus particulièrement mes professeurs des maths à l'Université Savoie Mont Blanc Georges Comte, Olivier Le Gal, Michel Raibault et Laurent Vuillon pour avoir cru en moi et m'avoir poussé à faire des maths, sans lesquelles je n'aurais pas pu faire cette thèse.

尽管已经出国多年并且回国的时间屈指可数，但这并没影响和你们之间的友情，在此特别感谢我在国内的朋友们，感谢梁嘉骏和刘邦在上海和邢凯在成都的款待，感谢梁嘉骏，宿辕，王骁恒，张建抽空从北京和上海到南京相聚，当然更感谢我多年好友于煊每次回国在南京的盛情款待和陪伴，和你们一起打魔兽吃鸡的日子都是我在法国平淡科研生活中最美好的点缀。

Finally, I would like to express my sincere gratitude to my family. I am very grateful to my cousin (or my little sister as I always explained to my friend) Anqi for coming visit me during all these years and for the passional talk about football with Tristan, it is always a great pleasure to see you guys. I would also like to thank my aunt for bringing me my favorite snacks from China, and I am so sorry that I did not have enough time to spend with you last time.

感谢我的姥姥姥爷小姨和罗超时常的微信问候和祝福。感谢我的父亲当年专程从昆明来到成都和我们认真商讨出国事宜，感谢我的母亲从一开始对我的选择的不支持到之后慢慢的理解和接受，没有你们经济上的支持，我很难想象如何走完这九年，同样也感谢你们这么多年的挂念和包容。

在此，也要同时感谢当初那些不相信我，对我的选择冷嘲热讽，不认为我会走下去的人，你们的质疑和能让你们闭嘴是我最大的动力。

Enfin, je remercie avec tout mon coeur ma copine 潘楠qui m'accompagne depuis plus de onze ans, avec qui j'ai fait toute cette aventure, merci pour ton amour et ton soutient inconditionnel, merci pour tes encouragements et ta confiance, merci de m'avoir supporté et d'avoir partagé toutes les fêtes, les joies ainsi que les moments difficiles avec moi, la moitié de cette thèse est dédiée à toi, merci!

Chapter 1

Introduction

1.1 Preliminary

1.1.1 Background and Motivation

The greenhouse effect is a process that warms up the Earth's surface, allowing life by maintaining Earth's temperature above freezing. However, this greenhouse effect is getting stronger as human activities release greenhouse gases in the atmosphere, trapping more and more heat and warming the climate of our planet. Since the pre-industrial period, it has been shown that Earth's global average temperature has increased by about 1 degree Celsius [61]. Among all the greenhouse gas emissions, carbon dioxide (CO_2) contributes up to 68 % of total emissions [24, 65]. According to a report by the Carbon Dioxide Information Analysis Center (CDIAC)[1], CO_2 emissions worldwide have increased from 11 millions metric tons in 1751 to 30619 millions metric tons in 2006. The continuous increase in emissions will have significant effects on future climates, ocean temperature, as well as on economic systems. Therefore, it is imperative to develop an appropriate technology to reduce the emissions and accumulation of CO_2. CO_2 fixation techniques can be divided into biological and physical methods [73]. Between these two techniques, biological CO_2 fixation appears to be a promising economical and environmentally viable technology [65, 76]. This techniques presents an attractive development option as plants or other photosynthetic organisms naturally capture and use CO_2 as part of their photosynthetic process. Although terrestrial plants are able to sequester vast amounts of CO_2 from the atmosphere, their growth is reduced due to the CO_2 availability. On the contrary, phytoplankton have faster growth rates and their CO_2 fixation efficiency is also between 10 and 30 times higher than the terrestrial plants [35, 79]. The biological mitigation of CO_2 by using phytoplankton could therefore offer huge advantages.

The word phytoplankton originally comes from Greek where phytón means plant and planktós means drifter. These micro-organisms comprise eukaryotic cells (microalgae) and prokaryotic cells (cyanobacteria) which can all do photosynthesis. They can grow naturally in all aquatic environments, for instance oceans, lakes, ponds, and rivers. Despite the fact that phytoplankton biomass in the oceans corresponds to less than 2% of the total global plant carbon, these organisms collectively capture approximately 40% of the global carbon sequestration per year [25, 49]. Therefore, the microalgae (synonym of phytoplankton in biotechnology and applied physiology) cultivation becomes an attractive alternative for reducing greenhouse gas emissions [121]. More precisely, no additional CO_2 is created during the photosynthetic process while biofuels could

[1] `https://cdiac.ess-dive.lbl.gov/ftp/ndp030/global.1751_2008.ems`

be produced from the lipids within the microalgae. Promising production potential of various secondary metabolites are also expected for numerous high added value commercial applications: pharmaceutical, cosmetics or food industries [47, 114].

Depending on the source of the light, these microorganisms are generally cultivated at industrial scale in open or closed photobioreactors. These devices vary from the most simple and cheapest open reactors to some high-tech closed photobioreactors. They can be run in batch, or continuously adding growth medium in the reactor. This so called chemostat was first introduced independently by Monod [100] and Novick and Szilard [103] in the 1950s for studying bacterial cultures. It is a perfectly mixed photobioreactor where the algae are permanently fed with a nutrient and simultaneously emptied such that the culture volume is kept constant. This classical device is often used to maintain a nutrient-limitation, which for microalgae can be modelled by the Droop model [41, 42] as presented in Subsection 1.2.1. Since the late 1960s, the chemostat has been widely used in microalgae research [69, 81, 98, 109]. At larger scale, the open raceway pond firstly introduced by Oswald [105] in the 1960s is currently the most frequently used and cheapest cultivation system for commercial production of microalgae. It is used worldwide including the United States, France, Thailand, China, Chile, and Israel. The pond is a shallow artificial hydraulic circuit divided into a rectangular grid, with each rectangle containing one oval-shaped channel. The water is kept in motion by a powered paddle wheel which also ensures the mixing. The industrial applications of microalgae for various industrial sectors, and especially using the cheaper raceway pond technologies, have motivated theoretical studies for modelling and optimization [8, 66, 67, 117].

1.1.2 Optimization aspects and contributions

There is a strong motivation to improve microalgal productivity and make the involved processes more efficient. Theoretical developments are complementing the experimental works, in the idea of guiding the way towards more effective algal production systems.

Researches for enhancing this bio-process followed various directions ranging from determining growth conditions more efficient for the physiology of the microalgae to the design of more efficient algal cultivation devices. Different environmental conditions can affect microalgal growth such as temperature, nutrient availability, light condition and pH. For instance, authors in [111] have investigated the impact of temperature for outdoor algal production. In [93], authors have studied the influence of the background turbidity in the photobioreactors on the algal production. Light intensity condition in reactors have also been investigated in [92], where authors have provided an optimal strategy to maximize the productivity in a light-limited chemostat. The influence of both light condition and nutrient availability has been optimized to improve the algal production [94]. The design of efficient cultivation devices has also been studied to optimize the industrial microalgal productivity. For instance, the authors in [77] have studied the algal productivity optimization on a algal rotating biofilm, where a flashing effect has been identified, meaning that the biofilm which rotates with an infinity velocity provides the maximal productivity. The coupling of biological system with hydrodynamics in raceways is studied [67] in order to optimize the raceway design.

The contributions of this thesis mainly focus on the optimization problems in algal production. In Chapter 2, we study the influence of light distribution on algal productivity. An optimal medium turbidity has been identified for general photobioreactors, corresponding to that has been found in literature [55, 94]. We then focus on a specific photobioreactor consisting of a raceway pond for the algal growth. We investigate the influence of the two main features of this device namely the paddle wheel and the topography of the raceway bottom. The idea is to bring more light resource to the algae at the lower part of the pond, since light is strongly

attenuated when passing through the algal culture. In Chapter 3, we focus on the optimal mixing of the paddle wheel. More precisely, we introduce a model to account for the mixing process and study the periodic regime of the algal growth (see also in [16]). The resulting problem consists of a specific allocation problem which gives rise to non trivial mixing strategies. We have then identified a periodic dynamical resource allocation problem, where we have developed a more complete theory which can be applied to problems other than the algal growth (see also in [15]). We then study the influence of the topography in Chapter 4. We introduce the methodology of optimization of the topography through a hydrodynamic-biologic system, where a non flat topography is observed for non periodic case (see also in [12]). In order to better understand the impact of the topography, we then extend the previous work to a larger range of setting (see also in [13]). In some cases, theoretical results enable to identify the critical topography. However, the increase on algal growth remains very limited when using our optimal topographies, therefore we combine the topography optimization along with the optimization of the mixing strategy with the paddle wheel, and an enhancement on the algal growth is then obtained (see also in [14]).

1.2 Biological and hydrodynamical models

In this section, we present some classical models related to the systems considered in this thesis. We start with the biological models to describe the algal growth, then we introduce the hydrodynamical models for the algal motion and end up with the light intensity modelling in the turbid medium which couple these two systems.

1.2.1 Biological model

Here, we give a brief review on some models often considered to describe algal systems. According to the application, these models account for describing different dynamical aspect of the growth of microalgae such as light, temperature, nutrient availability, salinity, pH, etc. We mainly focus on two models: the Droop model and the Han model.

Nutrient-Limited growth - The Droop model

One of the crucial elements which may limit microalgal growth is the nutrients. Co-limitation by two or several nutrients is more complex and will not be presented here, we refer to [22, 75, 80, 83] for further details. We rather focus on the case where only one nutrient is influencing microalgal growth, all the other being introduced in excess. The classical Monod kinetics [99], initially considered to model bacterial cultures, states that the growth rate denoted hereafter by μ $[d^{-1}]$ is directly related to the nutrient (inorganic nitrogen) concentration denoted by s $[\mathrm{g_N\,m^{-3}}]$ in the following way:

$$\mu(s) = \mu_{\max}\frac{s}{s+K_s},$$

with $\mu_{\max}$ $[d^{-1}]$ the maximal growth rate, i.e. the growth rate reached at infinite substrate and K_s $[\mathrm{g_N\,m^{-3}}]$ the half saturation constant for substrate uptake. The applicability of the Monod model has been shown in different works [57, 80, 83]. However, it has been firstly observed by Droop [41, 42] that microalgae keep growing for some time even after nutrients have been totally depleted. This behaviour does not correspond to Monod kinetics which are therefore not suitable to predict microalgae growth under nutrient limitation. In order to take nutrient-limited growth into account, Droop suggests [41] to separate the nutrient uptake rate denoted by ρ $[\mathrm{g_N\,g_C^{-1}\,d^{-1}}]$ from the growth rate μ which is related to the internal elemental nutrient

quota (amount of intracellular nutrient). This model has ever since then been widely studied in [9, 78, 119] and thoroughly validated experimentally [10, 42, 112, 119].

In a continuous and homogeneous microalgae culture, the dynamics of nutrient concentration s, the biomass concentration X [$\mathrm{g\,m^{-3}}$], and the carbon-specific nitrogen quota q [$\mathrm{g_N\,g_C{}^{-1}}$] of the cells are given by

$$\begin{cases} \dot{s} = Ds_{\mathrm{in}} - \rho(s)X - Ds, \\ \dot{X} = (\mu(q) - D)\,X, \\ \dot{q} = \rho(s) - \mu(q)q, \end{cases}$$

where D [$\mathrm{d^{-1}}$] denotes the dilution rates and s_{in} [$\mathrm{g_N\,m^{-3}}$] is the nutrient concentration in the feed.

In this model, the growth rate functions μ is taken as a Droop function [41]:

$$\mu(q) = \mu_{\max}\left(1 - \frac{q_0}{q}\right),$$

where q_0 [$\mathrm{g_N\,g_C{}^{-1}}$] stands for the minimal cell quota ($\mu(q_0) = 0$), meaning that no algal growth can take place for cell quota below this level. By taking the initial condition $q(0) \geq q_0$, it can be proved that $\forall t \geq 0$, $q(t) \geq q_0$ (as shown in [9]). As for the absorption functions ρ, it is generally taken as in the model proposed by Michaelis-Menten [28]:

$$\rho(s) = \rho_{\max}\frac{s}{s + K_s},$$

with $\rho_{\max}$ the maximal uptake rate.

Light intensity has a direct effect on algal growth through photosynthesis, on the same time nitrogen uptake can continue in the dark. However the classical Droop model cannot be used directly for varying light intensity. In order to account for this effect, an extension of the Droop model has recently been proposed by Bernard [18]. This approach consists in introducing light intensity, which will be denoted by I [$\mu\mathrm{mol\,m^{-2}\,s^{-1}}$], into the parameter $\mu_{\max} = \mu_{\max}(I)$:

$$\mu(q, I) = \mu_{\max}(I)\left(1 - \frac{q_0}{q}\right) = \mu_{\max}\frac{I}{I + K_I}\left(1 - \frac{q_0}{q}\right),$$

with K_I [$\mu\mathrm{mol\,m^{-2}\,s^{-1}}$] is the light half saturation coefficient. Note that in this case, the absorption function ρ also needs to depend on q as shown in [82]

$$\rho(s, q) = \rho_{\max}\frac{s}{s + K_s}\frac{q_l - q}{q_l - q_0},$$

with $q_l > q_0$.

Photosynthetic production and Photoinhibition - The Han model

The photosynthetic units (PSUs) are usually referred as a set of molecules including chlorophyll that capture photons to eventually oxidize a molecule of water (H_2O), produce dioxygen (O_2) or generate a flux of energetic co-factors such as ATP or NADPH. The PSUs can be associated with two types of photosystems: photosystem-I (PSI) and photosystem-II (PSII) [58, 53, 116, 120] where PSII leads to a flux of electrons and PSI generates the energy-rich cell co-factors. Among these two systems, PSII is generally assumed to play the main role in the photosynthetic dynamics since it involves a specific molecule (D1) in the reaction centre of the photosystems that is easily damaged by an excess of energy. For large light intensities, there is a risk that some PSUs are

damaged, leading to reduced photosynthetic activity. This photoinhibition mechanism must be taken into account to accurately estimate photosynthetic production at high light intensity [25, 48, 73, 110, 89]. Photoinhibition results in a decrease in photosynthesis rate in plants when they are exposed to high light intensity. In the last three decades, the understanding of photoinhibition mechanisms induced by photodamage to PSIIs has been largely improved motivated by the application of molecular biology [5, 95, 104, 113]. Therefore, quantitative representation of photoinhibition has received an increasing attention. As a consequence, number of models have been developed to represent and evaluate the effect of photoinhibition on photosynthesis [43, 44, 45, 60, 59, 91, 106, 125].

Among all these models, the Han model [59], which is initially inspired by the model of Eilers and Peeters [45], describes the effect of the light intensity and the dynamics of the reaction centres within the PSUs on microalgae growth. According to the Han model, the main contribution to photoinhibition is the damage of key proteins in PSUs. This model enables to describe complex photosynthetic processes only in terms of three possible physiological states of the PSUs, namely:

- A: open and ready to harvest a photon,
- B: closed while processing the absorbed photon energy,
- C: inhibited if several photons have been absorbed simultaneously.

The relations between these three states are schematically presented in Figure 1.1.

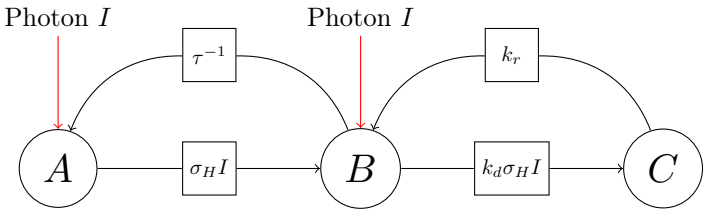

Figure 1.1: Scheme of the Han model, representing the probability of state transition, as a function of the photon flux density.

Their evolution satisfies the following dynamical system

$$\begin{cases} \dot{A} = -\sigma_H I A + \frac{B}{\tau}, \\ \dot{B} = \sigma_H I A - \frac{B}{\tau} + k_r C - k_d \sigma_H I B, \\ \dot{C} = -k_r C + k_d \sigma_H I B. \end{cases} \tag{1.1}$$

Here A, B and C are the relative frequencies of the three possible states with

$$A + B + C = 1, \tag{1.2}$$

This model separates the dynamics into two parts:

- the photosynthetic production corresponds to the transition between open state A and closed state B. Excitation is assumed to occur at a rate of $\sigma_H I$, with σ_H $[\mathrm{m}^2\,\mu\mathrm{mol}^{-1}]$ the effective cross-section of the PSUs, whereas deexcitation is assumed to occur at a rate of $\frac{1}{\tau}$, with τ [s] the turnover time of the electron transport chain. In particular, the photosynthesis rate is thus proportional to $\sigma_H I A$.

- the photo-inhibition mechanism occurs at high light intensity which corresponds to the transition from closed state B to inhibited state C. This process is assumed to occur at a rate of $k_d\sigma_H I$, with k_d [-] a damage constant. Finally, the reverse transition from inhibited state C to closed state B accounts for the repair of damaged PSUs by enzymatic processes in the cell, a mechanism which is assumed to occur at a constant rate k_r [s^{-1}].

The system (1.1) can be then reduced to two equations by using (1.2)

$$\begin{cases} \dot{A} = -(\sigma_H I + \frac{1}{\tau})A + \frac{1-C}{\tau}, \\ \dot{C} = -(k_r + k_d\sigma_H I)C + k_d\sigma_H I(1-A), \end{cases} \tag{1.3}$$

We then complete the system above with initial conditions

$$(A(0), C(0)) = (A_0, C_0) \in \{(x, y) \in \mathbb{R}^2_+ | x + y \in [0, 1]\}.$$

The dynamics of the open state A reaches its steady state following a process whose speed is very high compared to the dynamics of the photoinhibition state C [62] (for instance see Figure 1.2). This phenomenon is mainly due to the presence of the multiplicative parameter k_d which

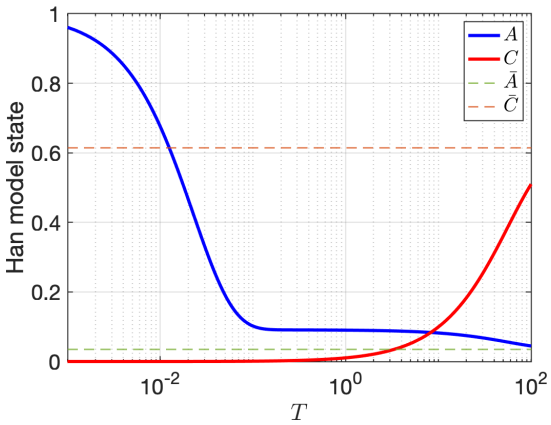

Figure 1.2: Evolution for open state A and photoinhibition state C with the initial condition $(A(0), C(0)) = (1, 0)$. Note that we use an Euler Explicit scheme to solve the system (1.3) by using the parameters presented in Table 1.1. A *log* scale is also used for the time variable.

is relatively small (see Table 1.1, where an example of possible values for the Han parameters is given). Since we usually focus on light variation at large time scale (larger than second) in real

k_r	4.8 10^{-4}	[s^{-1}]
k_d	2.99 10^{-4}	[-]
τ	6.849	[s]
σ_H	0.0029	[$m^2\,\mu mol^{-1}$]
k_H	3.6467 10^{-4}	[-]
I_s	1500	[$\mu mol\,m^{-2}\,s^{-1}$]

Table 1.1: Han model parameters taken from [77]

life applications, we can then apply a slow-fast dynamics using singular perturbation theory [72].

More precisely, this consists in equating the first equation of (1.3) to zero and find the pseudo steady state of A as $\frac{1-C}{\tau\sigma_H I+1}$. Replacing this into the second equation of (1.3), the previous two equations can finally be reduced to one equation, namely

$$\dot{C} = -\alpha(I)C + \beta(I), \tag{1.4}$$

where

$$\alpha(I) = \beta(I) + k_r, \quad \beta(I) = k_d\tau\frac{(\sigma_H I)^2}{\tau\sigma_H I + 1}.$$

As mentioned above, the growth rate is proportional to $\sigma_H IA$. Let us denote by k_H [-] the growth rate coefficient such that the growth rate is defined by

$$\mu(I) := k_H\sigma_H IA = \frac{k_H\sigma_H I}{\tau\sigma_H I + 1}(1 - C) = (1 - C)\gamma(I), \tag{1.5}$$

where

$$\gamma(I) = \frac{k_H\sigma_H I}{\tau\sigma_H I + 1}.$$

Remark

The net growth rate is defined from the growth rate by removing the respiration rate R [d^{-1}]:

$$\mu(I) - R = -\gamma(I)C + \zeta(I), \quad \zeta(I) = \gamma(I) - R. \tag{1.6}$$

An interesting property of the Han model is that the open, closed and inhibited states can be computed analytically from (1.1) as a function of the light intensity I at steady state. For instance, the steady-state expression $\bar{A}$ corresponding to the open state A is given by

$$\bar{A} = \frac{1}{\frac{k_d}{k_r}\tau(\sigma_H I)^2 + \tau\sigma_H I + 1}.$$

Therefore, one can compute the growth rate at steady state of the system by

$$\mu(I) = \frac{k_H\sigma_H I}{\frac{k_d}{k_r}\tau(\sigma_H I)^2 + \tau\sigma_H I + 1}. \tag{1.7}$$

Remark

Note that (1.4) can be solved explicitly for a constant light flux I. Hence explicit computations can also be carried out in this case for the average growth rate or the productivity. However, a continuous time-varying signal I may rapidly increase the difficulty of solving (1.4).

Definition 1.2.1. *A growth rate is said to be of Haldane type if it is of the form*

$$\mu(I) := \mu_{\max}\frac{I}{I + \frac{\mu_{\max}}{\theta}(\frac{I}{I^*} - 1)^2}, \tag{1.8}$$

where θ is the initial slope of μ, $\mu_{\max}$ stands for the maximal value of μ and I^* represents the optimal light intensity.

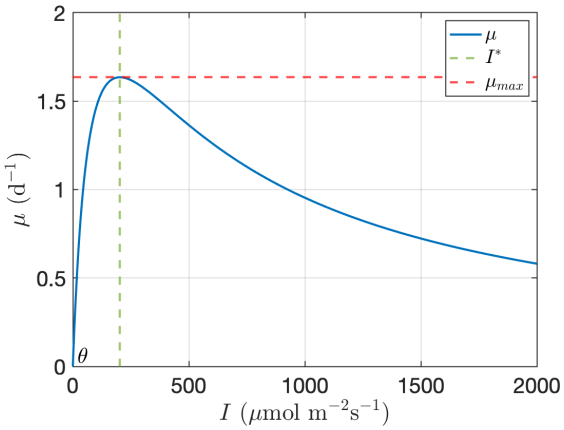

Figure 1.3: Growth rate for light intensity.

Proposition 1.2.1. *The growth rate at steady state of the Han model satisfies Haldane-type description.*

Proof. Expanding (1.8), one has

$$\mu(I) = \frac{\theta I}{\frac{I^2}{I^{*2}} + (\frac{\theta}{\mu_{\max}} - \frac{2}{I^*})I + 1}.$$

Then it remains to identify the coefficients with (1.7). We find that:

$$\theta = k_H \sigma_H, \quad I^* = \sqrt{\frac{k_r}{k_d \tau \sigma_H^2}}, \quad \mu_{\max} = \frac{k_H \sigma_H}{\tau \sigma_H + 2\sqrt{\frac{k_d \tau \sigma_H^2}{k_r}}}. \tag{1.9}$$

This concludes the proof. □

Remark

The Haldane form highlights the significant parameters of the growth rate as illustrated by Figure 1.3. This so-called PI curve shows the maximum value of the growth rate $\mu_{\max}$, the corresponding light intensity I^* and the initial angle of the growth rate θ.

1.2.2 Hydrodynamical model

Research related to geophysical fluid dynamics often consists in understanding the coupled dynamics of atmosphere and ocean on Earth or on other planets. The analysis and modeling of these geophysical flows are usually complex and challenging especially for free surface flows. The main difficulties come not only from the discretization and the simulation of the Navier-Stokes equations, but also from the fact that the considered problems may involve dynamics associated with very different scales. Therefore models with reduced complexity but still capable of representing complex flows are required. Among all, the Saint-Venant system introduced in [39] is a well known and efficient approximation of the Navier-Stokes system [115, 52, 90, 51, 21] for a large class of problems such as dam break, flooding, debris flow, etc.

The derivation of the Saint-Venant system from the Navier-Stokes equations is based on two main approximations namely:

- the vertical acceleration of the fluid can be neglected compared to the gravitational effects.
- the horizontal fluid velocity is approximated by its vertical average.

One can see for instance in [52] for the derivation of this model.

There are two ways to describe the fluid namely the Eulerian description and the Lagrangian description. The Eulerian description focuses on the macroscopic aspect meaning that a control volume is defined as well as its related properties such as pressure, velocity or acceleration, whereas the Lagrangian description pay attention to the properties of individual fluid particles, such as their positions or velocities, described as a function of time. In this thesis, we are interested in the Lagrangian description of the flow to adapt to the microscopic behaviour of the photosynthetic process in a raceway pond.

In this way, we first introduce the smooth steady state solutions of the Saint-Venant equations. Such steady states are governed by the following partial differential equations:

$$\partial_x(hu) = 0, \tag{1.10}$$

$$\partial_x(hu^2 + g\frac{h^2}{2}) = -gh\partial_x z_b, \tag{1.11}$$

where h [m] is the water elevation, u [$\mathrm{m\,s^{-1}}$] is the horizontal averaged velocity of the water, the constant g [$\mathrm{m\,s^{-2}}$] stands for the gravitational acceleration, and z_b [m] defines the topography. The free surface η [m] is given by $\eta := h + z_b$ and the averaged discharge Q [$\mathrm{m^2\,s^{-1}}$] is given by $Q := hu$. This system is presented in Figure 1.4. The z axis represents the vertical direction and

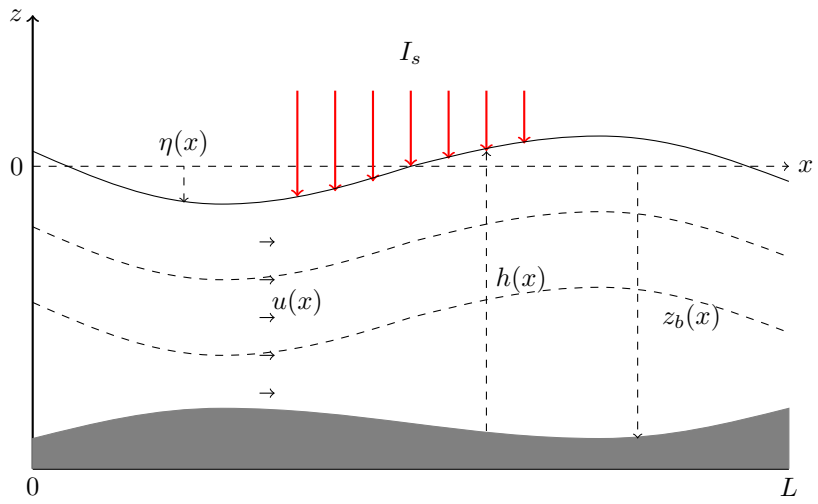

Figure 1.4: Representation of the hydrodynamic model.

the x axis represents the horizontal direction.

Remark

We assume that the solutions (h, u) are smooth such that we can carry out the following computation. Moreover, we focus only on the laminar regime of the flow.

Integrating (1.10), we get

$$hu = Q_0, \tag{1.12}$$

for a fixed positive constant Q_0 [$\mathrm{m}^2\,\mathrm{s}^{-1}$], which implies a constant discharge in space. Then (1.11) can be rewritten as

$$hu\partial_x u + h\partial_x gh + h\partial_x g z_b = 0. \tag{1.13}$$

Remark

This equation is a nonlinear ordinary differential equation, some solutions in specific cases have been widely studied. For instance, by assuming $h > 0$ and $Q_0 = 0$, we obtain the steady state of a lake at rest (see [96] and references therein), defined by

$$Q_0 = 0, \quad h + z_b = \text{cst}.$$

Let us assume that h is strictly positive. Dividing (1.13) by h and using (1.12) to eliminate u, we get

$$\partial_x\Big(\frac{Q_0^2}{2h^2} + g(h + z_b)\Big) = 0.$$

This equation corresponds to Bernoulli's principle. Now let us consider two fixed constants $h(0), z_b(0) \in \mathbb{R}$. For all $x \in [0, L]$, we obtain

$$\frac{Q_0^2}{2h^2} + g(h + z_b) = \frac{Q_0^2}{2h^2(0)} + g(h(0) + z_b(0)) =: M_0,$$

meaning that the topography z_b satisfies

$$z_b = \frac{M_0}{g} - \frac{Q_0^2}{2gh^2} - h. \tag{1.14}$$

Remark

Define the Froude number for the steady state by $Fr := u/\sqrt{gh}$. The situation $Fr < 1$ corresponds to the subcritical case (i.e. the flow regime is fluvial) while $Fr > 1$ is to the supercritical case (i.e. the flow regime is torrential). In particular, the threshold value of h for $Fr = 1$ is given by

$$h_c := (\frac{Q_0^2}{g})^{\frac{1}{3}}.$$

Because of (1.14), h is the solution of a third order polynomial equation. The following result ensures that (1.14) has a unique solution.

Lemma 1.2.1 (Lemma 1 in [96]). *Given a smooth topography z_b, if*

$$h_c + z_b + \frac{Q_0^2}{2gh_c^2} - \frac{M_0}{g} < 0.$$

there exists a unique positive smooth solution of (1.14) *which satisfies the subcritical flow condition.*

Let $z(t)$ be the depth of a particle at time t in the raceway pond. We determine the Lagrangian trajectory of an algal cell which starts at a given position $z(0)$ at time 0. From the incompressibility of the flow, one has $\nabla \cdot \underline{\mathbf{u}} = 0$ with $\underline{\mathbf{u}} = (u(x), w(x,z))$. Here, $u(x)$ is the horizontal velocity and $w(x,z)$ is the vertical velocity. Note that u only depends on x since a laminar regime is assumed. This implies that

$$\partial_x u + \partial_z w = 0. \tag{1.15}$$

Integrating (1.15) from z_b to z gives:

$$\begin{aligned} 0 &= \int_{z_b}^{z} \big(\partial_x u(x) + \partial_z w(x,z)\big)\mathrm{d}z \\ &= \partial_x \int_{z_b}^{z} u(x)\mathrm{d}z + \int_{z_b}^{z} \partial_z w(x,z)\mathrm{d}z \\ &= \partial_x\big((z-z_b)u(x)\big) + w(x,z) - w(x,z_b) \\ &= (z-z_b)\partial_x u(x) - u(x)\partial_x z_b + w(x,z), \end{aligned}$$

where we have used the kinematic condition at the bottom (i.e. $w(x,z_b) = u(x)\partial_x z_b$). It then follows from (1.14) that

$$w(x,z) = (\frac{M_0}{g} - \frac{3u^2(x)}{2g} - z)u'(x).$$

The Lagrangian trajectory is characterized by the system

$$\begin{pmatrix} \dot{x}(t) \\ \dot{z}(t) \end{pmatrix} = \begin{pmatrix} u(x(t)) \\ w(x(t), z(t)) \end{pmatrix}.$$

Remark

Note that a Brownian motion can be included in these equations to take into account the fluid viscosity. In this case, the optimisation procedure requires a large set of simulations and an averaging strategy. Such questions exceed the scope of this thesis.

Remark

Since the raceway pond is a circuit basin, it is natural to impose $h(0) = h(L)$ (or $z_b(0) = z_b(L)$), meaning that a space periodicity is assumed. One needs to account for this when dealing with the parameterization in the optimization part.

1.2.3 Light intensity modeling

The light intensity I plays an important role in algal growth, since it triggers photosynthesis. On the other hand, the position of the algae $z(t)$ will influence the light perceived as well as the efficiency of the photosynthesis process. Therefore, the light intensity is the main connection which couples the hydrodynamic model and the physiological evolution of the algae. We will present in this section a well-known model to describe the vertical light attenuation.

In most cases, the photobioreactors are illuminated from above by a light intensity denoted by I_s hereafter. The subscript s emphasizes that I_s is the light intensity at the illuminated surface, which is assumed to be a constant. It is often assumed for low-density cultures that all microalgae in the pond perceive the same light intensity as I_s [70]. However, in more general cases such as industrial applications and aquatic environments, a gradient of light intensity is observed when moving deeper into the culture medium. This is caused by light absorption and scattering by light-absorbing substances [17, 1, 74]. In order to take into account this phenomenon, the Beer-Lambert law is often chosen as a first approximation to determine the light attenuation at any position in the medium. This law states that I satisfies

$$\frac{\partial I}{\partial z} = -\varepsilon I,$$

where $\varepsilon \geq 0$ [m^{-1}] represents the light extinction coefficient and $z \in [0, h]$ denotes the vertical distance from the illuminated surface to the position of the culture with h [m] the depth of the reactor. Since the microalgae culture is often assumed to be perfectly mixed, light extinction coefficient ε does not depend on the depth of the culture z.

Therefore, we can integrate the previous equation to obtain:

$$I(z) := I_s \exp(-\varepsilon z). \tag{1.16}$$

The light extinction ε summarises the light absorption and diffusion in the system. In the case of a mono-culture, ε is mainly considered to be correlated to the biomass concentration X [74]. In a first approximation, one can assume an affine relation between these parameters, i.e.,

$$\varepsilon(X) := \alpha_0 X + \alpha_1, \tag{1.17}$$

where $\alpha_0 > 0$ [$\mathrm{m}^2\,\mathrm{g}^{-1}$] stands for the specific light extinction coefficient of the microalgae species and α_1 [m^{-1}] defines the background turbidity due to all non-microalgae components i.e. suspended solids and dissolved colored material. Typical values of the coefficient α_0 for some microalgae species are given in Table 1.2.

Extinction coefficient [$\mathrm{m}^2\,\mathrm{g}^{-1}$]	Algae species
0.214	Monodus subterraneu
0.175	Spirulina platensis
0.150	Porphyridium cruentum
0.200	Chlorella pyrenoidosa

Table 1.2: Values of the light extinction coefficient α_0 for different microalgae species see in [27].

It is usually assumed that the biomass concentration X is homogeneous. However, in order to use (1.17), the density of the culture X must be small enough to guarantee that most of the photons are diffused at most once. For multi-diffusion regimes, the latter condition is generally not satisfied [50]. Hence, various empirical expressions have been developed to account for multi-scattering, for instance, in [122] the authors have proposed the following expression:

$$\varepsilon(X) = \frac{\beta_0 X}{\beta_1 + X}.$$

with β_0 and β_1 determined empirically.

Remark

In this thesis, we focus only on light regime such that the light extinction can be described using (1.17).

As already mentioned, the light intensity I is the bridge to connect the hydrodynamical systems with the biological systems. In a raceway pond, it is often assumed that the photosynthetic units grow slowly such that the variations of biomass concentration X and background turbidity α_1 are negligible over one lap of the raceway. At such a time scale, these two quantities in (1.17) can be considered to be constant. Thus, the light extinction can be determined by measuring the light intensity at bottom of the reactor $I_b := I(h)$, so that we obtain for:

$$\varepsilon = \frac{1}{h}\ln(\frac{I_s}{I_b}).$$

From (1.16), one can compute the mean light intensity received by the algae culture

$$\bar{I} = I_s \int_0^h e^{-\varepsilon(X)z}\mathrm{d}z = \frac{I_s}{\varepsilon(X)}(1 - e^{-\varepsilon(X)h}).$$

The mean light intensity decreases with $\varepsilon(X)$, which confirms the intuition that high biomass concentration X or background turbidity α_1 (see Equation (1.17)) leads to high attenuation and low value of the mean light.

1.2.4 Mixing device modeling

Except for keeping a constant motion in the raceway pond, the powered paddle wheel also modifies the elevation of algal cultures each time when they pass through this device. Studies have shown that this device mixes the algae position to prevent cell sedimentation, to ensure nutrient homogeneity and to influence light reception at the cell scale in the system [37, 107]. However, modeling this complex device is challenging and involves stochastic behaviour when going through the device. In this thesis, we consider a generic mixing device and make a perfect mixing assumption, meaning that at each lap, the algae at the layer n_1 are supposed to be entirely transferred to the layer n_2 when passing through this mixing device. In this way, the mixing process can be modelled by a permutation matrix $P \in \mathcal{P}_N$, where $\mathcal{P}_N$ denotes the set of permutation matrices of size $N \times N$ with $N \in \mathbb{N}$. Denote also by $\sigma \in \mathfrak{S}_N$ the permutation corresponding to P where $\mathfrak{S}_N$ denotes the set of permutations of N elements. This mixing process is depicted schematically on an example in Figure 1.5.

1.3 Periodic Cauchy problem

In this section, we focus on the periodic Cauchy problem associated with the dynamics C (1.4). This will be useful to study periodic solutions of this biological model.

Let us first consider the Cauchy problem associated with (1.4). Given $I \in L^2(0,T;R_+)$ and an initial state $C_0 \in [0,1]$. Find $C \in \mathcal{C}(0,T;[0,1])$ such that

$$\begin{cases} \dot{C}(t) = -\alpha(I(t))C(t) + \beta(I(t)), \quad t \in [0,T] \\ C(0) = C_0 \end{cases} \tag{1.18}$$

The theorem below gives existence and uniqueness of a (weak) solution for this problem.

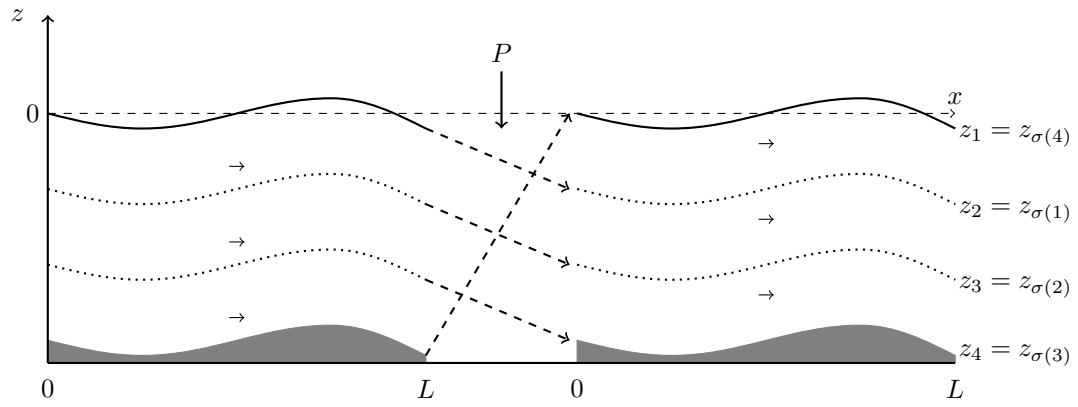

Figure 1.5: Schematic representation of the mixing process over two laps. Here, $N = 4$ and P corresponds to the cyclic permutation $\sigma = (1\ 2\ 3\ 4)$.

Theorem 1.3.1. *There exists a unique weak solution of* (1.18)*, i.e. a function* $C \in \mathcal{C}(0,T;[0,1])$ *satisfying*

$$C(t) = C_0 + \int_0^t -\alpha(I(s))C(s) + \beta(I(s))\mathrm{d}s, \tag{1.19}$$

for all $t \in [0,T]$.

Proof. Since $\alpha(I) = k_r + \beta(I)$, (1.4) can also be written as:

$$\dot{C}(t) = -k_r C(t) - \beta(I(t))C(t) + \beta(I(t)).$$

Note that the light intensity $I(t) \geq 0$ for all $t \in [0,T]$. Since τ, σ_H are all positive, then one has

$$\beta(I(t)) = k_d\tau\frac{(\sigma_H I(t))^2}{\tau\sigma_H I(t)+1} \leq k_d\tau(\sigma_H I(t))^2.$$

Consider now the mapping

$$\Phi : \begin{cases} \mathcal{C}(0,T;[0,1]) \to \mathcal{C}(0,T;[0,1]) \\ C \mapsto \Phi(C) \end{cases}$$

where $\Phi(C)$ is defined for $t \in [0,T]$ by the Duhamel's formula:

$$\Phi(C)(t) = e^{-k_r t}C_0 + \int_0^t e^{-k_r(t-s)}\Big(-\beta(I(s))C(s) + \beta(I(s))\Big)\mathrm{d}s. \tag{1.20}$$

Note first that Φ is well-defined: indeed since $C \in \mathcal{C}(0,T;[0,1])$ and $I \in L^2(0,T;R)$, $s \mapsto -\alpha(I(s))C(s) + \beta(I(s))$ is Lebesgue integrable. Let us now prove that Φ is a contraction. Let C_1 and $C_2 \in \mathcal{C}(0,T;[0,1])$. Since $t \geq s$, then $\exp(-k_r(t-s)) \leq 1$ which is a bounded function.

Therefore, we obtain

$$\begin{aligned}
\|\Phi(C_2) - \Phi(C_1)\|_{L^\infty(0,T;[0,1])} &= \sup_{t\in[0,T]} |\Phi(C_2)(t) - \Phi(C_1)(t)| \\
&= \sup_{t\in[0,T]} \left| \int_0^t e^{-k_r(t-s)} \beta(I(s))(C_2(s) - C_1(s)) \mathrm{d}s \right| \\
&\leq k_d \tau \sigma_H^2 \sup_{t\in[0,T]} \int_0^t I^2(s) \left| (C_2(s) - C_1(s)) \right| \mathrm{d}s \\
&\leq k_d \tau \sigma_H^2 \|C_2 - C_1\|_{L^\infty(0,T;[0,1])} \int_0^T I^2(s) \mathrm{d}s \\
&= k_d \tau \sigma_H^2 \|C_2 - C_1\|_{L^\infty(0,T;[0,1])} \|I\|^2_{L^2(0,T;\mathbb{R}_+)} .
\end{aligned}$$

According to $\|I\|_{L^2(0,T;\mathbb{R}_+)}$, two cases must be considered.

- If $\|I\|_{L^2(0,T;\mathbb{R}_+)}$ is small enough, the above inequality implies that Φ is a contraction. We deduce from the Banach fixed point theorem that Φ has a unique fixed-point, hence (1.18) admits a unique solution $C \in \mathcal{C}(0,T;[0,1])$.
- If $\|I\|_{L^2(0,T;\mathbb{R}_+)}$ is not small, we consider the partition $[0,T] = \bigcup_{l=0}^{N-1} [T_l, T_{l+1}]$, with $T_0 = 0$ and $T_N = T$, such that $\|I\|_{L^2(T_l,T_{l+1};\mathbb{R})}$ is small enough. Then by the Banach fixed-point theorem that Φ has a unique fixed point on each interval $[T_l, T_{l+1}]$ for all $l \in \{0, \cdots, N-1\}$.

Finally, by applying Banach fixed-point of Φ, we remark that the right sides of (1.20) and (1.19) are almost everywhere differentiable and that their derivatives are almost everywhere equal. This concludes the proof. □

We now consider a variant of the previous Cauchy problem, where the initial condition is unknown and must also satisfy the periodicity condition. Given $I \in L^2(0,T;R_+)$, this problem reads:

Find $(C_0, C) \in [0,1] \times \mathcal{C}(0,T;[0,1])$ *such that*

$$\begin{cases} \dot{C}(t) = -\alpha(I(t))C(t) + \beta(I(t)), & t \in [0,T] \\ C(T) = C_0 = C(0). \end{cases} \tag{1.21}$$

To prove the existence and uniqueness of a (weak) solution of this problem, we need the following result.

Lemma 1.3.1. *Given* $Z_0 \in [0,1]$*, let* $Z \in \mathcal{C}(0,T;[0,1])$ *be the weak solution of*

$$\begin{cases} \dot{Z}(t) = -\alpha(I(t))Z(t), & t \in [0,T] \\ Z(T) = Z_0 \end{cases} \tag{1.22}$$

For $t \in [0,T]$*:*

$$\|Z(t)\|_2 \leq e^{-k_r t} \|Z_0\|_2 . \tag{1.23}$$

Proof. Let $t \in [0,T]$, as a weak solution of (1.22), the function Z is almost everywhere differentiable and a direct computation gives

$$\frac{\mathrm{d}\|Z(t)\|_2^2}{\mathrm{d}t} = 2\langle Z(t), -\alpha(I(t))Z(t)\rangle \leq -2k_r \|Z(t)\|_2^2 , \tag{1.24}$$

where we have used the fact that $\alpha(I) = \beta(I) + k_r$, $\beta(I) \geq 0$ and $k_r > 0$. Defining $f(t) := \frac{\mathrm{d}\left\|Z(t)\right\|_2^2}{\mathrm{d}t} + 2k_r \left\|Z(t)\right\|_2^2$ and multiplying both sides by $e^{2k_r t}$, we obtain:

$$\frac{\mathrm{d}e^{2k_r t}\left\|Z(t)\right\|_2^2}{\mathrm{d}t} = e^{2k_r t} f(t),$$

which gives by integration over $[0, t]$ that

$$\left\|Z(t)\right\|_2^2 = e^{-2k_r t}\left\|Z_0\right\|_2^2 + \int_0^t e^{2k_r(s-t)} f(s)\mathrm{d}s.$$

Then using (1.24), $f(t) \leq 0$. This concludes the proof. □

We can now state an existence and uniqueness result in the periodic case.

Theorem 1.3.2. *There exists a unique couple* $(C_0, C) \in [0,1] \times \mathcal{C}(0, T; [0,1])$ *satisfying*

$$\begin{cases} C(t) = C_0 + \int_0^t -\alpha(I(s))C(s) + \beta(I(s))\mathrm{d}s, \\ C(T) = C_0 \end{cases} \tag{1.25}$$

for all $t \in [0, T]$.

Proof. Introduce the mapping $\Phi : [0,1] \to [0,1]$ defined by

$$\Phi(C_0) := C(T),$$

where C is the weak solution of (1.18) obtained in Theorem 1.3.1. Given $C_0^1 \in [0,1]$ and $C_0^2 \in [0,1]$, define $Z_0 = C_0^2 - C_0^1$ and $Z(t) = C^2(t) - C^1(t)$, where C^1 and C^2 are the weak solutions obtained by Theorem 1.3.1 with $C_0 = C_0^1$ and $C_0 = C_0^2$, respectively. Subtracting the corresponding weak representations (1.19), we see that Z satisfies the assumptions of Lemma 1.3.1 such that (1.23) holds. As a consequence,

$$\left\|C^2(T) - C^1(T)\right\|_2 \leq e^{-k_r T}\left\|C_0^2 - C_0^1\right\|_2,$$

which implies that Φ is a contraction. Applying Banach fixed-point theorem, it follows that there exists a unique $C_0 \in [0,1]$ such that $\Phi(C_0) = C_0$. The corresponding weak solution C of (1.18) satisfies (1.25). □

This result allows us to study the case when C is assumed to be periodic (see Subsection 4.3.2).

1.4 Adjoint methods for optimization problem

In this section, we briefly recall the basics of the adjoint method which will be used in Chapter 4 to solve the constrained optimization problem. The adjoint method originates from the theory of Lagrange multipliers in optimization which is presented in the following. Consider the problem

$$\begin{aligned} &\text{optimize } f(x), \\ &\text{subject to } g(x) = 0. \end{aligned}$$

where f, g are functions $\Omega \in \mathbb{R}$ of class $\mathcal{C}^1$ with Ω an open subset of $\mathbb{R}^n$.

Theorem 1.4.1. *If x^* is a local minimum or local maximum of f subject to the constraint $g = 0$ and if $\nabla g(x^*) \neq 0$, then there exists $\lambda \in \mathbb{R}$ such that the following system of equation is satisfied by x^* and λ:*

$$\begin{aligned} \nabla f(x^*) + \lambda \nabla g(x^*) &= 0, \\ g(x) &= 0. \end{aligned}$$

λ is so-called the Lagrange multiplier.

We refer to [46, Chapter 3, Section 3] for more details about this theorem.

The adjoint method is an extension of this theorem in the framework of optimal control and optimization. In this way, the variable x is the union of a state variable $\tilde{x}$ and a control state u. The constraint $g(\tilde{x}, u) = 0$ gives the state $\tilde{x}$ in terms of the control u. In such cases, the Lagrange multiplier λ is often called the adjoint state. This approach was first developed by Pontryagin [20] to ordinary differential equations and by Lions [86] to partial differential equations.

We illustrate this method for the time-dependent problem which are often treated by semi-discretization on the spatial variable of a partial differential equation. Consider the following problem:

$$\begin{aligned} \text{optimize } & \int_0^T f(x, a, t), \\ \text{subject to } & h(x, \dot{x}, a, t) = 0, \\ & g(x(0), a) = 0. \end{aligned}$$

where a represents a vector of unknown parameters, x stands for a (often vector) function of time, $h(x, \dot{x}, a, t) = 0$ is an ordinary differential equation in implicit form and $g(x(0), a) = 0$ is the initial condition which may be a function of some of the unknown parameters. Note that the ordinary differential equation h may be the result of a spatial semi-discretization of a partial differential equation.

The gradient-based optimization algorithm requires to compute the total derivative

$$\mathrm{d}_a \int_0^T f(x, a, t)\mathrm{d}t = \int_0^T \left(\partial_x f \mathrm{d}_a x + \partial_a f\right) \mathrm{d}t.$$

where $\mathrm{d}_a x$ denotes the total derivative of x with respect to the unknown parameters a which is challenging to compute in most cases. To overcome this difficulty, we first introduce the Lagrangian corresponding to the optimization problem:

$$\mathcal{L} = \int_0^T f(x, a, t) + \lambda_1 h(x, \dot{x}, a, t)\mathrm{d}t + \lambda_2 g(x(0), a),$$

where λ_1, λ_2 are two Lagrange multipliers with λ_1 a function of time. Taking then the total derivative of the Lagrangian

$$\mathrm{d}_a \mathcal{L} = \int_0^T \partial_x f \mathrm{d}_a x + \partial_a f + \lambda_1 \left(\partial_x h \mathrm{d}_a x + \partial_{\dot{x}} h \mathrm{d}_a \dot{x} + \partial h\right) \mathrm{d}t + \lambda_2 \left(\partial_{x(0)} g \mathrm{d}_a x + \partial_a g\right). \tag{1.26}$$

Integrating by parts helps us to eliminate $\mathrm{d}_a \dot{x}$ as

$$\int_0^T \lambda_1 \partial_{\dot{x}} h \mathrm{d}_a \dot{x} \mathrm{d}t = \left[\lambda_1 \partial_{\dot{x}} h \mathrm{d}_a x\right]_0^T - \int_0^T \left(\dot{\lambda}_1 \partial_a h + \lambda_1 \mathrm{d}_t \partial_{\dot{x}} h\right) \mathrm{d}_a x \mathrm{d}t.$$

The next step consists in substituting the previous result into (1.26)

$$\begin{aligned}\mathrm{d}_a\mathcal{L} = \int_0^T \Big[\Big(\partial_x f + \lambda_1(\partial_x h - \mathrm{d}_t\partial_{\dot{x}}h) - \dot{\lambda}_1\partial_{\dot{x}}h\Big)\,\mathrm{d}_a x + \partial_a f + \lambda_1\partial_a h\Big] \\ + \lambda_1\partial_{\dot{x}}h\mathrm{d}_a x|_T + (-\lambda_1\partial_{\dot{x}}h + \lambda_2\partial_{x(0)}g)|_0\mathrm{d}_a x(0) + \lambda_2\partial_a g.\end{aligned}$$

Since the two constraints $h = 0$ and $g = 0$ are always satisfied by construction, then we can set $\lambda_1(T) = 0$ and $\lambda_2 = \lambda_1\partial_{\dot{x}}h|_0\partial^{-1}_{x(0)}g$. Finally we can avoid computing $\mathrm{d}_a x$ for all $t > 0$ by setting

$$\partial_x f + \lambda_1(\partial_x h - \mathrm{d}_t\partial_{\dot{x}}h) - \dot{\lambda}_1\partial_{\dot{x}}h = 0,$$

one finds the total derivative as

$$\mathrm{d}_a\int_0^T f(x,a,t) = \int_0^T \partial_a f + \lambda_1\partial_a h\mathrm{d}t + \lambda_1\partial_{\dot{x}}h|_0\partial^{-1}_{x(0)}g\partial_a g.$$

1.5 Summary

In this section, we give a general summary of each contribution. This thesis can be separated into three parts:

- In Chapter 2, we focus on the optimal conditions to maximize the productivity in photobioreactors. More precisely, we investigate the influence of the light extinction and the background turbidity of the medium on growth and productivity. In this way, a general light attenuation function relying on biomass concentration is considered which also accounts for the background turbidity of the system. The concept of optical productivity is introduced to better understand the influence of the optical depth in the system dynamics. A global optimal optical depth is determined which depends only on the model settings. From a biological point of view, this optimal condition consists in canceling the net growth rate of the algae at the bottom of the reactors. This optimal condition can then be used to characterize the optimization of the surface biomass productivity in some specific cases, whereas an asymptotic behaviour has been observed in more general case. In practise, this optimal condition helps to establish a relation between the algal biomass concentration and the reactor depth. We develop a nonlinear controller and prove the global asymptotic stability of the biomass concentration towards the desired optimal value. This part of the work corresponds to a submitted journal article [11].

- Chapter 3 deals with a general class of problem where N resources are distributed to N activities, each activity then uses the assigned resource to evolve during a given time $T > 0$ after which the resources will be re-distributed. This problem is part of a large class of allocation problems, with the particularity that it includes a dynamical system. In such problems, the goal is to find the best allocation strategies to optimize the cost or the benefit of the system. We apply this theory to the industrial microalgal raceway where a mixing device, such as a paddle wheel, is considered to control the rearrangement of the depth of the algae cultures hence the light perceived at each lap. Non trivial permutation strategies are obtained with a significant increase in the algal growth. This part of the work corresponds to the theory we progressively developed in a conference proceeding [16] and a submitted journal article [15].

- Chapter 4 is dedicated to the analysis of the influence of the shape of the topography on al-

gal growth in raceway ponds. A coupled biological-hydrodynamical model is considered to describe this complex dynamical system. For this problem, we apply an adjoint-based optimization scheme which includes the constraints associated with the shallow water regime. On the contrary to a widespread belief, the flat topography is proved to be the optimal topography in a periodic regime, whereas non-trivial topographies can be obtained in other contexts, e.g., when the periodic assumption is removed or when an extra mixing strategy is included in the model. Note that in the examples considered in our numerical tests, such topographies slightly improved the biomass production, whereas a combination of the mixing strategies with the topographies can enhance this result. This chapter corresponds to the conference proceedings [12, 14] and a submitted journal article [13].

1.5.1 Optimal condition for algal production

The biomass production in photobioreactors depends on the photosynthesis efficiency of the microalgae which mainly relies on the light radiation in the system. As shown in Subsection 1.2.3, the light intensity decreases rapidly along the photobioreactor depth. This phenomenon can be described by a Beer-Lambert law (1.16). Although a linear dependence of the biomass concentration has often been used in literature to describe the light extinction (as shown in (1.17)), experimental studies show that nonlinear behaviour can be obtained in some cases (hence a general nonlinear formulation must be considered). For instance, Morel calibrates in [101] the optical behaviour in the attenuation process of radiant energy based on oceanic water for which phytoplankton and their derivative play a predominant role in determining their optical properties. The background turbidity of the system may also have an influence on the average growth rate of the algae [93]. These two parameters are considered here, in order to describe the light extinction in photobioreactors. In the quest for optimising areal biomass productivity, authors in [94] have found an optimal condition by using the Droop description (Subsection 1.2.1) of algal growth rate and a linear light extinction function. This condition expresses that respiration rate compensates exactly the algal growth rate at the bottom of the reactor. In Chapter 2, we extend [94] by using a Haldane-type description (1.8) combined with a more general light extinction function:

$$\varepsilon(X) := \alpha_0(s)X^s + \alpha_1,$$

where $0 < s \leq 1$, $\alpha_0(s) > 0$ stands for the specific light extinction coefficient and α_1 defines the background turbidity of the medium due to dissolved turbidity, bacteria, particulate matter and other microalgae.

In the first part, we introduce the concept of optical productivity P as the product between the average growth rate $\bar{\mu} - R$ with the optical depth $Y := \varepsilon(X)h$ (see (2.8)) and provide the following result to determine the optimal optical depth Y_{opt}:

Theorem 1.5.1. *For a given light intensity I_s, there exists an optimum Y_{opt} to maximize the optical productivity P which satisfies $\mu\left(I(Y_{opt})\right) = R$. This optimum can be computed explicitly as a function of the growth rate at the surface $\mu(I_s)$:*

$$Y_{opt} = \begin{cases} \ln\left(\dfrac{\frac{2I_s R\mu_{\max}}{\theta I^{*2}}}{\mu_{\max} - R + \frac{2R\mu_{\max}}{\theta I^*} - \sqrt{(\mu_{\max}-R)(\mu_{\max}-R+\frac{4R\mu_{\max}}{\theta I^*})}}\right), & \mu(I_s) > R, \\ \ln\left(\dfrac{\frac{2I_s R\mu_{\max}}{\theta I^{*2}}}{\mu_{\max} - R + \frac{2R\mu_{\max}}{\theta I^*} + \sqrt{(\mu_{\max}-R)(\mu_{\max}-R+\frac{4R\mu_{\max}}{\theta I^*})}}\right), & \mu(I_s) \leq R, \end{cases}$$

where $\mu_{\max}, \theta, I^*$ are defined in Definition 1.2.1.

The optimal optical depth Y_{opt} represents the case where the growth rate at the bottom of the reactor equals the respiration rate R. Since the value of Y_{opt} only depends on the choice of the model parameter (i.e. $I_s, R, \mu_{\max}, \theta, I^*$), one can use it as a criterion to evaluate the optimum for different biomass concentrations or different reactor depths. Some results can be deduced directly from this theorem in particular one concerning the productivity Π (defined in (2.6)) with a fixed biomass concentration X.

Corollary 1.5.1. *For a given biomass concentration X_1, there exists a unique h_1 satisfied $\varepsilon(X_1)h_1 = Y_{opt}$ which maximizes the productivity $\Pi(X_1, \cdot)$.*

On the contrary to the previous case, dealing with a fixed reactor depth h is more tricky since the light extinction function plays an important role. More precisely, we have found the following result.

Theorem 1.5.2. *If $\alpha_1 > 0$, there is no global optimum for the productivity $\Pi(\cdot, \cdot)$ in $\mathbb{R}_+ \times \mathbb{R}_+$.*

We then define a sequence $(X_n, h_n)_{n>0}$ to study the asymptotic behaviour in this situation. For a given X_0, this sequence is defined by:

$$h_n = \frac{Y_{\text{opt}}}{\varepsilon(X_{n-1})}, \quad X_n := \text{argmax}_{X \in \mathbb{R}_+} \Pi(X, h_n).$$

Using this sequence, one has the following result on the productivity Π:

Theorem 1.5.3. *The productivity Π for the sequence $(X_n, h_n)_{n>0}$ is given by*

$$\lim_{n\to\infty} \Pi(X_n, h_n) = \begin{cases} \frac{P(Y_{opt})}{\alpha_0}, & s = 1, \\ +\infty, & s < 1. \end{cases}$$

In practise, the reactor depth h is always a fixed constraint (e.g., $h = 0.4\,\text{m}$ for raceway ponds and $h = 1\,\text{mm}$ for biofilm reactors). In this way, choosing a biomass concentration to cancel the net growth rate at bottom may usually not be an optimal strategy to maximize the productivity Π. As shown in Figure 1.6, the blue point corresponds to the case when the net growth rate at

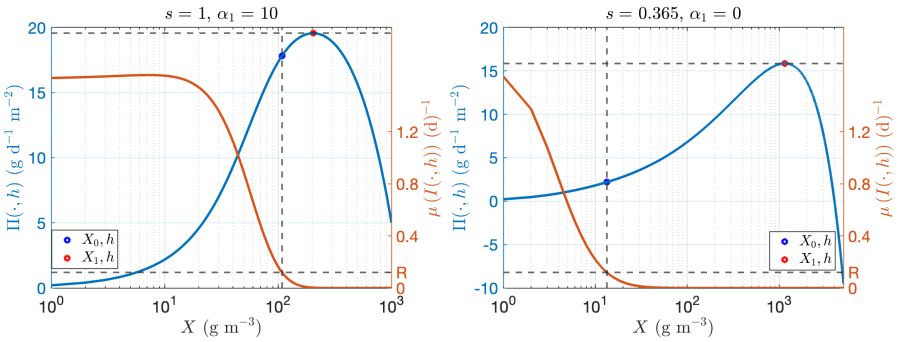

Figure 1.6: Productivity (Π) with respect to biomass concentration (X) for $h = 0.15\,\text{m}$. Blue point: $\varepsilon(X_0)h = Y_{\text{opt}}$ Red point: $X_1 = \text{argmax}_{X \in \mathbb{R}_+} \Pi(X, h)$.

the bottom is zero and the red point corresponds to the optimal biomass concentration for this given reactor depth h. In particular, the choice of such biomass concentration can have a huge impact on the productivity as shown on the right figure. In this case, one needs to have the

specific formulation of the average growth rate $\bar{\mu}$ (or the productivity Π) to locate the optimal biomass concentration.

1.5.2 Optimal mixing strategy for algal production

The classical resource allocation problem consists in finding an optimal strategy to assign a number of resources to the different activities. Due to its simple structure, this problem is encountered in a number of applications, for instance load scheduling [123], manufacturing [124], portfolio selection [63] and computational biology [3]. The optimization of these complex systems is challenging and the available works in the literature, especially when dealing with dynamics, are still rare.

In this way, we focus on the following problem: Given a period T, and initial time T_0 and a sequence $(T_k)_{k\in\mathbb{N}}$, with $T_k = kT + T_0$, we consider the following resource allocation problem: Consider N resources denoted by $(I_n)_{n=1}^N \in \mathbb{R}^N$ which can be allocated to N activities denoted by $(x_n)_{n=1}^N$ where x_n consists of a real function of time. On a time interval $[T_k, T_{k+1})$, each activity uses the assigned resource and evolves according to a linear dynamics

$$\dot{x}_n = -\alpha(I_n)x_n + \beta(I_n),$$

where $\alpha : \mathbb{R} \to \mathbb{R}_+$ and $\beta : \mathbb{R} \to \mathbb{R}_+$ are given. At time T_{k+1}, the resources is re-assigned, meaning that $x(T_{k+1}) = Px(T_{k+1}^-)$ for some permutation matrix $P \in \mathcal{P}_N$. In order to evaluate the quality of the mixing associated with P, we define the benefit attached to each time period $[T_k, T_{k+1})$ by

$$f^k := \langle u, \frac{1}{T}\int_{T_k}^{T_{k+1}} x(t)\mathrm{d}t\rangle,$$

with $u \in \mathbb{R}^N$ an arbitrary vector. Then the average benefit after K operations is given by $\frac{1}{K}\sum_{k=0}^K f^k$.

The first challenging issue that appears at this step is related to the periodicity of the permutation matrix P. Since we are interested in the average benefit for K operations, then it is natural to assume the periodicity on the system, meaning that $x(T_K) = x(T_0)$. This assumption is very useful when it comes to e.g., crop harvesting or scheduling of appliances. A natural choice for K would be the order of the permutation associated with P. Indeed, in this case K is the minimal number of re-assignments required to recover the initial allocation. However, different permutation matrices may be associated with different order K, and some of these orders K can be very large such that computations will be time consuming and memory resource demanding. The following result helps us to overcome this difficulty.

Theorem 1.5.4. *$(x(T_k))_{k\in\mathbb{N}}$ is a constant sequence and for all $k \in \mathbb{N}$, we have*

$$x(T_k) = (\mathcal{I}_N - PD)^{-1}Pv.$$

This result shows that every $KT-$periodic evolution will actually be $T-$periodic. This property is decisive to formulate an optimization problem independent of K. In addition, the computations to solve the optimization problem will be reduced, since the CPU time required to assess the quality of a permutation will not depend on its order. In this way, let us consider the functional deduced from the average benefit as

$$J(P) := \langle u, (\mathcal{I}_N - PD)^{-1}Pv\rangle.$$

Here lies the second challenge. Since the cardinal of the permutation set is $N!$, this problem

cannot be tackled in realistic cases where large values of N must be considered, e.g., to keep a good numerical accuracy. To overcome this difficulty, we propose an approximation of this problem whose optimum can be determined explicitly. For this purpose, we expand the functional $J(P)$ as follows

$$\langle u,(I-PD)^{-1}Pv\rangle=\sum_{l=0}^{+\infty}\langle u,(PD)^{l}Pv\rangle=\langle u,Pv\rangle+\sum_{l=1}^{+\infty}\langle u,(PD)^{l}Pv\rangle,$$

and consider as an approximation of $J(P)$ the first term of this series, namely

$$J^{\text{approx}}(P):=\langle u,Pv\rangle.$$

For this sub-problem, the optimal solution can be determined explicitly by using the following result.

Lemma 1.5.1. *Let $\sigma_+,\ \sigma_-\in\mathfrak{S}_N$ such that $v_{\sigma_+(1)}\leq v_{\sigma_+(2)}\cdots\leq v_{\sigma_+(N)}$ and $v_{\sigma_-(N)}\leq v_{\sigma_-(N-1)}\leq\cdots\leq v_{\sigma_-(1)}$ and $P_+,\ P_-\in\mathcal{P}_N$, the corresponding permutation matrices. Then*

$$P_+=\text{argmax}_{P\in\mathcal{P}_N}J^{approx}(P),\quad P_-=\text{argmin}_{P\in\mathcal{P}_N}J^{approx}(P).$$

In other words, this result states that once u and v are given, P_+ will be the matrix which associates the largest coefficient of u with the largest coefficient of v, the second largest coefficient with the second largest, and so on. In the same way, P_- is the matrix which associates the largest coefficient of u with the smallest coefficient of v, the second largest coefficient with the second smallest, and so on.

We then provide the next criterion to evaluate this optimal strategy corresponding to this sub-problem.

Theorem 1.5.5. *Assume that u and v have positive entries and define*

$$\phi(m_1):=\frac{1}{s_{\lceil\frac{m_1}{2}\rceil}}\Big(\sum_{l=1}^{+\infty}d_{\max}^{l}F^{+}_{(l+1)m_1}-d_{\min}^{l}F^{-}_{(l+1)m_1}\Big),\tag{1.27}$$

where s and F^+,F^- are independent of the optimum of $J(P)$ and can be pre-computed explicitly (see (3.12) and (3.13) in Chapter 3 Section 3.2.2), $d_{\max}:=\max_{n=1,\dots,N}(d_n)$ and $d_{\min}:=\min_{n=1,\dots,N}(d_n)$. Assume that:

$$\max_{m_1\geq 2}\phi(m_1)\leq 1.$$

Then the problem $\max_{P\in\mathcal{P}_N}\langle u,(I-PD)^{-1}Pv\rangle$ (resp. $\min_{P\in\mathcal{P}_N}\langle u,(I-PD)^{-1}Pv\rangle$) and the problem $\max_{P\in\mathcal{P}_N}\langle u,Pv\rangle$ (resp. $\min_{P\in\mathcal{P}_N}\langle u,Pv\rangle$) have the same solution.

This periodic dynamical resource allocation theory is then applied to the optimization of a mixing strategy to enhance the growth rate in a microalgal raceway system. In [29], authors have shown that the paddle wheel, which set the hydrodynamic system in motion in raceway ponds, homogenises the medium, ensures an equidistribution of the nutrients and guarantees that each cell will have regularly access to the light. In the present work, the paddle wheel is identified to a mixing device and modeled by a permutation. We then focus on the influence of the mixing strategy on the algal productivity in a flat raceway system with a constant average velocity for which the above resource allocation setting applies. Non-trivial optimal strategies have been observed, see, e.g., Figure 1.7 where the optimal matrix is represented by its stencil.

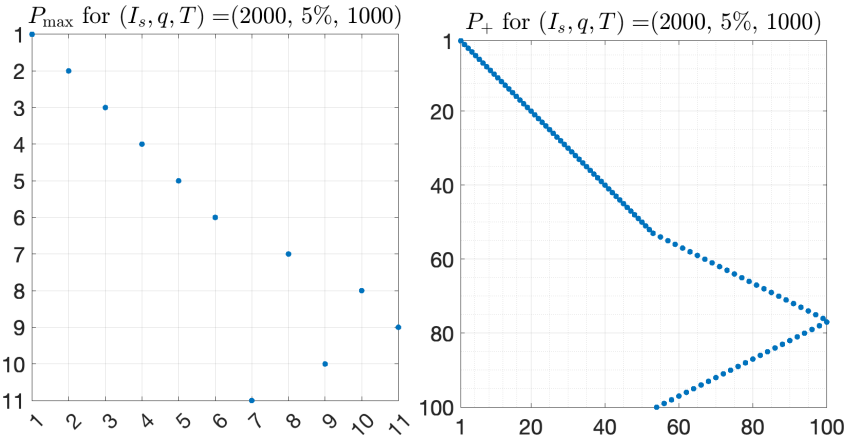

Figure 1.7: Optimal matrix $P_{\max}$ for $N = 11$ obtained with functional $J(P)$ (Left) and P_+ for $N = 100$ obtained with functional $J^{\text{approx}}(P)$ (Right). The blue points represent non-zero entries, i.e., entries equal to 1.

As for the quality of the sub-problem and the criterion, one can see in Figure 1.8 that for large values of time duration T, the optimum approximation almost always coincides with the true optimum (purple stars). Nevertheless, we observe that the criterion (1.27) becomes less

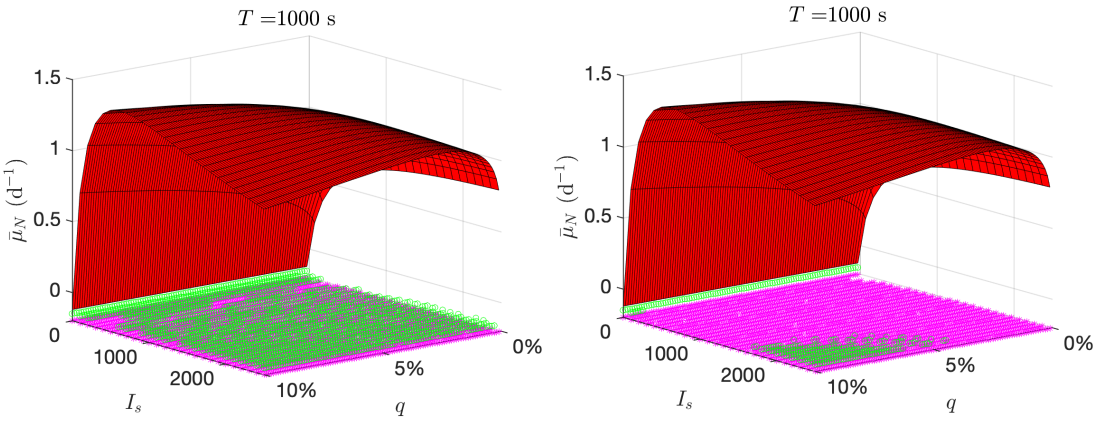

Figure 1.8: Average net specific growth rate $\bar{\mu}_N$ for $T = 1000\,\text{s}$. Left: $N = 5$. Right: $N = 9$. The red surface is obtained with $P_{\max}$ and the blue surface is obtained with P_+. The purple stars represent the cases where $P_{\max} = P_+$ or, in case of multiple solution, $\bar{\mu}_N(P_{\max}) = \bar{\mu}_N(P_+)$. The green circles represent the cases where the criterion (1.27) is satisfied.

efficient for larger N in the sense that it is not satisfied even in the cases where two solutions coincide (green circles).

1.5.3 Optimal topography for algal production

Studies on the shape of the topography (or the bathymetry) have always been a challenging problem, since this problem usually involves the free-surface incompressible Navier-Stokes system.

In particular, explicit computation some time may be difficult to provide due to the complexity of the chosen model. On the other hand, large computational resources are often needed to provide numerical simulations and experimental results. The goal of Chapter 4 is to investigate the influence of the topography of the raceway system. More precisely, we base on a common belief that some specific topographies can bring more light to the algae (at the lower part of the raceway), since they are closer to the surface when reaching the peak of these topographies. In this way, this chapter aims at answering the following question: *Do non-flat topographies enable to increase the light perceived at the lower part of the raceway?*

The first challenge to consider is to answer this question coming from the modeling aspect of this complex system. Indeed, this algal raceway system contains both a macroscopic aspect - the hydrodynamical behaviour of the fluid transporting the algae culture and a microscopic aspect - the photosynthesis within the chlorophyll cells. Therefore, finding a model which takes into account these two aspects is challenging. To overcome it, we limit ourselves to the 1D case and consider the Saint-Venant model (1.10)- (1.11) to describe the hydrodynamical behaviour and the Han model (1.1) to describe the photosynthetic process. The crucial element to couple these two models is the light intensity perceived by the algae culture which is described by the Beer-Lambert law (1.16). More precisely, we use the Saint-Venant model to compute the Lagrangian trajectories of the algae cells, which enables us to determine their depth. The trajectory is then used in the Beer-Lambert law to estimate the perceived light intensities . Finally, the Han model relates the light to the algal growth dynamics[2]. Facing at this coupled model, the second challenge rises up as: *How to optimize concretely the topography?*

In a first study [12], we consider one lap of the algal movement in the raceway pond and use the Lagrangian trajectory as an optimization constraint. For the sake of simplicity, we illustrate here the optimization problem with a single algal culture:

$$\begin{aligned}\max_{a\in\mathbb{R}^N} \frac{1}{T}\int_0^T & -\gamma(I(x,z;a))C+\zeta(I(x,z;a))\mathrm{d}t,\\ \dot{C} &= -\alpha(I(x,z;a))C+\beta(I(x,z;a)),\\ \dot{x} &= u(x;a),\\ \dot{z} &= w(x,z;a).\end{aligned}$$

where w stands for the vertical velocity of the algae cell and a is a parameter that encodes the topography and is supposed to be optimized. The general form of this problem can be found in Chapter 4. We then apply the adjoint-based method described in Section 1.4 to solve this optimization problem. Figure 1.9 represents the optimal topography obtained using a truncated Fourier series parameterization. The reason using this parameterization is presented in Subsection 4.4.2. The optimization procedure starts with a flat topography and ends up with a non-trivial topography as shown in this figure.

In a further step, a second analysis is given in [13] where we reduce the optimization constraints to a single constraint related to C by using the special form of the Lagrangian trajectory in the Saint-Venant description. The optimization problem for a single algal culture in this case

[2]Note that one can also use this approach for more complicated hydrodynamical model as soon as the Lagrangian trajectory can be computed.

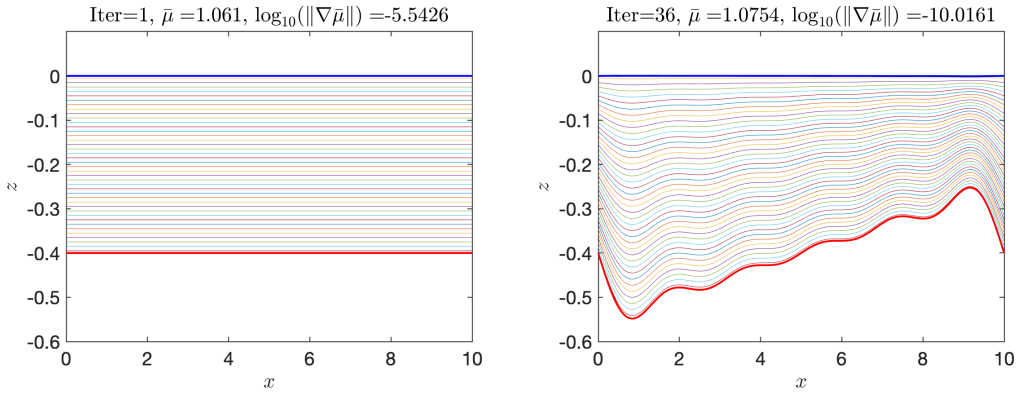

Figure 1.9: The initialization (Left) and the final iteration (Right) of the optimization procedure for truncated Fourier number $N = 5$. The red thick curve represents the topography (z_b), the blue thick curve represents the free surface (η), and all the other curves between represent the trajectories for different layers.

reads:

$$\max_{a\in\mathbb{R}^N} \frac{1}{V}\int_0^L -\gamma(I(x,z;a))C + \zeta(I(x,z;a))h(x;a)\mathrm{d}x,$$
$$C' = \frac{-\alpha(I(x,z;a))C + \beta(I(x,z;a))}{Q_0}h(x;a).$$

This simplification consists in providing a time free formulation of the Lagrangian trajectories of the algal cells. It reduces the computational cost of the reconstruction of the hydrodynamical behaviour of the fluid since high order numerical schemes are often required to compute the Lagrangian trajectory as a function of time.

Another improvement with respect to the results presented in [12] is related to the periodic behaviour of the biological state C which is a desirable property for industrial production. In this case, one can prove directly that the flat topography is a critical point for the previous optimization problem as stated in the following theorem.

Theorem 1.5.6. *Assume the volume of the system is fixed, then flat topography cancels the gradient of the net average growth rate* (4.25) *(defined in Chapter 4).*

Note that this result is true only in the case where C is periodic. The numerical experiments show that flat topography is actually optimal as shown in Figure 1.10 where we use a random initial topography to proceed the optimization procedure.

In the last part of this work, we consider the case where depth can vary, so that the volume is also optimized. In this case, the biomass concentration X can no longer be considered as a constant. Therefore we apply the optimal condition found in Chapter 2 to established a relation between the biomass concentration X with the volume of the system V. In this framework, maximizing areal productivity is a relevant target. Productivity per unit of surface for a given biomass concentration X is given by:

$$\Pi := \bar{\mu}X\frac{V}{S},$$

Unlike the previous theorem, the flat topography does not cancel the gradient $\nabla\Pi$.

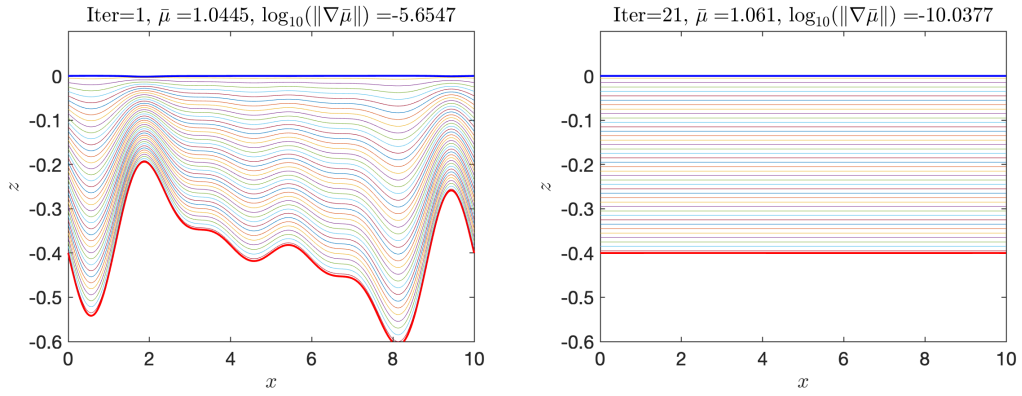

Figure 1.10: The initialization (Left) and the final iteration (Right) of the optimization procedure for truncated Fourier number $N = 5$ in the case C periodic.

Theorem 1.5.7. *Assume that the net growth rate at the surface satisfies $\mu(I_s) > 0$ and that I_{a_0} solves (4.35). Let $\tilde{a}_f = [a_0, a_f]$ the flat topography with an average depth a_0, then $\nabla\Pi(\tilde{a}_f) \neq 0$.*

This result shows that no optimal solution can be found in this case.

In a third work [14], we are interested in combining the mixing strategies presented in Chapter 3 with the topographies. The goal is to investigate numerically the optimal shape of the topographies when including permutation strategies. The optimization problem in this case reads

$$\max_{P\in\mathcal{P}_N}\max_{a\in\mathbb{R}^N}\frac{1}{V}\sum_{i=1}^{N_z}\int_0^L -\gamma(I(x,z_i;a))C_i^P+\zeta(I(x,z_i;a))h(x;a)\mathrm{d}x,$$

$$C_i^{P\prime}=\frac{-\alpha(I(x,z_i;a))C_i^P+\beta(I(x,z_i;a))}{Q_0}h(x;a).$$

Since $N_z!$ permutation strategies needs to be tested in combination with the optimization of the topography, one can only test with a small number of N_z.

In this case, the periodic result in [12] is no longer valid since an extra permutation matrix is added into the optimization problem. Moreover, we have observed in the variable volume case that the optimization procedure stops because of the violation of the minimal water depth constraint (in practice 5 cm). Indeed, it appears that a small volume (or in other words a small water elevation) is better for increasing the productivity. This result is similar to the one found in Theorem 2.3.3 which shows that the productivity is increasing when considering high level of concentration and small water depth.

Chapter 2

Optimal optical conditions for algal production in photobioreactors

2.1 Introduction

Most of the time, the light attenuation is considered to be described by a Beer-Lambert law where the light extinction rate varies with the process type and algal concentration. Some studies have more accurately represented the way light is attenuated in the process, especially to deal with the very dense multiscattering medium where a photon can be scattered several times before being eventually absorbed [101]. The influence of the background turbidity and the reactor depth on the average growth rate of the algae have also been considered in [93]. On the other hand, a range of biological models with different complexities describe various aspects of the growth of microalgae considering different mechanisms. For instance, authors in [94] have used the Droop model [41, 42] combining with the growth rate description in [18] to give an optimal condition to maximize the surface biomass productivity. This condition consists in cancelling the net growth rate at bottom of the reactor and is much more convenient in practice to find the relation between the biomass concentration and the reactor depth, for instance authors in [13] have used this condition to study the algal growth in a raceway pond with a varying volume. Optimization of the microalgal productivity has also been studied intensively in the last decade [55, 15, 38, 34, 33].

On top of light extinction and water depth which have been already deeply studied, in this chapter, we focus on understanding how the productivity in photobioreactors is also influenced by the background turbidity of the reactors. Our first contribution was to extend the work in [94] by choosing a more realistic description of the algal growth dealing with photoinhibition. Our second contribution consisted in considering a general biomass dependent light extinction function accounting for the background turbidity of the system. The concept of optical depth productivity is introduced and a condition is derived on the optical depth for globally maximizing productivity. This optimum corresponds to the *compensation condition*, where the respiration compensates exactly the algal growth rate at the bottom of the reactors. We then use this optimal condition to characterize the optimization of the surface biomass productivity depending on the minimum achievable water depth. When the light extinction rate is affine with respect to the algal biomass, an upper limit to the productivity (obtained for an infinitely small depth) is given. A nonlinear controller is given and is proved to stabilize the evolution of the biomass towards the optimal desired value. The optimal behaviours are illustrated in different cases by numerical

experiments.

This chapter is organised as follows. In Section 2.2, we define the key concepts such as average growth rate and light distribution. We then study the optimization problem in Section 2.3. More precisely we investigate the global behaviour of the optical depth productivity and the optimal condition in Subsection 2.3.1. The optimal biomass concentration for a given reactor depth to maximize the surface biomass productivity is investigated in Subsection 2.3.2. A nonlinear controller is then introduced in Section 2.4 to stabilize the biomass concentration towards its optimal value. We illustrate and discuss the behaviour of the optima in different cases by some numerical experiments in Section 2.5.

2.2 Description of the model

For a given light intensity I, the growth rate of microalgae is defined by a Haldane-type description like one presented in Definition 1.2.1, which is recalled here:

$$\mu(I) := \mu_{\max} \frac{I}{I + \frac{\mu_{\max}}{\theta}(\frac{I}{I^*} - 1)^2}, \tag{2.1}$$

where θ is the initial slope of μ, $\mu_{\max}$ denotes the maximum value of μ and I^* represents the optimal light intensity. This description results from a mechanical consideration of the light harvesting dynamics represented by the Han system [59] (see Subsection 1.2.1 for more details). The light attenuation is described by a Beer-Lambert law

$$I(X, z) := I_s \exp\Big(\varepsilon(X) z\Big), \tag{2.2}$$

where X represents the biomass concentration, $z \in [-h, 0]$ denotes the vertical position of the algae cells with h the depth and I_s is the light intensity at the reactor surface. The light extinction ε, which summarises the light absorption and diffusion, is considered to be correlated to the biomass concentration X

$$\varepsilon(X) := \alpha_0(s) X^s + \alpha_1, \tag{2.3}$$

where $0 < s \leq 1$, $\alpha_0(s) > 0$ stands for the specific light extinction coefficient of the microalgae species. It depends on the parameter s. The background turbidity α_1 is due to all non-microalgae components i.e. suspended solids and dissolved colored material. The dependence of s in α_0 will be omitted hereafter when no confusion may occur.

From (2.2) one can compute the mean light intensity received by the algae culture

$$\bar{I} = I_s \int_{-h}^{0} e^{\varepsilon(X) z} \mathrm{d}z = \frac{I_s}{\varepsilon(X)} \Big(1 - e^{-\varepsilon(X) h}\Big).$$

This quantity is a decreasing function of $\varepsilon(X)$, which confirms the intuition that a higher biomass concentration or a higher background turbidity leads to lower mean light received in the reactor, due to stronger light attenuation effect.

Replacing I by (2.2) in (2.1), one can see that the growth rate varies with depth of the reactor. Lower growth rate in the upper part of the reactor results from the photo-inhibition caused by high light density. Similarly, the growth rate is weak in the lower part of the reactor because of

low light intensity. The mean growth rate in the reactor is defined by

$$\bar{\mu} := \frac{1}{h}\int_{-h}^{0} \mu(I(X,z))\mathrm{d}z. \tag{2.4}$$

Applying then a change of the variable $y = \varepsilon(X)z$, it can be written as

$$\bar{\mu} := \frac{1}{\varepsilon(X)h}\int_{0}^{\varepsilon(X)h} \mu(I(-y))\mathrm{d}y, \tag{2.5}$$

so that the mean growth rate depends on the *optical depth* $\varepsilon(X)h$. This quantity is denoted by Y [-] hereafter. In this case, the average growth rate (2.5) can also be written as a function of Y (i.e. $\bar{\mu}(X,h) = \bar{\mu}(Y)$). Our aim is to optimize the surface biomass productivity (units: $\mathrm{g}\cdot\mathrm{m}^{-2}\cdot\mathrm{d}^{-1}$) which is defined by

$$\Pi := (\bar{\mu} - R)Xh. \tag{2.6}$$

Remark

The evolution of the biomass concentration X is given by

$$\dot{X} = (\bar{\mu} - R - D)X, \tag{2.7}$$

where R is the respiration rate and D denotes the reactor dilution rate. At equilibrium, the biomass surface productivity Π is the product between dilution rate ($D = \bar{\mu} - R$) and surface biomass Xh.
Note that a nonlinear controller for D is introduced in section 2.4 to stabilize (2.7) to the value of X optimizing productivity.

2.3 Analysis of the optimal productivity

In this section, we investigate the optimization problem associated with the productivity Π. Note that the biomass concentration X and the depth h are both defined in $\mathbb{R}_+$.

2.3.1 Global optimality condition

First of all, let us define the optical depth productivity[1] (units: d^{-1}) by

$$P := (\bar{\mu} - R)Y. \tag{2.8}$$

[1] also called "optical productivity"

Remark

According to the definition of the optical depth productivity (2.8), a thin reactor with high biomass concentration is equivalent to a deep reactor with low biomass concentration as long as they both share the same optical depth Y. A low value of Y means a weaker photon harvesting since less light is absorbed. On the reverse, a too high Y means that light hardly reaches the bottom of the reactor, with an area where respiration (loss of CO_2) exceeds growth (fixation of CO_2). Hence, it is necessary to determine the optimal Y value maximizing the efficiency of the productivity P.

Theorem 2.3.1. *Given a surface light intensity I_s, there exists an optimum Y_{opt} which maximizes the optical productivity P. This value satisfies $\mu\left(I(Y_{opt})\right) = R$ and can be computed explicitly according to the growth rate at the surface $\mu(I_s)$:*

$$Y_{opt} = \begin{cases} \ln\left(\dfrac{\frac{2I_s R\mu_{\max}}{\theta I^{*2}}}{\mu_{\max}-R+\frac{2R\mu_{\max}}{\theta I^*}-\sqrt{(\mu_{\max}-R)(\mu_{\max}-R+\frac{4R\mu_{\max}}{\theta I^*})}}\right), & \mu(I_s) > R, \\ \ln\left(\dfrac{\frac{2I_s R\mu_{\max}}{\theta I^{*2}}}{\mu_{\max}-R+\frac{2R\mu_{\max}}{\theta I^*}+\sqrt{(\mu_{\max}-R)(\mu_{\max}-R+\frac{4R\mu_{\max}}{\theta I^*})}}\right), & \mu(I_s) \leq R. \end{cases} \tag{2.9}$$

Proof. For a given Y, the optical productivity P can be written from (2.5) and (2.8)

$$\begin{aligned} P(Y) =& \int_0^{Y_{\text{opt}}} \mu(I(-y)) - R\mathrm{d}y + \int_{Y_{\text{opt}}}^{Y} \mu(I(-y)) - R\mathrm{d}y \\ =& P(Y_{\text{opt}}) + \int_{Y_{\text{opt}}}^{Y} \mu(I(-y)) - R\mathrm{d}y, \end{aligned} \tag{2.10}$$

where Y_{opt} is chosen according to (2.9). On the other hand, for the function

$$\mu(I(-y)) = \frac{\mu_{\max} I(-y)}{I(-y) + \frac{\mu_{\max}}{\theta}(\frac{I(-y)}{I^*} - 1)^2},$$

there exists a $y^* > 0$ with $\mu(I(-y^*)) = \mu_{\max}$ such that $\mu(I(-y))$ is increasing from 0 to y^* and decreasing from y^* to 0. According to the value of $\mu(I(0))$ (i.e. $\mu(I_s)$), two cases must be considered:

- if $\mu(I(0)) = \mu(I_s) > R$, the second term of (2.10) is always negative. Indeed, in the case where Y is smaller than Y_{opt}, using the concavity of $\mu(I(-y))$, one finds $\mu\left(I(-y)\right) > R$, $\forall y < Y_{\text{opt}}$. In other words, the second term of (2.10) removes the microalgae which grow more than they respire. Otherwise, Y is greater than Y_{opt}, one finds $\mu\left(I(-y)\right) < R$, $\forall y > Y_{\text{opt}}$ (for the same reason as above). This means that the second term of (2.10) adds the microalgae which respire more than their growth.

- if $\mu(I(0)) = \mu(I_s) \leq R$, then there exists a $\tilde{y} \in [0, y^*)$ such that $\mu(I(-\tilde{y})) = R$. Then if Y is greater than $\tilde{y}$, the second term of (2.10) is negative for the same reason as above. Otherwise, the productivity $P(Y)$ is negative.

In both cases, the second term of (2.10) is negative. Thus Y_{opt} maximizes the quantity P.

In order to compute Y_{opt}, one needs to solve $\mu(I) = R$, or equivalently:

$$\frac{R\mu_{\max}}{\theta {I^*}^2} I^2 + (R - \mu_{\max} - \frac{2R\mu_{\max}}{\theta I^*})I + \frac{R\mu_{\max}}{\theta} = 0.$$

The discriminant of this second order polynomial equation is given by $\Delta = (\mu_{\max} - R)(\mu_{\max} - R + \frac{4R\mu_{\max}}{\theta I^*}) > 0$, which implies that there exists two real roots. The sum and the product of two roots are both positive, hence both of these two roots are also positive. Finally Y_{opt} can be determined by the growth rate at the surface $\mu(I_s)$:

- if $\mu(I_s) > R$, then there exists one root in the interval $(0, I_s)$ and one root in the interval $(I_s, +\infty)$. In this case, one has

$$Y_{\text{opt}} = \ln\left(\frac{\frac{2I_s R\mu_{\max}}{\theta {I^*}^2}}{\mu_{\max} - R + \frac{2R\mu_{\max}}{\theta I^*} - \sqrt{(\mu_{\max} - R)(\mu_{\max} - R + \frac{4R\mu_{\max}}{\theta I^*})}}\right).$$

- if $\mu(I_s) \leq R$, then two roots both lie into the interval $(0, I_s]$. In this case, we choose the smaller one (since it represents the light at lower part of the reactors)

$$Y_{\text{opt}} = \ln\left(\frac{\frac{2I_s R\mu_{\max}}{\theta {I^*}^2}}{\mu_{\max} - R + \frac{2R\mu_{\max}}{\theta I^*} + \sqrt{(\mu_{\max} - R)(\mu_{\max} - R + \frac{4R\mu_{\max}}{\theta I^*})}}\right).$$

This concludes the proof. □

Remark

As shown in (2.9), the value of Y_{opt} only depends on the model parameters (θ, $\mu_{\max}$, I^*, R) and on the light intensity at the reactor surface I_s. In other words, the cancellation of the net growth rate at the bottom of the reactor is the optimal strategy to maximize optical depth productivity (see in Figure 2.2 for illustrations).

2.3.2 Surface biomass productivity

In this section, we focus on the surface biomass productivity Π. From the definition of Π (2.6) and the definition of P (2.8), one has

$$\Pi = \frac{X}{\varepsilon(X)} P. \tag{2.11}$$

In general, it is not possible to apply the same strategy (as in the proof of Theorem 2.3.1) to optimize Π, since P and Π do generally not have the same behaviour. Only in the case where $s = 1$ and $\alpha_1 = 0$, the factor $\frac{X}{\varepsilon(X)}$ simplifies, leading to the same optimum. Using then Theorem 2.3.1, we deduce directly the following results.

Corollary 2.3.1. *If the light extinction function defined by* (2.3) *satisfies* $\alpha_1 = 0$ *and* $s = 1$*, then* Y_{opt} *defined by* (2.9) *maximizes the productivity* Π *and* Y_{opt} *is the global optimum. Moreover,* $\tilde{Y}_{opt} := Y_{opt}/\alpha_0$ *is the optimal surface biomass.*

Proof. Since $\alpha_1 = 0$ and $s = 1$, $Y = \varepsilon(X)h = \alpha_0\tilde{Y}$ with $\tilde{Y} := Xh$ the surface biomass. Meanwhile, using (2.11), one has $P(\cdot) = \alpha_0\Pi(\cdot)$, then following the same analysis, one finds that Y_{opt} maximizes $P(\cdot)$, therefore the productivity $\Pi(\cdot)$. Finally, $\tilde{Y}_{\text{opt}}$ is given by Y_{opt}/α_0. □

Corollary 2.3.2. *If the objective is to reach a biomass concentration X_1, there exists a unique reactor depth h_1 which satisfies $\varepsilon(X_1)h_1 = Y_{opt}$ and maximizes the productivity $\Pi(X_1, \cdot)$ for this target biomass.*

Proof. Since X_1 is fixed, then using (2.11), one has directly that the optimum is given by Y_{opt}. In this case, h_1 is defined by $Y_{\text{opt}}/\varepsilon(X_1)$. □

In Corollary 2.3.2, we have studied the case with a fixed biomass concentration X. This result does not depend on the considered law $\varepsilon(X)$. However, optimizing X is more tricky, Corollary 2.3.1 provides a result in the case with a specific value of α_1 and s. In more general case, the strategy used in the proof of Theorem 2.3.1 may fail when optimizing X. In this way, we focus on the case where the background turbidity α_1 is not zero in this section. According to the value of s, we separate the study into two parts.

The standard case $s = 1$

Let h_1 a given depth and (X_1, h_1) which satisfies $Y_{\text{opt}} = \varepsilon(X_1)h_1$. For a biomass concentration $X > X_1$, one has $Y = \varepsilon(X)h_1 > Y_{\text{opt}}$. Applying then Theorem 2.3.1, one finds $P(Y) < P(Y_{\text{opt}})$. On the other hand, one has $\frac{X}{\varepsilon(X)} > \frac{X_1}{\varepsilon(X_1)}$ using the definition (2.3) for $s = 1$. According to (2.11), it is not clear to see if $\Pi(X_1, h_1)$ is larger than $\Pi(X, h_1)$. Indeed, by using the explicit formulation given in Appendix 2.A, one can show that there always exists $X > X_1$ such that $\Pi(X, h_1) > \Pi(X_1, h_1)$ in the case $s = 1$.

According to Corollary 2.3.2, the couple (X_1, h_1) satisfies $\varepsilon(X_1)h_1 = Y_{\text{opt}}$ and corresponds to the optimum of $\Pi(X_1, \cdot)$ for a given X_1. However, this is not the optimal condition to optimize $\Pi(\cdot, h_1)$ for a given h_1. We deduce then the next theorem.

Theorem 2.3.2. *If $\alpha_1 > 0$, there is no global optimum for the productivity $\Pi(\cdot, \cdot)$ in $\mathbb{R}_+ \times \mathbb{R}_+$.*

Proof. Let us assume that there exists a global optimum for the productivity Π denoted by (X^*, h^*). Since (X^*, h^*) is a global optimum, in particular, this is an optimum in the direction of h. Using Corollary 2.3.2, we find $\varepsilon(X^*)h^* = Y_{\text{opt}}$. However, there exists $\tilde{X}^* > X^*$ such that $\Pi(\tilde{X}^*, h^*) > \Pi(X^*, h^*)$. This contradicts the fact that (X^*, h^*) is a global optimum. Therefore, the productivity $\Pi(\cdot, \cdot)$ has no global optimum. □

Since no global optimum for the productivity Π can be found when $\alpha_1 > 0$, then we would like to study the asymptotic behaviour of Π. In the following, we focus on the optimum in the direction of X and in the direction of h separately. Given X_0 and consider the sequence $(X_n, h_n)_{n\in\mathbb{N}}$ defined by

$$h_n = \frac{Y_{\text{opt}}}{\varepsilon(X_{n-1})}, \quad X_n := \text{argmax}_{X\in\mathbb{R}_+}\Pi(X, h_n). \tag{2.12}$$

From the definition above, the sequence $(X_{n-1}, h_n)_{n>0}$ corresponds to the optimum in the direction of h for X_{n-1}, whereas the sequence $(X_n, h_n)_{n>0}$ corresponds to the optimum in the direction of X for h_n. In plain words, these two sequences defined by (2.12) aims at searching the local optima by optimizing in the direction of h and in the direction of X alternately. Let us provide some more information about the sequence $(X_n, h_n)_{n>0}$.

Lemma 2.3.1. *The sequence* (X_n, h_n) *verifies* $\lim_{n\to\infty} \varepsilon(X_n)h_n = Y_{opt}$*, and the growth rate at the reactor bottom satisfies* $\lim_{n\to\infty} \mu(I(X_n, h_n)) = R$*.*

Proof. From the definition of the sequence $(X_{n-1}, h_n)_{n>0}$, one has $\varepsilon(X_{n-1})h_n = Y_{\text{opt}}$, which means

$$\lim_{n\to\infty} \varepsilon(X_n)h_n = Y_{\text{opt}} \lim_{n\to\infty} \frac{\varepsilon(X_{n-1})}{\varepsilon(X_n)} = Y_{\text{opt}}.$$

Denoting by $Y_n = \varepsilon(X_n)h_n$, since $\mu \circ I(-y)$ is a continuous function with respect to y in $\mathbb{R}_+$, one has

$$\lim_{n\to\infty} \mu(I(X_n, h_n)) = \lim_{n\to\infty} \mu(I(Y_n)) = \mu(I(Y_{\text{opt}})) = R.$$

This concludes the proof. □

This lemma enables us to prove the next theorem, without constraint on the minimal reactor depth.

Theorem 2.3.3. $\lim_{n\to\infty} X_n = \infty$*,* $\lim_{n\to\infty} h_n = 0$ *and* $\lim_{n\to\infty} \Pi(X_n, h_n) = \frac{P(Y_{opt})}{\alpha_0}$*.*

Proof. Since $(X_n)_{n\in\mathbb{N}}$ is a strictly increasing sequence, the sequence $(h_n)_{n\in\mathbb{N}^*}$ is strictly decreasing by its construction (2.12). Since for each $n \in \mathbb{N}^*$, $h_n > 0$, then this sequence converges to a limit that we denote by h_{lim}. Assume that $h_{\text{lim}} > 0$, then from (2.12), one has

$$h_{\text{lim}} = \lim_{n\to\infty} h_n = \lim_{n\to\infty} \frac{Y_{\text{opt}}}{\varepsilon(X_{n-1})} = Y_{\text{opt}} \lim_{n\to\infty} \frac{1}{\alpha_0 X_{n-1} + \alpha_1},$$

which means that $\lim_{n\to\infty} X_n =: X_{\text{lim}} < \infty$. Then $(X_{\text{lim}}, h_{\text{lim}})$ is a global optimum, hence a contradiction with Theorem 2.3.2. Therefore $h_{\text{lim}} = 0$, which means that $X_{\text{lim}} = \infty$.

On the other hand, by the construction of these two sequences $(X_{n-1}, h_n)_{n>0}$, $(X_n, h_n)_{n>0}$, one has

$$\Pi(X_{n-1}, h_n) < \Pi(X_n, h_n) < \Pi(X_n, h_{n+1}).$$

Using (2.11), one has $\Pi(X_{n-1}, h_n) = \frac{X_{n-1}}{\varepsilon(X_{n-1})} P(Y_{\text{opt}})$ and $\Pi(X_n, h_{n+1}) = \frac{X_n}{\varepsilon(X_n)} P(Y_{\text{opt}})$. Taking the limit similarly as in the above inequalities gives $\lim_{n\to\infty} \Pi(X_n, h_n) = \frac{P(Y_{\text{opt}})}{\alpha_0}$. This concludes the proof. □

Case $s < 1$

In the case $s < 1$, one can still use the explicit formula of Π given in Appendix 2.A to show that the couple (X_1, h_1) satisfying $\varepsilon(X_1)h_1 = Y_{\text{opt}}$ is not the optimum in the direction of X for a given h_1. There exists $X > X_1$ such that $\Pi(X, h_1) > \Pi(X_1, h_1)$. Therefore, one can keep the same definition of the sequences (2.12). Lemma 2.3.1 remains true in this case by the definition of the sequence (X_n, h_n). However the last limit in Theorem 2.3.3 will be different as shown in the next theorem.

Theorem 2.3.4. $\lim_{n\to\infty} X_n = \infty$*,* $\lim_{n\to\infty} h_n = 0$ *and* $\lim_{n\to\infty} \Pi(X_n, h_n) = +\infty$*.*

Proof. Following the similar strategy as in Theorem 2.3.3, one can show that $\lim_{n\to\infty} X_n = \infty$, $\lim_{n\to\infty} h_n = 0$.

On the other hand, by the construction of the two sequences $(X_{n-1}, h_n)_{n>0}$, $(X_n, h_n)_{n>0}$, one has

$$\Pi(X_{n-1}, h_n) < \Pi(X_n, h_n) < \Pi(X_n, h_{n+1}).$$

Using (2.11) and passing to the limit, one finds

$$\lim_{n\to\infty} \Pi(X_{n-1}, h_n) = \lim_{n\to\infty} \frac{X_{n-1}}{\varepsilon(X_{n-1})} P(Y_{\text{opt}}) = \frac{P(Y_{\text{opt}})}{\alpha_0} \lim_{n\to\infty} X_{n-1}^{1-s} = +\infty,$$
$$\lim_{n\to\infty} \Pi(X_n, h_{n+1}) = \lim_{n\to\infty} \frac{X_n}{\varepsilon(X_n)} P(Y_{\text{opt}}) = \frac{P(Y_{\text{opt}})}{\alpha_0} \lim_{n\to\infty} X_n^{1-s} = +\infty.$$

Therefore, $\lim_{n\to\infty} \Pi(X_n, h_n) = +\infty$. □

Note that for real reactors, there is a constraint on the minimal reactor depth h_{lim} (below which mixing is no more possible). An optimal solution can then be found in this case. Indeed, as shown in Theorem 2.3.4 (or Theorem 2.3.3), a higher productivity can be obtained for higher biomass concentration and smaller reactor depth. Considering the minimal reactor depth, one can find the optimal biomass concentration maximizing the productivity.

2.4 Optimal control implementation in closed loop

As shown in previous section, there exists optimal biomass concentration for a given reactor depth h. In this section, let us show that the evolution of the biomass concentration X (defined in (2.7)) can be stabilized to a desired biomass concentration by applying an appropriate controller. More precisely, we consider the dilution rate D in (2.7) as a controller. Let us denote by $X^\star \in (0, X(0))$ the desired biomass concentration.

Assumption 2.4.1 (H1)**.** *We assume that:*

a. the quantity $\Phi := (\bar{\mu}(X, h) - R)X$ is measured on-line from the plant,

b. the growth rate for the influent light intensity is larger than the respiration (i.e. $\mu(I_s) > R$),

c. the maximal dilution rate $D_{\max}$ is larger than the maximal growth rate $\mu_{\max}$.

The quantity Φ denotes the average oxygen production which is available from the reactor. Indeed, oxygen sensors or numerical estimators can be applied to obtain the quantity Φ. In the sequel, we assume that (H1) holds. Then we have the following result.

Proposition 2.4.1. *The control law*

$$D = \begin{cases} D_{\max} & X \geq \bar{X} \\ (\bar{\mu}(X, h) - R)\frac{X}{X^\star} & X < \bar{X} \end{cases} \tag{2.13}$$

globally stabilizes equation (2.7) *towards the positive point $X^\star$.*

Remark

$\bar{X} > X^\star$ is chosen to determine the area where the control will be at its maximum rate. It is defined so that $(\mu_{\max} - R)\frac{\bar{X}}{X^\star} < D_{max}$.

Proof. From the definition of (2.13), the control variable D is positive. On the other hand, $\bar{\mu}(0, h) > R$, $\lim_{X\to\infty} \bar{\mu}(X, h) = 0$ and $\bar{\mu}(\cdot, h)$ is continuously decreasing with respect to X. If the initial state $X(0) \geq \bar{X}$, then replacing $D = D_{\max}$ into (2.7) gives

$$\dot{X} = (\bar{\mu}(X, h) - R - D_{\max})X.$$

In particular, $\bar{\mu}(X(0),h) - R - D_{\max} < 0$, hence there exists a time $t_1 > 0$ such that the state X decreases from 0 to t_1 and $X(t_1) = \bar{X}$. When $t > t_1$, $D = \frac{\Phi}{X^\star}$. Replacing $D = \frac{\Phi}{X^\star}$ into (2.7) gives

$$\dot{X} = (\bar{\mu}(X,h) - R)\frac{X}{X^\star}(X^\star - X) = \frac{\Phi}{X^\star}(X^\star - X). \tag{2.14}$$

Note that the system is now in the positive invariant region $X < \bar{X}$ and cannot come back again to $X \geq \bar{X}$. Moreover, $0 < \bar{\mu}(X,h) - R < \mu_{\max} - R$. Then, integrating (2.14) gives $\forall t \geq t_1, \quad 0 < X^\star \leq X(t) \leq X(0)$.

In the case the initial state $X(0) \in (0, \bar{X})$, the control variable $D = \frac{\Phi}{X^\star}$ and the evolution equation (2.7) once again becomes (2.14), hence we follow the small strategy as above.

Finally we find in both two cases that

$$\forall t \geq 0, \quad 0 < X^\star \leq X(t) \leq X(0).$$

Therefore, the state $X^\star$ is globally exponentially stable for the evolution equation (2.7) by using the control law (2.13). □

2.5 Numerical results

In this section, we will illustrate some optimal conditions to maximize the algal productivity. In this way, we first introduce an algorithm to compute the sequences defined in (2.12). We then give the parameters that we use for the numerical experiments and show some numerical results.

2.5.1 Numerical algorithm

In practise, one can use the next algorithm to compute two sequences $(X_{n-1}, h_n)_{n>0}$ and $(X_n, h_n)_{n>0}$ defined by (2.12).

Algorithm 1 Search Optimum

1: **Input**: Y_{opt}, $n_{\max}$ and X_0.
2: **Output**: $(X_n, h_n)_{n>0}$
3: Set $n := 0$.
4: **while** $n < n_{\max}$ **do**
5: Set $n = n + 1$.
6: Compute $h_n = Y_{\text{opt}}/\varepsilon(X_{n-1})$.
7: Compute X_n such that $\mathrm{d}\Pi_X(X_n, h_n) = 0$.
8: **end while**

2.5.2 Parameter settings

The Han model parameters are taken from [54] and recalled in Table 2.1. Then one can use (1.9) to find $\mu_{\max}, \alpha, I^*$. The considered surface light intensity is set to be $I_s = 2000\,\mu\text{molm}^{-2}\text{s}^{-1}$. For $s = 1$, we take from Table 1.2 the specific light extinction coefficient for the species *Chlorella pyrenoidosa* $\alpha_0 = 0.2\,\text{m}^2 \cdot \text{g}^{-1}$ and the background turbidity $\alpha_1 = 10\,\text{m}^{-1}$. Note that for the case where $s < 1$, we compute the coefficient $\alpha_0(s)$ to find the one providing an extinction coefficient as close as possible to the reference linear case which is generally the one measured:

$$\alpha_0(s) = \text{argmax}_{\text{X}\in[\text{X}_{\min},\text{X}_{\max}]} \left|\alpha_0(1)\text{X} - \alpha_0(\text{s})\text{X}^{\text{s}}\right|. \tag{2.15}$$

Table 2.1: Parameter values for Han Model.

k_r	$6.8\ 10^{-3}$	s^{-1}
k_d	$2.99\ 10^{-4}$	-
τ	0.25	s
σ	0.047	$m^2 \cdot (\mu mol)^{-1}$
k	$8.7\ 10^{-6}$	-
R	$1.389\ 10^{-7}$	s^{-1}

2.5.3 Numerical study

In this section, we provide some numerical tests to illustrate the influence of the water depth h, the biomass concentration X and the light extinction function $\varepsilon(X)$ on algal productivity.

Evaluation of different light extinction coefficient

As mentioned in the previous section, the light extinction coefficient α_0 needs to be better estimated when $s < 1$, in comparison with the reference case $s = 1$. For this reason, let us set biomass concentration X in a range of $[0, 1000]$ $(g \cdot m^{-3})$. We then use (2.15) to find α_0 that provide the same average extinction rate. Figure 2.1 shows $\varepsilon(X)$ for different values of s when the background turbidity $\alpha_1 > 0$.

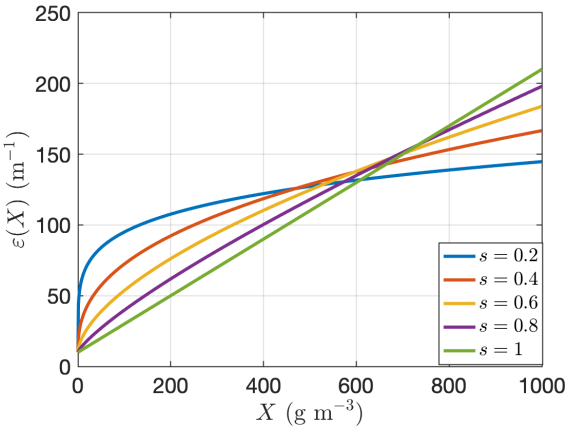

Figure 2.1: $\varepsilon(X)$ with respect to X for $s \in \{0.2, 0.4, 0.6, 0.8, 1\}$.

Global optimum of optical depth

The optimal optical depth (Y_{opt}) can be computed explicitly using (2.9) once the light intensity at the reactor surface I_s and the model parameters (θ, $\mu_{\max}$, I^*, R) are fixed. Figure 2.2 presents the evolution of the growth rate μ and optical depth productivity (P) with respect to y for different value of s and α_1. One can see that the optimum is obtained with $Y_{\text{opt}} = 6.337$, which also satisfies numerically $\mu(I(Y_{\text{opt}})) = R$ in our case. Moreover, as mentioned in Remark 2.3.1, Y_{opt} does not change for other values of α_1 and s.

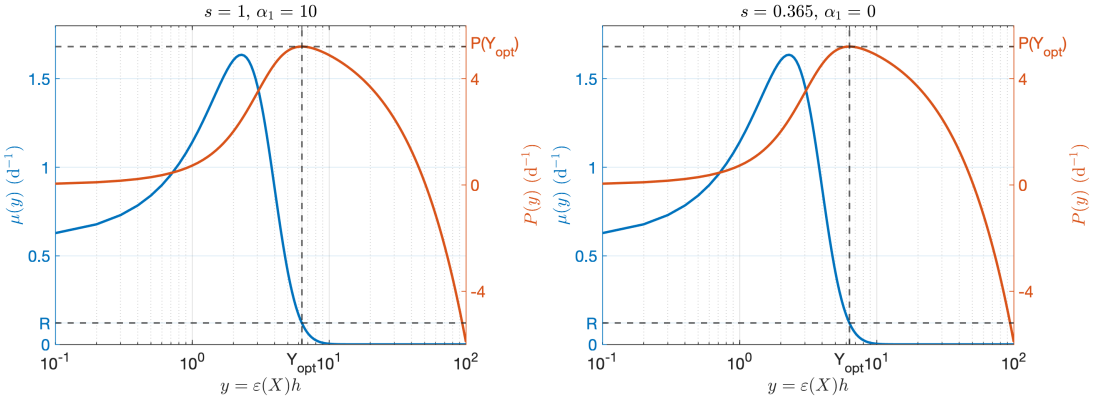

Figure 2.2: Growth rate μ and optical depth productivity P with respect to y. Left: $s = 1$ and $\alpha_1 = 10\,\mathrm{m}^{-1}$. Right: $s = 0.365$ and $\alpha_1 = 0\,\mathrm{m}^{-1}$.

In the same way, for a given biomass concentration X, Corollary 2.3.2 provides a condition to determine the optimal depth to maximize the surface biomass productivity Π. Figure 2.3 illustrates this corollary with a biomass concentration $X = 50\,\mathrm{g}\cdot\mathrm{m}^{-3}$ for different values of s and α_1. Note that the optimal depth h^* satisfies the relation $\varepsilon(X)h^* = Y_{\mathrm{opt}}$. In other words,

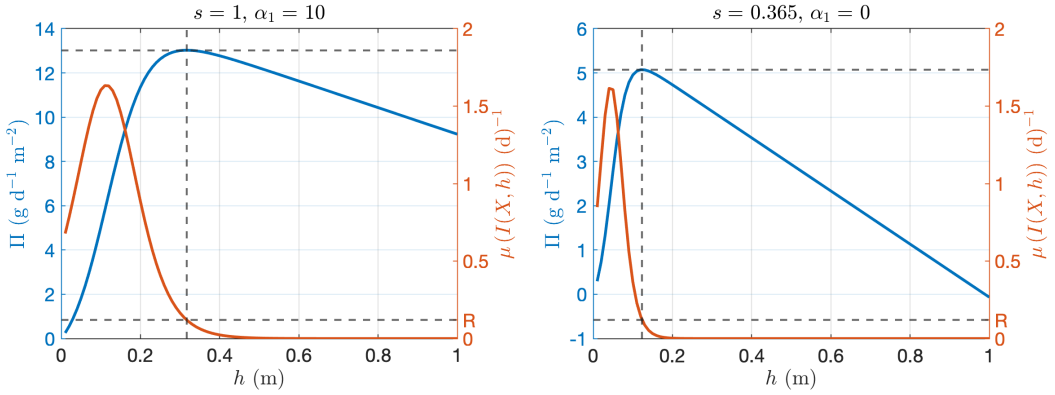

Figure 2.3: Productivity (Π) and net growth rate ($\mu_{\mathrm{net}}(X,h)$) with respect to depth (h) for $X = 50\,\mathrm{g}\cdot\mathrm{m}^{-3}$. Left: $s = 1$ and $\alpha_1 = 10\,\mathrm{m}^{-1}$. Right: $s = 0.365$ and $\alpha_1 = 0\,\mathrm{m}^{-1}$.

one can see that this optimal satisfies $\mu\,(I(X,h^*)) = R$. It is worth remarking that the range of the productivity Π changes for different value of s and α_1, this motivates to better understand how these parameters affect growth.

Influence of the background turbidity and s

Here we study the influence of the background turbidity α_1 and the value of s on the productivity Π. We keep the biomass concentration value $X = 50\,\mathrm{g}\cdot\mathrm{m}^{-3}$ and compute h by using the relation $\varepsilon(X)h = Y_{\mathrm{opt}}$ for different values of α_1 and s. Note that the depth h computed in this way is the optimum to maximize the productivity for the given biomass concentration. Figure 2.4 represents the optimal surface biomass productivity Π with respect to the background turbidity.

As we can expect intuitively, the larger the background turbidity is, the smaller the productivity

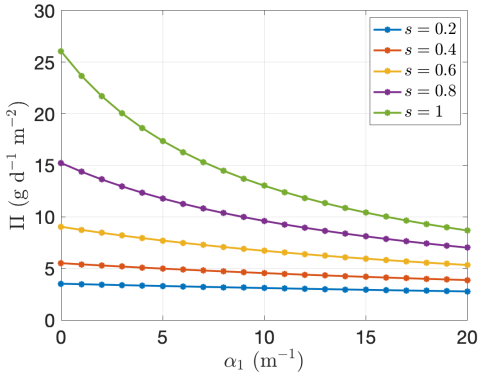

Figure 2.4: Optimal surface biomass productivity with respect to the background turbidity α_1 for $X = 50\,\mathrm{g}\cdot\mathrm{m}^{-3}$ and different value of s.

is. Furthermore, the productivity increases with the value of s for a fixed value of turbidity α_1.

Local optima in the case $s = 1$

In real life applications, the depth h depends on the type reactors, for instance, $h = 0.1\,\mathrm{m} - 0.5\,\mathrm{m}$ for raceway ponds, $h = 1\,\mathrm{cm} - 10\,\mathrm{cm}$ for tubular photobioreactors and $h = 0.1\,\mathrm{m} - 1\,\mathrm{mm}$ for biofilm reactors (where the microalgal biomass is fixed on a support). By knowing the lowest bound admissible for the reactor depth (depending on the process type), we only need to optimize the productivity in the direction of X. Note that the turbidity α_1 may change the optimal condition to maximize the surface biomass productivity Π. Indeed, Figure 2.5 illustrates this for a reactor depth $h = 0.15\,\mathrm{m}$. Note that X_0 satisfies the relation $\varepsilon(X_0)h = Y_{\mathrm{opt}}$ which also means

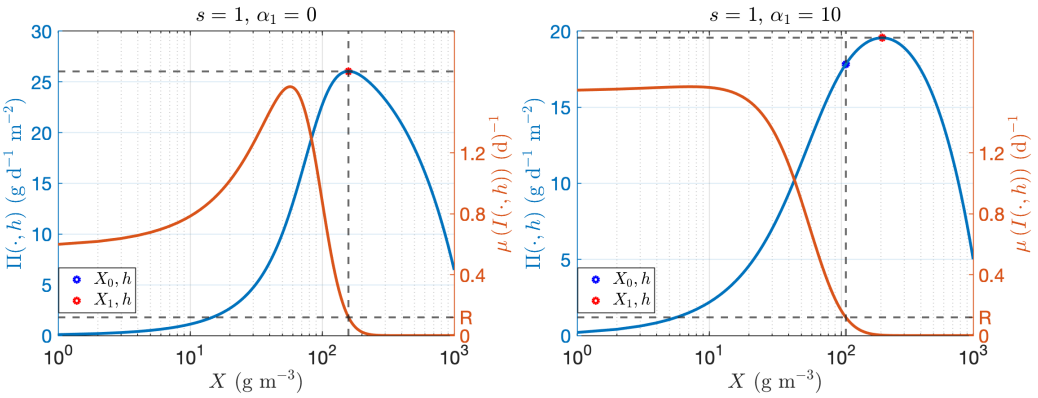

Figure 2.5: Productivity (Π) with respect to biomass concentration (X) for $h = 0.15\,\mathrm{m}$. Left: $\alpha_1 = 0\,\mathrm{m}^{-1}$. Right: $\alpha_1 = 10\,\mathrm{m}^{-1}$.

that the net growth rate at the bottom of the reactor is zero (see the blue point in these two figures). On the other hand, the red point (X_1, h) is the optimum which maximizes the surface biomass productivity Π for this given depth h. One can see that $X_0 = X_1 = 158.427\,\mathrm{g}\cdot\mathrm{m}^{-3}$ in the case the background turbidity is zero in the system (Left), meaning that the optimum

is the point which cancels the net average growth rate at the reactor bottom as mentioned in Corollary 2.3.1. However, as mentioned in Subsection 2.3.2, that by taking account into the background turbidity (Right), these two points are no longer the same and the optimum then satisfies $X_1 = 204.190\,\mathrm{g}\cdot\mathrm{m}^{-3} > X_0 = 108.427\,\mathrm{g}\cdot\mathrm{m}^{-3}$.

The global behaviour of the surface biomass productivity Π is represented on Figure 2.6, for $h \in (0, 1]$ and $X \in (0, 1000]$. To discuss the influence of the background turbidity, we consider two possible values, $\alpha_1 = 0\,\mathrm{m}^{-1}$ and $\alpha_1 = 10\,\mathrm{m}^{-1}$. Note that the blue points in the left figure

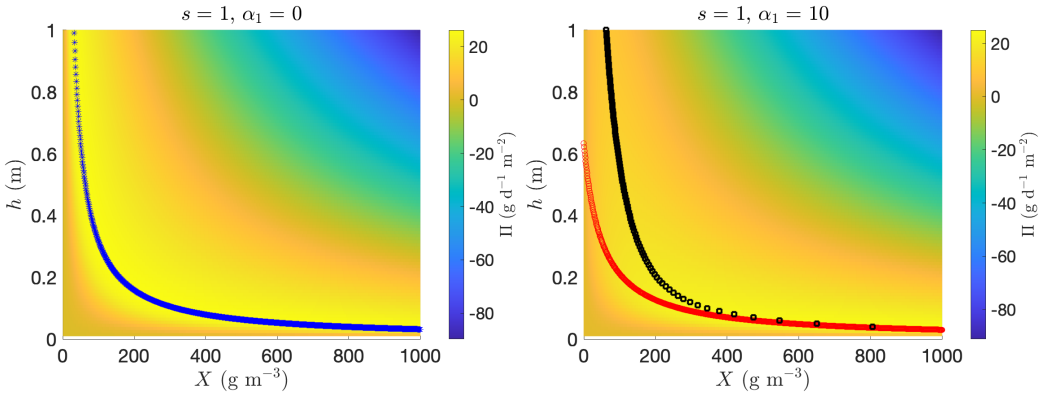

Figure 2.6: Global behaviour of productivity (Π) with respect to depth (h) and biomass concentration (X). Left: $\alpha_1 = 0\,\mathrm{m}^{-1}$. The blue stars represent the optimal couple (X, h) such that Π finds its global maximum. Right: $\alpha_1 = 10\,\mathrm{m}^{-1}$. The red circles represent the suboptimal couple (X, h) where Π finds its maximum in the direction of h for a given X. The black squares represent the suboptimal couple (X, h) where Π finds its maximum in the direction of X for a given h.

(X, h) satisfy the relation $\varepsilon(X)h = Y_{\mathrm{opt}}$ which is also the global optimum. However, by taking account into the background turbidity (see figure on the right), no global optimum exists in this case as mentioned in Theorem 2.3.2. Instead, for a given biomass concentration, the optimal depths can still be found using the relation $\varepsilon(X)h = Y_{\mathrm{opt}}$ (represented by the red circles in the right figure). For a given water depth, the optimal concentrations are obtained by cancelling the derivative of $\Pi(\cdot, h)$ (represented by the black squares in the right figure). Furthermore, one can observe that this two suboptima become closer when X increases and h decreases, meanwhile the productivity also increases in this direction.

Let us set $X_0 = 50\,\mathrm{g}\cdot\mathrm{m}^{-3}$, $\alpha_1 = 10\,\mathrm{m}^{-1}$ and $n_{\max} = 10^4$. Figure 2.7 illustrates the proprieties of these two sequences constructed by Algorithm 1. Starting from the figure on the top, the blue point and the yellow point are the first-two element of the sequence $(X_{n-1}, h_n)_{n>0}$, the red point and the purple point are the first-two element of the sequence $(X_n, h_n)_{n>0}$. Recall that the sequence $(X_{n-1}, h_n)_{n>0}$ always satisfies $\varepsilon(X_{n-1})h_n = Y_{\mathrm{opt}}$ and the net growth rate at the reactor bottom is always 0. We then only study the asymptotic behaviour of the sequence $(X_n, h_n)_{n>0}$. As shown in bottom left figure, the surface biomass $X_n h_n$ converges to $\frac{Y_{\mathrm{opt}}}{\alpha_0}$ and the optical depth $\varepsilon(X_n)h_n$ converges to Y_{opt}, as proved in Lemma 2.3.1. The productivity $\Pi(X_n, h_n)$ converges to $P(Y_{\mathrm{opt}})/\alpha_0$, see bottom right figure as proved in Theorem 2.3.3. Finally, the net growth rate at the reactor bottom converges to zero, which is the global optimum condition in the case where the background turbidity is 0 (see Corollary 2.3.1). In particular, since (X_n, h_n) are the optima in the direction of X for each h_n, one can see that the net growth rate at the reactor bottom for these optima are always negative, meaning that the compensation condition is only satisfied

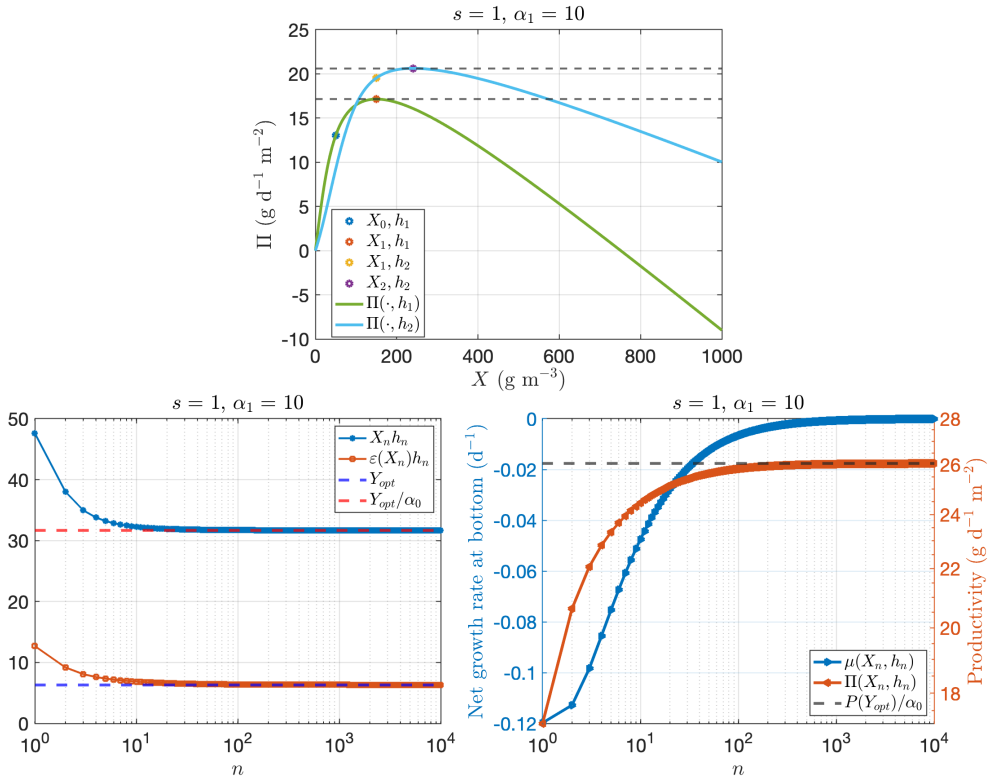

Figure 2.7: Up: First-two elements of these two sequences. Down Left: Surface biomass $(X_n h_n)$ and optical depth $(\varepsilon(X_n)h_n)$ for the sequence $(X_n, h_n)_{n>0}$. Down Right: Productivity $\Pi(X_n, h_n)$ and net growth rate at the reactor bottom $\mu(X_n, h_n) - R$ for the sequence $(X_n, h_n)_{n>0}$.

asymptotically.

Local optima in the case $s < 1$

We start with a similar study as in Figure 2.5 in the case $s < 1$. Recall that the depth of the reactor is given by $h = 0.15\,\mathrm{m}$ and two background turbidity values are given by $\alpha_1 = 0\,\mathrm{m}^{-1}$ and $\alpha_1 = 10\,\mathrm{m}^{-1}$. Figure 2.8 illustrates the results for $s = 0.365$. Recall that the blue point

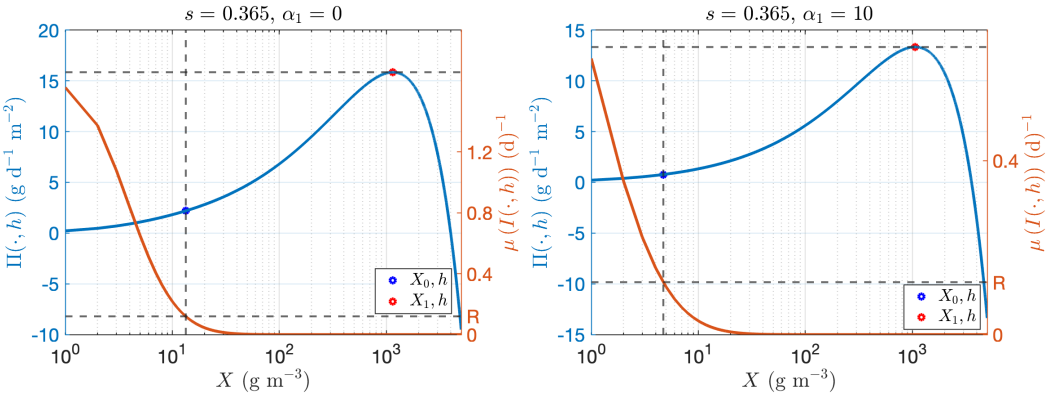

Figure 2.8: Productivity (Π) with respect to biomass concentration (X) for $h = 0.15\,\mathrm{m}$. Left: $\alpha_1 = 0\,\mathrm{m}^{-1}$. Right: $\alpha_1 = 10\,\mathrm{m}^{-1}$.

(X_0, h) satisfies the relation $\varepsilon(X_0)h = Y_{\mathrm{opt}}$ which also means that the net growth rate at the reactor bottom of the reactor is zero, and the red point (X_1, h) represents the optimum which maximizes the productivity for this depth h. In the case $\alpha_1 = 0\,\mathrm{m}^{-1}$, we find $X_0 = 13.327\,\mathrm{g}\cdot\mathrm{m}^{-3}$ and $X_1 = 1149.298\,\mathrm{g}\cdot\mathrm{m}^{-3}$, whereas we obtain $X_0 = 4.715\,\mathrm{g}\cdot\mathrm{m}^{-3}$ and $X_1 = 1064.574\,\mathrm{g}\cdot\mathrm{m}^{-3}$ in the case $\alpha_1 = 10\,\mathrm{m}^{-1}$. These two points do not coincide even when the background turbidity is zero, which is different from the case $s = 1$.

Figure 2.9 shows the global behaviour of surface biomass productivity in the case $s = 0.365$. Unlike for the case $s = 1$ (Figure 2.6), the influence of the background turbidity becomes smaller when $s < 1$. However, similarly to this $s = 1$ case (Right), the productivity becomes larger when the biomass concentration X increases and the water depth h decreases. Furthermore, Figure 2.10 shows the divergence of the productivity Π, as proved in Theorem 2.3.4.

Controller test

We present the efficiency of the controller D designed in Proposition 2.4.1. Let us set $h = 0.1\,\mathrm{m}$, $s = 1$, $X(0) = [2500, 50]\mathrm{g}\,\mathrm{m}^{-3}$, $D_{\max} = 10\mu_{\max}$ and keep other parameter settings. Figure 2.11 illustrates the behaviour of the biomass concentration X under our controller D. Note that the desired biomass concentration $X^\star = \mathrm{argmax}_{X\in\mathbb{R}_+}\Pi(X, h)$. One can see that the evolution of the biomass concentration X in closed loop converges to the desired optimal biomass concentration (after five days).

2.6 Conclusion

The concept of optical productivity P has been defined and a global optimum Y_{opt} has been found to maximize P. This condition corresponds to a situation where the net growth rate at

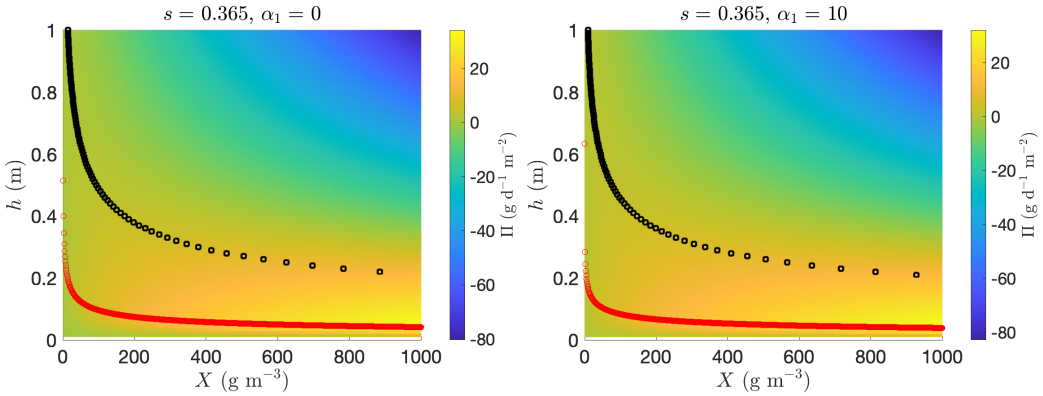

Figure 2.9: Global behaviour of productivity (Π) with respect to depth (h) and biomass concentration (X). Left: $\alpha_1 = 0\,\mathrm{m}^{-1}$. Right: $\alpha_1 = 10\,\mathrm{m}^{-1}$. The red circles represent the suboptimal couple (X, h) where Π finds its maximum in the direction of h for a given X. The black squares represent the suboptimal couple (X, h) where Π finds its maximum in the direction of X for a given h.

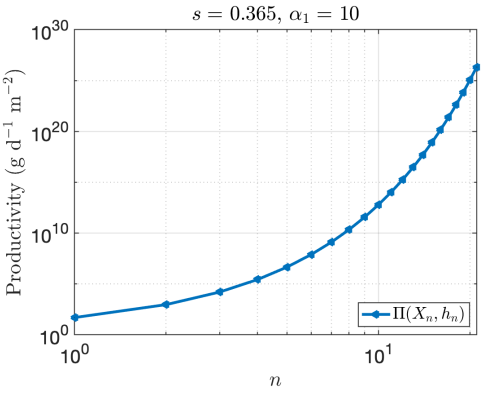

Figure 2.10: Productivity $\Pi(X_n, h_n)$ for the sequence $(X_n, h_n)_{n>0}$.

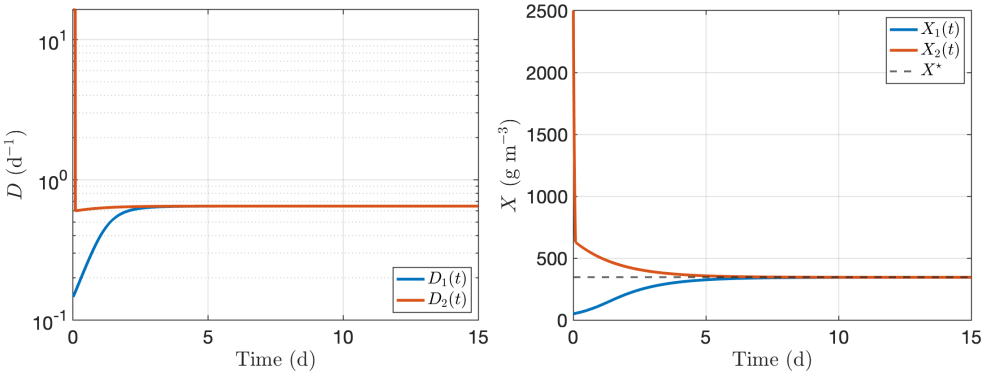

Figure 2.11: Evolution of the biomass concentration X in closed loop for two initial conditions.

the reactor bottom is zero. This optimum can be used to characterize the optimal water depth which maximizes surface biomass productivity Π for a target biomass concentration value. When the light extinction rate is affine with respect to the biomass concentration, an upper limit to the productivity is given which is obtained for an infinitely small depth and an infinitely large biomass concentration.

The proposed nonlinear controller stabilizes the biomass concentration to its optimal value $X^\star$. It could be improved by integrating an extremum seeking strategy [88, 56] to automatically target the desired biomass without identifying it in advance.

2.A Explicit computations for average growth rate

In this section, we provide details about the computation on $\bar{\mu}$. As mentioned in Subsection 1.2.1, the growth rate described by Han model can be easily written in the Haldane description. We choose to present the corresponding computation hereafter with Han model parameters. From the definition of $\bar{\mu}$ (2.4), one has

$$\bar{\mu} = \frac{1}{h}\int_{-h}^{0} \mu(I(X,z))\mathrm{d}z = \frac{k_r k\sigma}{h\varepsilon(X)}\int_{I_b}^{I_s} \frac{1}{k_d\tau(\sigma I)^2 + k_r(\tau\sigma I + 1)}\mathrm{d}I,$$

where $I_b = I_s\exp(-\varepsilon(X)h)$. Define $a = k_d\tau\sigma^2, b = k_r\tau\sigma, c = k_r$. According to the sign of the discriminant Δ of equation $aI^2 + bI + c$, three cases must be considered.

- $\Delta > 0$: Then there exists two reel roots denoted by $d_1 = \frac{-b+\sqrt{b^2-4ac}}{2a}$ and $d_2 = \frac{-b-\sqrt{b^2-4ac}}{2a}$. Hence one has
$$\bar{\mu} = \frac{k_r k\sigma}{ah\varepsilon(X)}\Big(e_1\ln\left|\frac{I_s - d_1}{I_b - d_1}\right| + e_2\ln\left|\frac{I_s - d_2}{I_b - d_2}\right|\Big).$$
with $e_1 + e_2 = 0$ and $e_1 d_2 + e_2 d_1 = -1$, i.e. $e_1 = \frac{1}{d_1 - d_2} = \frac{a}{\sqrt{b^2-4ac}}$ and $e_2 = \frac{1}{d_2 - d_1} = -\frac{a}{\sqrt{b^2-4ac}}$. Using $e_2 = -e_1$, we find
$$\bar{\mu} = \frac{k_r k\sigma e_1}{ah\varepsilon(X)}\ln\left|\frac{(I_s - d_1)(I_b - d_2)}{(I_b - d_1)(I_s - d_2)}\right|.$$

- $\Delta = 0$: Then there exists a unique root denoted by $d = -\frac{b}{2a}$. And one has
$$\bar{\mu} = \frac{k_r k\sigma}{h\varepsilon(X)}\frac{I_s - I_b}{(I_s - d)(I_b - d)}$$

- $\Delta < 0$: Then one has
$$aI^2 + bI + c = \frac{4ac - b^2}{4a}\Big(\big(\frac{I + \frac{b}{2a}}{\sqrt{\frac{4ac-b^2}{4a^2}}}\big)^2 + 1\Big).$$
Applying a change of variable by setting $y = \frac{I+\frac{b}{2a}}{\sqrt{\frac{4ac-b^2}{4a^2}}}$, one gets
$$\bar{\mu} = \frac{k_r k\sigma}{h\varepsilon(X)}\frac{2}{\sqrt{4ac - b^2}}\big(\arctan(\frac{2aI_s + b}{\sqrt{4ac - b^2}}) - \arctan(\frac{2aI_b + b}{\sqrt{4ac - b^2}})\big).$$

Since one has the explicit formulation of the average growth rate $\bar{\mu}$, the surface biomass concentration Π can be then computed explicitly including its derivatives. This is at the basis of the determination of the optimal biomass concentration X for a given depth h.

Chapter 3

Periodic resource allocation in dynamical systems, application to raceway microalgal production

3.1 Introduction

Considering a fixed amount of the resources and a set of activities, we look for a distribution strategy which optimizes a given objective function. This is the so-called resource allocation problem [68]. Due to its simple structure, this problem is encountered in a number of applications including load scheduling [123], manufacturing [124], portfolio selection [63] and computational biology [3]. Periodic versions have also been considered. The periodic scheduling problem was first addressed in [87] in the framework of operation research. Later on, the concept of *proportionate fairness* constraint has been introduced [6] to design allocation algorithms which schedule the resources in proportion to task weight. Periodic resource allocation problems are also used in ecology, e.g., in [32, 108] where the authors investigate long-term behaviour of harvesting policies for a forest composed of multiple species with different maturity ages. In such problems, the state can also be described in terms of dynamical systems. As an example, hospital resources (hospital beds) continuous allocation is studied in [2] as a strategy to control the dengue fever, associated with a patient recovery rate. In the same way, a population of a single species with logistic growth in a patchy environment is considered in [102]. The problem here consists of the maximization of the total population by re-distributing the limited resources among the patches.

In general, resource allocation problems are related to the assignment of a resource to a sequence of two or more tasks at the same time. However, we focus in this chapter on problems where N resources are assigned to N tasks over some time intervals. Additionally, we consider permanent regimes which are often relevant in the case of long term processes, as, e.g., crop harvesting, scheduling of appliances, etc. Moreover, here we also account for the dynamical evolution of the system between two re-allocations, further increasing the difficulty of the analysis. In this way, our work is related to the fields of switched systems [84], impulse control [7, 64] and to periodic control [31]. These techniques are usually used to tackle stabilization issues. In this chapter, we consider them in view of optimization issues.

In order to model the allocation process in the periodic system, we study the following resource allocation problem : *Consider a system with N resources and N activities, each activity uses the allocated resource to evolve during a given time $T > 0$. At time T, the resources will be re-allocated*

according to a given permutation. It is proven that if the dynamics of the system is periodic, then it is one period corresponding to one allocation process whatever the order of the considered permutation matrix is. A nonlinear objective functional to be optimized is then introduced in order to find best allocation strategies. Since $N!$ permutations need to be tested in the general case, it can be numerically solved only for a limited number of N. To overcome this difficulty, we propose a second optimization problem - a typical assignment problem - associated with a suboptimal solution of the initial problem, which can be determined explicitly. In addition, a sufficient condition to characterize cases where the two problems have the same solution is given.

For the sake of concreteness, we illustrate our theory by an industrial application, namely the mixing of microalgae cells in a cultivation set-up. Outdoor algal cultivation is mainly carried out in open raceway ponds exposed to solar radiation. This hydrodynamic system is set in motion by a paddle wheel which homogenises the medium for ensuring an equidistribution of the nutrients and guarantees that each cell will have regularly access to the light [29]. Microalgae then grow between two re-distributions depending on the light intensity received in their layer. Different strategies have been proposed to optimize the production of the biomass in this algal raceway system [38, 36, 34, 33, 4, 12, 13, 14]. However, the mixing policy has not been investigated up to now. In the current study, the paddle wheel is identified to a mixing device and modeled by permutation. We then focus on the influence of the mixing strategy on the algal productivity in a flat raceway system with a constant average velocity.

This chapter is organized as follows. We introduce our periodic resource allocation problem and the considered dynamical system in Section 3.2. More precisely, the optimization problem together with a simpler version based on an approximated functional are introduced in Subsection 3.2.2. Some technical lemmas are given in Subsection 3.2.3 and a criterion to guarantee that the original problem and its approximation share the same solution is given in Subsection 3.2.4. Some implementation remarks conclude this section in Subsection 3.2.5. Section 3.3 is devoted to the application to algal production. We present the models associated with the biological and the mixing device in a raceway pond in Subsection 3.3.1. The considered parameters are given in Subsection 3.3.2. We illustrate the performance of our strategies by numerical experiments in Subsection 3.3.4. Finally, we conclude with some perspectives of our work in Section 3.4.

Notation. In what follows, $\mathbb{N}$ denotes the set of non-negative integers, $\mathcal{P}_N$ denotes the set of permutation matrices of size $N \times N$ with $N \in \mathbb{N}$ and $\mathfrak{S}_N$ denotes the associated set of permutations of N elements. The cardinal of a set E is denoted by $\#E$. Given a matrix M, we denote by $\ker(M)$ its kernel and by $M_{i,j}$ its coefficient (i,j). In the same way, W_n denotes the n-th coefficient of a vector W. $\langle \cdot, \cdot \rangle$ denotes the scalar product in $\mathbb{R}^2$.

3.2 Description of the problem and optimization

Given a period T, and initial time T_0 and a sequence $(T_k)_{k\in\mathbb{N}}$, with $T_k = kT + T_0$, we consider the following resource allocation problem: Consider N resources denoted by $(I_n)_{n=1}^N \in \mathbb{R}^N$ which can be allocated to N activities denoted by $(x_n)_{n=1}^N$ where x_n consists of a real function of time. On a time interval $[T_k, T_{k+1})$, each activity uses the assigned resource and evolves according to a linear dynamics

$$\dot{x}_n = -\alpha(I_n)x_n + \beta(I_n), \tag{3.1}$$

where $\alpha : \mathbb{R} \to \mathbb{R}_+$ and $\beta : \mathbb{R} \to \mathbb{R}_+$ are given. At time T_{k+1}, the resources is re-assigned, meaning that $x_{n_1}(T_{k+1}) = x_{n_2}(T_{k+1}^-)$ for some $n_1, n_2 \in \{1, \dots, N\}$. In this way, $k \in \mathbb{N}$ represents the number of re-assignments and T_k^- represents the moment just before re-assignment. This problem can also be defined using the permutation matrix $P \in \mathcal{P}_N$. In particular, the assignment process can be formulated by $x(T_k) = Px(T_k^-)$.

Assume that the resource $(I_n)_{n=1}^N$ are constant with respect to time, then the evolution equation (3.1) can be computed explicitly. Indeed, for a given initial vector of states $(x_n(T_0))_{n=1}^N$, we have

$$x(t) = D(t)x(T_k) + v(t), \quad t \in [T_k, T_{k+1}), \tag{3.2}$$

where $D(t)$ is a time dependent diagonal matrix with $D_{nn}(t) := e^{-\alpha(I_n)(t-T_k)}$ and $v(t)$ is a time dependent vector with

$$v_n(t) := \frac{\beta(I_n)}{\alpha(I_n)}(1 - e^{-\alpha(I_n)(t-T_k)}). \tag{3.3}$$

The detail about the computations giving rise to (3.2) is presented in Appendix 3.A. For the sake of simplicity, we write hereafter D, v instead of $D(T), v(T)$.

Let $u \in \mathbb{R}^N$ an arbitrary vector. Define

$$f^k := \langle u, \frac{1}{T}\int_{T_k}^{T_{k+1}} x(t)\mathrm{d}t\rangle, \tag{3.4}$$

the benefit attached to the time period $[T_k, T_{k+1})$ after k times of re-assignment. Then the average benefit after K operations is given by

$$\frac{1}{K}\sum_{k=0}^{K} f^k.$$

Remark

Such a formalization is used in the context of forest maintenance and exploitation in [32]. In this work, an infinite sum is considered to study the total benefit of all the operations.

3.2.1 Periodic regime

Consider $P \in \mathcal{P}_N$ the permutation matrix describing the resource assignment process. According to (3.2) and by the definition of P, we have

$$x(T_{k+1}) = P(Dx(T_k) + v). \tag{3.5}$$

Before studying the sequence $(x(T_k))_{k\in\mathbb{N}}$, let us give a first simple result. We denote by I the identity matrix of size N.

Lemma 3.2.1. *Given $k \in \mathbb{N}$ and $P \in \mathcal{P}_N$, the matrix $\mathcal{I}_N - (PD)^k$ is invertible.*

Proof. Assume $\mathcal{I}_N - PD$ is not invertible, then there exists a non-null vector $X \in \ker(\mathcal{I}_N - PD)$, which means $X = PDX$. Let us denote $d_n = D_{nn}$, $n = 1, \dots, N$. Denoting by σ the permutation associated with P, we find that $(DX)_n = d_n X_n$ and $X_n = (PDX)_n = d_{\sigma(n)}X_{\sigma(n)}$. In the same way, we have

$$X_n = \left((PD)^k X\right)_n = d_{\sigma^k(n)} \dots d_{\sigma(n)} X_{\sigma^k(n)},$$

where $\sigma^k(n)$ denotes the $k-$times repeated composition of σ with itself. Denoting by K the order of σ, we have

$$X_n = \left((PD)^K X\right)_n = d_{\sigma^K(n)} \dots d_{\sigma(n)} X_{\sigma^K(n)} = d_{\sigma^K(n)} \dots d_{\sigma(n)} X_n.$$

Since, $0 < d_n < 1$ for $n = 1, \dots, N$, then $0 < d_{\sigma^K(n)} \dots d_{\sigma(n)} < 1$. This implies that $X_n = 0$, which contradicts our assumption. Therefore, $\mathcal{I}_N - PD$ is invertible. That $\mathcal{I}_N - (PD)^k$ is invertible can be proved in much the same way. □

Assume now that the state x is KT-periodic in the sense that after K times of re-assignment, the state of each activity returns to its initial state $x_n(T_K) = x_n(T_0)$. A crucial property of $(x(T_k))_{k\in\mathbb{N}}$ is given in the next proposition.

Theorem 3.2.1. *We keep the notation of the previous lemma and assume that the state x is KT-periodic. Then $(x(T_k))_{k\in\mathbb{N}}$ is a constant sequence and we have for all $k \in \mathbb{N}$*

$$x(T_k) = (\mathcal{I}_N - PD)^{-1}Pv.$$

Proof. Thanks to Lemma 3.2.1, there exists a unique $\bar{x}$ satisfying $\bar{x} = P(D\bar{x} + v)$. Let us then define the sequence $(e^k)_{k\in\mathbb{N}}$ by

$$e^k := x(T_k) - \bar{x}.$$

We have

$$e^{k+1} = (PD)e^k.$$

Since x is assumed to be KT-periodic, we have

$$e^0 = e^K = (PD)^K e^0.$$

According to Lemma 3.2.1, $\mathcal{I}_N - (PD)^K$ is invertible, meaning that $e^0 = 0$. It follows that $e^k = 0$, for $k \in \mathbb{N}$. The result follows. □

A natural choice for K would be the order of the permutation associated with P. Indeed, in this case K is the minimal number of re-assignments required to recover the initial state of x. The previous result shows that every $KT-$periodic evolution will actually be $T-$periodic. In the next section, we show that this property is decisive to formulate an optimization problem. In addition, the computations to solve the optimization problem will be reduced, since the CPU time required to assess the quality of a permutation will not depend on its order.

3.2.2 Objective function

Let us take the benefit (3.4) and replace $x(t)$ by its solution (3.2), one has

$$f^k = \frac{1}{T}\langle u, \tilde{D}x(T_k) + \tilde{v}\rangle = \frac{1}{T}\langle \tilde{D}u, x(T_k)\rangle + \langle u, \tilde{v}\rangle,$$

where $\tilde{D}_{nn} = \int_{T_k}^{T_{k+1}} D_{nn}(t)\mathrm{d}t$ and $\tilde{v}_n = \int_{T_k}^{T_{k+1}} v_n(t)\mathrm{d}t$. The only term depends on the re-assignment process is $x(T_k)$. On the other hand, using Theorem 3.2.1, one finds

$$\langle \tilde{D}u, x(T_k)\rangle = \langle \tilde{D}u, x(T_0)\rangle = \langle \tilde{D}u, (\mathcal{I}_N - PD)^{-1}Pv\rangle,$$

meaning that the benefit is the same for each re-assignment process.

Without loss of generality, let us still denote $\tilde{D}u$ by u. We now consider both minimization and maximization problems associated with the functional

$$J(P) := \langle u, (\mathcal{I}_N - PD)^{-1}Pv\rangle, \tag{3.6}$$

where $P \in \mathcal{P}_N$. Since $\#\mathfrak{S}_N = N!$, this problem cannot be tackled in realistic cases where large values of N must be considered, e.g., to keep a good numerical accuracy. To overcome this difficulty, we propose in this section an approximation of this problem whose optimum can be determined explicitly. For this purpose, we expand the functional (3.6) as follows

$$\langle u, (\mathcal{I}_N - PD)^{-1} Pv \rangle = \sum_{l=0}^{+\infty} \langle u, (PD)^l Pv \rangle = \langle u, Pv \rangle + \sum_{l=1}^{+\infty} \langle u, (PD)^l Pv \rangle,$$

and consider as an approximation the first term of this series, namely

$$J^{\text{approx}}(P) := \langle u, Pv \rangle. \tag{3.7}$$

Without loss of generality (see Appendix 3.B for the details), we assume that the entries of u are sorted in an ascending order, meaning that $u_1 \leq \ldots \leq u_N$. Note that optimizing J^{approx} amount to solving an assignment problem [26]. Indeed, we have for example

$$\min_{P \in \mathcal{P}_N} J^{\text{approx}}(P) = \min_{\sigma \in \mathfrak{S}_N} \sum_{n=1}^{N} u_n v_{\sigma(n)}.$$

This reads as an assignment problem associated with the matrix $[u_i v_j]_{(i,j=1,\ldots,N)}$. To make our exposition self-contained, we give the solution of this problem in Section 3.2.4.

Remark

A fairly common approach to deal with permutation optimization is to relax the problem by extending the optimization to the set of bistochastic matrices. As an example, this technique corresponds to the Kantorovitch relaxation considered in optimal transport [71], see also [19] for a more general presentation of the linear case, and [85] for a similar strategy in the context of quantum chemistry. This approach allows the optimization to be performed by gradient-type methods. At the theoretical level, the goal is then to prove that the convergence takes place towards extremal points, i.e. permutation matrices. We have tested this approach to the nonlinear problem (3.6). Our results indicate that the obtained limits are indeed permutation matrices. However, we have observed that the obtained matrices are not always optimal, which leads us to conjecture the existence of local non-global minima for this extended form of J.

3.2.3 Some technical lemmas

Let us state some preliminary properties about the permutation set $\mathfrak{S}_N$ that we will use in the next section. Given $k \in \mathbb{N}$, and two arbitrary permutations $\sigma, \widetilde{\sigma} \in \mathfrak{S}_N$, let us define

$$\begin{aligned} E_k(\sigma, \widetilde{\sigma}) &:= \left\{ n = 1, \ldots, N \mid \sigma^k(n) \neq \widetilde{\sigma}^k(n) \right\}, \\ G_k(\sigma, \widetilde{\sigma}) &:= \{ n = 1, \ldots, N \mid \forall k' \leq k,\ \sigma^{k'}(n) = \widetilde{\sigma}^{k'}(n) \}, \end{aligned}$$

and

$$m_k := \# E_k(\sigma, \widetilde{\sigma}).$$

We have the following result.

Lemma 3.2.2. *For $k \in \mathbb{N}$, we have $m_k \leq k m_1$ and $\# G_k(\sigma, \widetilde{\sigma}) \geq \max(N - k m_1, 0)$.*

Proof. To shorten notation, we write in this proof E_k instead of $E_k(\sigma,\widetilde{\sigma})$, E_{k+1} instead of $E_{k+1}(\sigma,\widetilde{\sigma})$, G_k instead of $G_k(\sigma,\widetilde{\sigma})$, etc. From the definition of E_k, we have:

$$E_{k+1} = ((\{1,\dots,N\}\setminus E_1)\cap E_{k+1})\cup(E_1\cap E_{k+1}).$$

The first subset in the right hand side satisfies

$$\sigma\left((\{1,\dots,N\}\setminus E_1)\cap E_{k+1}\right) = \widetilde{\sigma}\left((\{1,\dots,N\}\setminus E_1)\cap E_{k+1}\right)\subset E_k,$$

so that $\#\left((\{1,\dots,N\}\setminus E_1)\cap E_{k+1}\right)\leq \#E_k =: m_k$.

On the other hand, $(E_1\cap E_{k+1})\subset E_1$, hence $\#(E_1\cap E_{k+1})\leq m_1$. As a consequence, $m_{k+1}\leq m_k+m_1$. This implies $m_k\leq km_1$.

As for G_k, we have:

$$G_k = (G_{k+1}\cap G_k)\cup(\sigma^{-k}(E_1)\cap G_k). \tag{3.8}$$

Indeed, let $n\in G_k$, i.e, $\sigma^k(n)=\widetilde{\sigma}^k(n)$. If $\sigma^{k+1}(n)=\widetilde{\sigma}^{k+1}(n)$, then $n\in G_{k+1}$. Otherwise, $\sigma^{k+1}(n)\neq\widetilde{\sigma}^{k+1}(n)$, meaning that $\sigma^{k+1}(n)\neq\widetilde{\sigma}(\sigma^k(n))$ which implies $\sigma^k(n)=\widetilde{\sigma}^k(n)\in E_1$, so that $n\in\sigma^{-k}(E_1)$. This proves (3.8), and we get as a by-product

$$(G_{k+1}\cap G_k)\cap(\sigma^{-k}(E_1)\cap G_k)=\emptyset.$$

Moreover, since $G_{k+1}\subset G_k$, we get $G_{k+1}\cap G_k = G_{k+1}$. It follows that

$$\#G_k = \#G_{k+1}+\#\{\sigma^{-k}(E_1)\cap G_k\}.$$

Since $\#\{\sigma^{-k}(E_1)\cap G_k\}\leq \#E_1 = m_1$, we obtain $\#G_{k+1}\geq \#G_k - m_1$. The result follows. □

In what follows, a transposition in $\mathfrak{S}_N$ between two elements $i\neq j$ is denoted by $(i\ j)$. By abuse of notation, $(n\ n)$ denotes the identity for all $n=1,\dots,N$. Given a permutation $\sigma\in\mathfrak{S}_N$, we consider the sequence of permutations $(\sigma_n)_{n=0,\dots,N}$ defined by

$$\begin{aligned}&\sigma_0=\sigma\\&\sigma_n=(n\ \sigma_{n-1}(n))\circ\sigma_{n-1}.\end{aligned} \tag{3.9}$$

For all $n\leq N$, it immediately follows from this definition that

$$\sigma_n|_{\{1,\dots,n\}} = Id|_{\{1,\dots,n\}} \text{ and } \sigma_{N-1}=\sigma_N=Id,$$

where Id denote the identity permutation. Let us give two additional properties of this sequence.

Lemma 3.2.3. *Let $\sigma\in\mathfrak{S}_N$ and $(\sigma_n)_{n=1,\dots,N-1}$ defined by* (3.9)*. One has:*

$$\{i=1,\dots,N\mid\sigma(i)=i\}=\{i=1,\dots,N\mid\forall n=1,\dots,N-1,\ \sigma_n(i)=i\}.$$

Proof. Given i with $1\leq i\leq N$, such that $\sigma(i)=i$, let us prove that $\sigma_n(i)=i$ by induction on n. Since $\sigma_0=\sigma$, the result holds for $n=0$. Suppose it holds at a rank $n-1$, meaning that $\sigma_{n-1}(i)=i$. By definition of $(\sigma_n)_{n=1,\dots,N}$, one has:

$$\sigma_n(i)=(n\ \sigma_{n-1}(n))\circ\sigma_{n-1}(i)=(n\ \sigma_{n-1}(n))(i).$$

If $i=n$, then $(n\ \sigma_{n-1}(n))(i)=\sigma_{n-1}(n)=\sigma_{n-1}(i)=i$. If $i=\sigma_{n-1}(n)$, then $i=\sigma_{n-1}(i)=\sigma_{n-1}(n)$ and $i=n$, so that we conclude as in the previous case. In the other cases, $\sigma_n(i)=\sigma_{n-1}(i)=i$. The result follows. □

Lemma 3.2.4. *Let $i, j \in \{1, \dots, N\}$, with $i < j$. Let $\sigma \in \mathfrak{S}_N$ $\sigma = (i\ j) \circ \sigma'$, where $(i\ j)$ and σ' have disjoint supports, i.e., $\sigma'(i) = i$ and $\sigma'(j) = j$. One has: $\sigma_j = \sigma_{j-1}$.*

Proof. From the definition of $(\sigma_n)_{n=1,\dots,N}$, one has

$$\sigma_j = (j\ \sigma_{j-1}(j)) \circ \sigma_{j-1}.$$

We need to prove that $\sigma_{j-1}(j) = j$. Since σ' and $(i\ j)$ are disjoint, then for $n < i$, $\sigma_n = (i\ j) \circ \sigma'_n$, where σ'_n is defined by (3.9), with the initial term $\sigma'_0 = \sigma'$. In particular, $\sigma_n(i) = j$ for $n < i$.

In the case $n = i$, one has

$$\sigma_i = (i\ \sigma_{i-1}(i)) \circ \sigma_{i-1} = (i\ j) \circ \sigma_{i-1} = (i\ j) \circ (i\ j) \circ \sigma'_{i-1} = \sigma'_{i-1}.$$

In particular, $\sigma_i(j) = j$.

Finally, since $\sigma'_{i-1}(i) = i$, we find that $\sigma'_i = \sigma'_{i-1}$, and it follows by induction that for $n > i$, $\sigma_n = \sigma'_n$, which means $\sigma_n(j) = j$. In particular $\sigma_{j-1}(j) = j$. This concludes the proof. □

The sequence $(\sigma_n)_{n=0,\dots,N}$ can be used to decompose $J(I) - J(P)$ for an arbitrary $P \in \mathcal{P}_N$, as stated in the next Lemma.

Lemma 3.2.5. *Let $\sigma \in \mathfrak{S}_N$ and $P \in \mathcal{P}_N$ the associated permutation matrix, we have:*

$$\langle u, (\mathcal{I}_N - P)v \rangle = \sum_{n=1}^{N-1} (u_n - u_{\sigma_{n-1}^{-1}(n)})(v_n - v_{\sigma_{n-1}(n)}).$$

Proof. Given $j \in \{0, \dots, N\}$, define $S_j = \sum_{n=1}^{N} u_n v_{\sigma_j(n)}$. Since $\sigma_j(n)$ and $\sigma_{j-1}(n)$ might only differ for $n = j$ and $n = \sigma_{j-1}^{-1}(j)$, we have

$$\begin{aligned}
S_j - S_{j-1} &= \sum_{n=j}^{N} u_n (v_{\sigma_j(n)} - v_{\sigma_{j-1}(n)}) \\
&= u_j (v_{\sigma_j(j)} - v_{\sigma_{j-1}(j)}) + u_{\sigma_{j-1}^{-1}(j)} (v_{\sigma_j(\sigma_{j-1}^{-1}(j))} - v_{\sigma_{j-1}(\sigma_{j-1}^{-1}(j))}) \\
&= u_j (v_j - v_{\sigma_{j-1}(j)}) + u_{\sigma_{j-1}^{-1}(j)} (v_{\sigma_{j-1}(j)} - v_j) \\
&= (u_j - u_{\sigma_{j-1}^{-1}(j)})(v_j - v_{\sigma_{j-1}(j)}).
\end{aligned}$$

The result then follows from $\langle u, (\mathcal{I}_N - P)v \rangle = S_{N-1} - S_0$. □

3.2.4 Solutions of the optimization problems

The previous lemma enables us to solve the problems $\max_{P \in \mathcal{P}_N} J^{\text{approx}}(P)$ and $\min_{P \in \mathcal{P}_N} J^{\text{approx}}(P)$. Recall that the entries of u are sorted in an ascending order.

Lemma 3.2.6. *Let $\sigma_+,\ \sigma_- \in \mathfrak{S}_N$ such that $v_{\sigma_+(1)} \leq v_{\sigma_+(2)} \cdots \leq v_{\sigma_+(N)}$ and $v_{\sigma_-(N)} \leq v_{\sigma_-(N-1)} \leq \cdots \leq v_{\sigma_-(1)}$ and $P_+,\ P_- \in \mathcal{P}_N$, the corresponding permutation matrices. Then*

$$P_+ = \text{argmax}_{P \in \mathcal{P}_N} J^{approx}(P), \quad P_- = \text{argmin}_{P \in \mathcal{P}_N} J^{approx}(P).$$

Proof. Let $P \in \mathcal{P}_N$ and $\sigma \in \mathfrak{S}_N$ the associated permutation, we have

$$\begin{aligned}\langle u, (P_+ - P)v\rangle =& \langle u, (\mathcal{I}_N - PP_+^{-1})w\rangle \\ =& \sum_{n=1}^{N-1} (u_n - u_{(\sigma'_{n-1})^{-1}(n)})(w_n - w_{\sigma'_{n-1}(n)}),\end{aligned} \tag{3.10}$$

where $w = (w_n)_{n=1}^N := (v_{\sigma_+(n)})_{n=1}^N$ and σ'_n is the sequence defined by (3.9) with $\sigma' := \sigma_+^{-1} \circ \sigma$ the permutation associated with PP_+^{-1}. Since $(w_n)_{n=1}^N$ by its definition is an increasing sequence, $\sigma'_{n-1}(n) \geq n$ and $(\sigma'_{n-1})^{-1}(n) \geq n$, we find that $\langle u, (P_+ - P)v\rangle \geq 0$. The proof of the problem $\min_{P\in\mathcal{P}_N} \langle u, Pv\rangle$ is similar. □

We immediately deduce from this lemma that once u and v are given, the matrix P_+, P_- of Lemma 3.2.6 can be determined explicitly. More precisely, P_+ is the matrix corresponding to the permutation which associates the largest coefficient of u with the largest coefficient of v, the second largest coefficient with the second largest, and so on. In the same way, P_- is the matrix corresponding to the permutation which associates the largest coefficient of u with the smallest coefficient of v, the second largest coefficient with the second smallest, and so on.

Remark

The optimal matrices P_+ and P_- are not unique as soon as either u or v contains at least two identical entries.

We focus now on the case where u as well as v have entries with a constant sign. Since the results in this section hold both for minimization and maximization problems, we can assume without loss of generality that u, v are both positive. Using the properties given in the previous section, we will show that in some cases, the problem $\max_{P\in\mathcal{P}_N} J(P)$ (resp. $\min_{P\in\mathcal{P}_N} J(P)$) and $\max_{P\in\mathcal{P}_N} J^{\text{approx}}(P)$ (resp. $\min_{P\in\mathcal{P}_N} J^{\text{approx}}(P)$) have the same solution.

We keep the notation of Lemma 3.2.6. Define for $n = 1, \ldots, N$,

$$\widetilde{p}_n := \min_{i,j=1,\ldots,N, i\neq n, j\neq n} |(u_n - u_i)(v_{\sigma_+(n)} - v_{\sigma_+(j)})|. \tag{3.11}$$

Denote by i_n and j_n the solutions of the previous problem. Since $u_n, v_{\sigma_+(n)}$ are sorted in an ascending order, we find immediately that if $n = 1$ (resp. N), then $i_n = j_n = 2$ (resp. $i_n = j_n = N - 1$). Otherwise, $i_n = n - 1$ or $i_n = n + 1$, and the same result holds for j_n. Sort $(\widetilde{p}_n)_{n=1}^N$ and denote by $(p_n)_{n=1}^N$ the resulting sequence, i.e., $p_1 \leq, \ldots, \leq p_N$. Define then for $m = 1, \ldots, N$

$$s_m := \sum_{n=1}^{m} p_n, \tag{3.12}$$

and

$$F_m^- := \sum_{n=1}^{\min(m,N)} u_n v_{\sigma_-(N-m+n)}, \quad F_m^+ := \sum_{n=\max(1,N-m+1)}^{N} u_n v_{\sigma_+(n)}. \tag{3.13}$$

From the definition of these sequences, we have $F_m^+ \geq F_m^-$. See Appendix 3.C for the case where u or v negative. We are now in a position to give the main result of this section.

Theorem 3.2.2. *Assume that u and v have positive entries and define*

$$\phi(m_1) := \frac{1}{s_{\lceil \frac{m_1}{2} \rceil}} \Big(\sum_{l=1}^{+\infty} d_{\max}^l F^+_{(l+1)m_1} - d_{\min}^l F^-_{(l+1)m_1} \Big), \tag{3.14}$$

where m_1 refers to the notation in Lemma 3.2.2, $d_{\max} := \max_{n=1,\dots,N}(d_n)$ and $d_{\min} := \min_{n=1,\dots,N}(d_n)$. Assume that:

$$\max_{m_1 \geq 2} \phi(m_1) \leq 1. \tag{3.15}$$

Then the problem $\max_{P\in\mathcal{P}_N} \langle u, (I - PD)^{-1}Pv\rangle$ (resp. $\min_{P\in\mathcal{P}_N} \langle u, (I - PD)^{-1}Pv\rangle$) and the problem $\max_{P\in\mathcal{P}_N} \langle u, Pv\rangle$ (resp. $\min_{P\in\mathcal{P}_N} \langle u, Pv\rangle$) have the same solution.

Proof. We keep the notation in Section 3.2.3 and give the proof in the case of the maximization problem. The case of the minimization problem can be handled in the very same way. Let $P \in \mathcal{P}_N$ and $\sigma \in \mathfrak{S}_N$ the associated permutation, we have

$$\begin{aligned} & \langle u, (I - P_+D)^{-1}P_+v\rangle - \langle u, (I - PD)^{-1}Pv\rangle & (3.16)\\ = & \sum_{l=0}^{+\infty} \langle u, \big((P_+D)^lP_+ - (PD)^lP\big)v\rangle \\ = & \langle u, (P_+ - P)v\rangle + \sum_{l=1}^{+\infty} \langle u, \big((P_+D)^lP_+ - (PD)^lP\big)v\rangle. & (3.17) \end{aligned}$$

From the definition $E_k(\sigma_+, \sigma)$ and $G_k(\sigma_+, \sigma)$, we have in particular

$$E_1(\sigma_+, \sigma) \sqcup G_1(\sigma_+, \sigma) = \{1, \dots, N\}.$$

Let us denote by $(w_n)_{n=1}^N = (v_{\sigma_+(n)})_{n=1}^N$ and by σ'_n the sequence defined by (3.9) with $\sigma'_0 := \sigma_+^{-1} \circ \sigma$. From the definition of $E_1(\sigma_+, \sigma)$ and $G_1(\sigma_+, \sigma)$, we have $\sigma(G_1(\sigma_+, \sigma)) = \sigma_+(G_1(\sigma_+, \sigma))$ and $\sigma(E_1(\sigma_+, \sigma)) = \sigma_+(E_1(\sigma_+, \sigma))$, which implies $\sigma'_0(E_1(\sigma_+, \sigma)) = E_1(\sigma_+, \sigma)$, and for any $i \in G_1(\sigma_+, \sigma)$, $\sigma'_0(i) = i$. Using these properties and (3.10), we have

$$\begin{aligned} \langle u, (P_+ - P)v\rangle &= \sum_{n=1}^{N-1} (u_n - u_{(\sigma'_{n-1})^{-1}(n)})(w_n - w_{\sigma'_{n-1}(n)}) \\ &= \sum_{n\in E_1(\sigma_+,\sigma)} (u_n - u_{(\sigma'_{n-1})^{-1}(n)})(w_n - w_{\sigma'_{n-1}(n)}) \\ &\quad + \sum_{n\in G_1(\sigma_+,\sigma)} (u_n - u_{(\sigma'_{n-1})^{-1}(n)})(w_n - w_{\sigma'_{n-1}(n)}) \\ &= \sum_{n\in E_1(\sigma_+,\sigma)} (u_n - u_{(\sigma'_{n-1})^{-1}(n)})(w_n - w_{\sigma'_{n-1}(n)}). \end{aligned} \tag{3.18}$$

In the case where there exists a transposition $(i\ i')$ with $i < i'$ in σ', Lemma 3.2.4 implies that $u_{(\sigma'_{i'-1})^{-1}(i')} = u_{i'}$ and $w_{\sigma'_{i'-1}(i')} = w_{i'}$. The maximum number of transpositions in σ'_0 is $\frac{m_1}{2}$ if m_1 is even, $\frac{m_1-3}{2}$ otherwise. Hence, the smallest number of non-zero terms present in the last sum of (3.18) is given by $m_1 - \frac{m_1}{2} = \frac{m_1}{2}$ if m_1 is even, $\frac{m_1-1}{2}$ otherwise. In other words, there

exists at least $\lceil \frac{m_1}{2} \rceil$ non zero terms in the last sum of (3.18), which implies

$$\langle u, (P_+ - P)v \rangle = \sum_{n \in E_1(\sigma_+, \sigma)} (u_n - u_{(\sigma'_{n-1})^{-1}(n)})(w_n - w_{\sigma'_{n-1}(n)}) \geq s_{\lceil \frac{m_1}{2} \rceil}. \tag{3.19}$$

For $n \in \{1, \dots, N\}$ and $l \in \mathbb{N}^*$, let us denote by

$$d_{\sigma,l,n} := d_{\sigma^l(n)} d_{\sigma^{l-1}(n)} \cdots d_{\sigma(n)}.$$

Considering now the second term of the right hand side of (3.17), we get

$$< u, (PD)^l Pv >= \sum_{n=1}^{N} u_n d_{\sigma^l(n)} d_{\sigma^{l-1}(n)} \cdots d_{\sigma(n)} v_{\sigma^{l+1}(n)} = \sum_{n=1}^{N} u_n d_{\sigma,l,n} v_{\sigma^{l+1}(n)}.$$

Using this notation and Lemma 3.2.2, we find

$$\begin{aligned}
&\left| \langle u, (P_+ D)^l P_+ v - (PD)^l Pv \rangle \right| \\
=&\left| \sum_{n=1}^{N} u_n (d_{\sigma_+,l,n} v_{\sigma_+^{l+1}(n)} - d_{\sigma,l,n} v_{\sigma^{l+1}(n)}) \right| \\
=&\left| \sum_{n \notin G_{l+1}(\sigma_+, \sigma)} u_n (d_{\sigma_+,l,n} v_{\sigma_+^{l+1}(n)} - d_{\sigma,l,n} v_{\sigma^{l+1}(n)}) \right| \\
=&\left| \sum_{n \notin G_{l+1}(\sigma_+, \sigma)} u_n d_{\sigma_+,l,n} v_{\sigma_+^{l+1}(n)} - \sum_{n \notin G_{l+1}(\sigma_+, \sigma)} u_n d_{\sigma,l,n} v_{\sigma^{l+1}(n)} \right| \\
\leq& d_{\max}^l \sum_{n \notin G_{l+1}(\sigma_+, \sigma)} u_n v_{\sigma_+(n)} - d_{\min}^l \sum_{n \notin G_{l+1}(\sigma_+, \sigma)} u_n v_{\sigma_-(n)} \\
\leq& d_{\max}^l F^+_{(l+1)m_1} - d_{\min}^l F^-_{(l+1)m_1}.
\end{aligned} \tag{3.20}$$

This result combined with (3.15), gives

$$\begin{aligned}
\left| \sum_{l=1}^{+\infty} \langle u, (P_+ D)^l P_+ v - (PD)^l Pv \rangle \right| \leq& \sum_{l=1}^{+\infty} d_{\max}^l F^+_{(l+1)m_1} - d_{\min}^l F^-_{(l+1)m_1} \\
\leq& s_{\lceil \frac{m_1}{2} \rceil}.
\end{aligned}$$

Considering now (3.19), we obtain

$$|\langle u, (P_+ - P)v \rangle| \geq \left| \sum_{l=1}^{+\infty} \langle u, (P_+ D)^l P_+ v - (PD)^l Pv \rangle \right|.$$

It follows that the first term of (3.17) dominates the second one. As a consequence, the former has the same sign as (3.16). The result follows. □

3.2.5 Implementation Remarks

Let us conclude with some Remarks on the computation of the function $\phi(m_1)$, more precisely of the sum in (3.14). Given $m_1 \in \{2, \dots, N\}$, define by l^* such that

$$l^* := \left\lfloor \frac{N}{m_1} \right\rfloor - 1.$$

We have

$$\begin{aligned}
&\sum_{l=1}^{+\infty} \left(d_{\max}^l F_{(l+1)m_1}^+ - d_{\min}^l F_{(l+1)m_1}^- \right) \\
=&\sum_{l=1}^{l^*} \left(d_{\max}^l F_{(l+1)m_1}^+ - d_{\min}^l F_{(l+1)m_1}^- \right) + \sum_{l=l^*+1}^{+\infty} \left(d_{\max}^l F_{(l+1)m_1}^+ - d_{\min}^l F_{(l+1)m_1}^- \right) \\
=&\sum_{l=1}^{l^*} \left(d_{\max}^l F_{(l+1)m_1}^+ - d_{\min}^l F_{(l+1)m_1}^- \right) + \frac{d_{\max}^{l^*+1}}{1-d_{\max}} F_N^+ - \frac{d_{\min}^{l^*+1}}{1-d_{\min}} F_N^-.
\end{aligned}$$

As for the evaluation of $s_{\lceil \frac{m_1}{2} \rceil}$, only $\left\lceil \frac{N}{2} \right\rceil$ terms need to be computed. Examples of behaviour of s_m and F_m^+, F_m^- are presented in Figure 3.3, whereas examples of behaviour of the function (3.14) with respect to m_1 are shown in Figure 3.4.

3.3 Application to algal production

In this section, we apply the theory developed in the previous section to an algal production case and provide some numerical results to evaluate the efficiency of the mixing strategies and their approximation.

3.3.1 Raceway modeling

We consider the Han model [59] to describe the dynamics of the photosynthetic units characterizing the growth of the algae after each allocation. Each light harvesting unit is assumed to have three different states: open and ready to harvest a photon (A), closed while processing the absorbed photon energy (B), or inhibited if several photons have been absorbed simultaneously leading to an excess of energy (C). Their dynamics is described by the following system

$$\begin{cases}
\dot{A} = -\sigma_H I A + \dfrac{1}{\tau} B, \\
\dot{B} = \sigma_H I A - \dfrac{1}{\tau} B + k_r C - k_d \sigma_H I B, \\
\dot{C} = -k_r C + k_d \sigma_H I B.
\end{cases}$$

Here A, B and C are the relative frequencies of the three possible states with $A+B+C = 1$, and I is a continuous time-varying signal representing the photon flux density. The coefficient σ_H stands for the specific photon absorption, τ is the turnover rate, k_r represents the photosystem repair rate and k_d is the damage rate. As shown in Subsection 1.2.1, one can use a fast-slow approximation and singular perturbation theory to reduce this system to a single evolution

equation on the photo-inhibition state C:

$$\dot{C} = -\alpha(I)C + \beta(I), \tag{3.21}$$

where

$$\alpha(I) := k_d\tau\frac{(\sigma_H I)^2}{\tau\sigma_H I + 1} + k_r, \quad \beta(I) := k_d\tau\frac{(\sigma_H I)^2}{\tau\sigma_H I + 1}.$$

The net specific growth rate is obtained by balancing photosynthesis and respiration, which gives

$$\mu(C, I) := -\gamma(I)C + \zeta(I),$$

where

$$\gamma(I) := \frac{k_H\sigma_H I}{\tau\sigma_H I + 1}, \quad \zeta(I) := \frac{k_H\sigma_H I}{\tau\sigma_H I + 1} - R.$$

Here, R denotes the respiration rate and k_H is a factor which relates the photosynthetic activity to the growth rate.

We assume that the system is perfectly mixed such that the biomass concentration (X) in (4.4) is homogeneous. Furthermore, it is often assumed that the photosynthetic units grow slowly so that the variations of biomass concentration (X) and background turbidity (α_1) are negligible over one lap of the raceway. As a consequence, the turbidity (α_1) and the biomass concentration (X) is supposed to be constant over the considered time scale. In this framework, we use the Beer-Lambert law to describe the light attenuation as a function of the depth z, i.e.

$$I(z) = I_s \exp(\varepsilon z), \tag{3.22}$$

where I_s is the light intensity at the free surface and ε is the light extinction coefficient. The average net specific growth rate over the domain is then defined by

$$\bar{\mu} := \frac{1}{T}\int_0^T \frac{1}{h}\int_{-h}^0 \mu\big(C(t,z), I(z)\big)\mathrm{d}z\mathrm{d}t, \tag{3.23}$$

where h is the depth of the raceway pond and T is the average duration of one lap of the raceway pond.

Let us now see how this model can be included in the framework of Section 3.2. In order to compute numerically (3.23), we introduce a vertical discretization of the fluid. More precisely, we consider N layers uniformly distributed on a vertical grid. The depth of the layer n is given by

$$z_n := -\frac{n - \frac{1}{2}}{N}h, \quad n = 1, \dots, N. \tag{3.24}$$

For a given initial photo-inhibition state $C_n(0)$, let $C_n(t)$ be the solution of (3.21) at time t. In this semi-discrete setting, the average net specific growth rate in the raceway pond can be defined by

$$\bar{\mu}_N := \frac{1}{T}\int_0^T \frac{1}{N}\sum_{n=1}^N \mu(C_n(t), I_n)\mathrm{d}t, \tag{3.25}$$

where I_n is the light intensity received in the layer n. The solution of (3.21) can be computed explicitly to get a formula that takes the form of (3.2). It follows that (3.25) satisfies

$$\bar{\mu}_N = \frac{1}{NT}\Big(\langle\Gamma, C(0)\rangle + \langle\mathbf{1}, Z\rangle\Big), \tag{3.26}$$

where $\mathbf{1}$ is a vector of size N whose coefficients are equal to 1, and Γ, Z are two vectors such that

$$\Gamma_n := \frac{\gamma(I_n)}{\alpha(I_n)}(e^{-\alpha(I_n)T} - 1),$$
$$Z_n := \frac{\gamma(I_n)\beta(I_n)}{\alpha(I_n)^2}(1 - e^{-\alpha(I_n)T}) - \frac{\gamma(I_n)\beta(I_n)}{\alpha(I_n)}T + \zeta(I_n)T.$$

The detail about the computations giving rise to (3.26) is presented in Appendix 3.A.

In this framework, the light intensity at different layers represents the resource I_n in the system and the photosynthesis at each layer represents the activity. Suppose now that at each lap, the algae at the layer n_1 are supposed to be entirely transferred to the layer n_2 when passing through the mixing device. During a lap, the photosynthesis of the algae follows a (3.1) type of evolution and the goal is to find the optimal resource allocation strategy to increase the productivity of the system. This mixing process is depicted schematically on an example in Figure 3.1. The interest of such a device is to mix the algae to better balance their exposure to

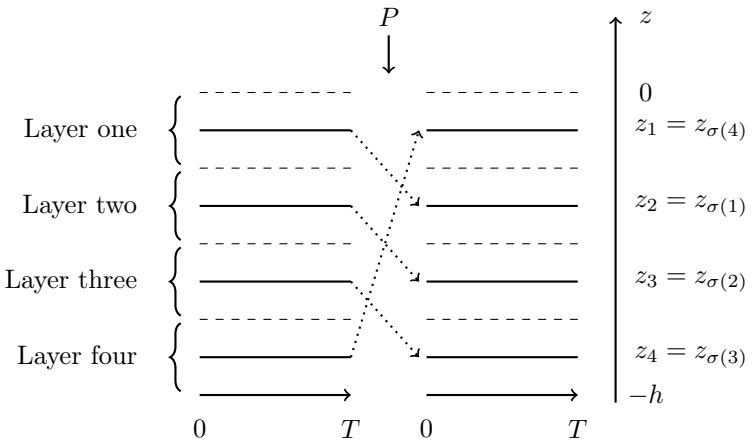

Figure 3.1: Schematic representation of the mixing process over two laps. Here, $N = 4$ and P corresponds to the cyclic permutation $\sigma = (1\ 2\ 3\ 4)$.

light and increase the production. Note that in actual raceway ponds, this device is generally a paddle wheel (see for example [40]).

Focusing on permanent regimes, we assume the system to be KT-periodic. From Theorem 3.2.1, we get immediately that $C(0) = (\mathcal{I}_N - PD)^{-1}PV$. Our goal is to maximize the average growth rate $\bar{\mu}_N$. Since only $C(0)$ in (3.26) depends on the permutation matrix P, we find that the objective function has the form of (3.6) with $u = \Gamma$ and $v = V$.

3.3.2 Parameter settings

Consider a raceway whose water elevation $h = 0.4\,\mathrm{m}$, which corresponds to typical raceway pond setting. All the numerical parameters values considered in this section for Han's model are taken from [54] and recalled in Table 3.1. Recall that I_s is the light intensity at the free surface. In order to fix the value of the light extinction coefficient ε in (3.22), we assume that only a fraction q of I_s reaches the bottom of the raceway pond, meaning that $I_b = qI_s$, where $q \in [0, 1]$ and I_b

Table 3.1: Parameter values for Han Model

k_r	$6.8\ 10^{-3}$	s^{-1}
k_d	$2.99\ 10^{-4}$	-
τ	0.25	s
σ_H	0.047	$\mathrm{m}^2\,\mu\mathrm{mol}^{-1}$
k_H	$8.7\ 10^{-6}$	-
R	$1.389\ 10^{-7}$	s^{-1}

is the light intensity at the bottom. It follows that ε can be computed by

$$\varepsilon = (1/h)\ln(1/q).$$

In practice, this quantity can be implemented in the experiments by adapting the biomass harvesting frequency, or the dilution rate for continuous cultivation. In what follows, the varying parameters are I_s , the ratio q and T. We consider $I_s \in [0, 2500]\mu\mathrm{mol}\,\mathrm{m}^{-2}\,\mathrm{s}^{-1}$, $q \in [0.1\%, 10\%]$ and $T \in [1, 1000]$s. The number of layers N remains small as we need to test numerically $N!$ permutation matrices for each triplet (I_s, q, T).

3.3.3 Examples of optimal devices

In this section, we present some examples of optimal solution of (3.6). Set $N = 11$ the number of layers, meaning that we test numerically $N!$ (i.e. 39916800) permutation matrices. The light intensity at the free surface is set to be $I_s = 2000\,\mu\mathrm{mol}\,\mathrm{m}^{-2}\,\mathrm{s}^{-1}$ which corresponds to a maximum value during summer in the south of France.

Let us start with a series of tests with the average time duration for one lap of the raceway pond $T = 1000\,\mathrm{s}$. When the light attenuation ratio $q = 10\%$, we find that $P_{\max} = I$. When $q = 1\%$, the optimal permutation matrix $P_{\max}$ is given by (3.27).

$$P_{\max} = \begin{pmatrix} 0 & 1 & 0 & 0 & 0 & 0 & 0 & 0 & 0 & 0 & 0 \\ 0 & 0 & 0 & 1 & 0 & 0 & 0 & 0 & 0 & 0 & 0 \\ 0 & 0 & 0 & 0 & 0 & 1 & 0 & 0 & 0 & 0 & 0 \\ 0 & 0 & 0 & 0 & 0 & 0 & 0 & 1 & 0 & 0 & 0 \\ 0 & 0 & 0 & 0 & 0 & 0 & 0 & 0 & 0 & 1 & 0 \\ 0 & 0 & 0 & 0 & 0 & 0 & 0 & 0 & 0 & 0 & 1 \\ 0 & 0 & 0 & 0 & 0 & 0 & 0 & 0 & 1 & 0 & 0 \\ 0 & 0 & 0 & 0 & 0 & 0 & 1 & 0 & 0 & 0 & 0 \\ 0 & 0 & 0 & 0 & 1 & 0 & 0 & 0 & 0 & 0 & 0 \\ 0 & 0 & 1 & 0 & 0 & 0 & 0 & 0 & 0 & 0 & 0 \\ 1 & 0 & 0 & 0 & 0 & 0 & 0 & 0 & 0 & 0 & 0 \end{pmatrix}. \tag{3.27}$$

When $q = 0.1\%$, the optimal permutation matrix $P_{\max}$ is given by (3.28). For all three cases,

$P_+ = P_{\max}$.

$$P_{\max} = \begin{pmatrix} 0 & 0 & 0 & 0 & 1 & 0 & 0 & 0 & 0 & 0 & 0 \\ 0 & 0 & 0 & 0 & 0 & 0 & 1 & 0 & 0 & 0 & 0 \\ 0 & 0 & 0 & 0 & 0 & 0 & 0 & 0 & 1 & 0 & 0 \\ 0 & 0 & 0 & 0 & 0 & 0 & 0 & 0 & 0 & 0 & 1 \\ 0 & 0 & 0 & 0 & 0 & 0 & 0 & 0 & 0 & 1 & 0 \\ 0 & 0 & 0 & 0 & 0 & 0 & 0 & 1 & 0 & 0 & 0 \\ 0 & 0 & 0 & 0 & 0 & 1 & 0 & 0 & 0 & 0 & 0 \\ 0 & 0 & 0 & 1 & 0 & 0 & 0 & 0 & 0 & 0 & 0 \\ 0 & 0 & 1 & 0 & 0 & 0 & 0 & 0 & 0 & 0 & 0 \\ 0 & 1 & 0 & 0 & 0 & 0 & 0 & 0 & 0 & 0 & 0 \\ 1 & 0 & 0 & 0 & 0 & 0 & 0 & 0 & 0 & 0 & 0 \end{pmatrix}. \tag{3.28}$$

We next study a much extreme case where the time duration of one lap $T = 1\,\mathrm{s}$. When the ratio $q = 10\%$, we find the optimal matrix $P_{\max} = I$. When $q = 1\%$, the optimal permutation matrix $P_{\max}$ is a two-block matrix consisting of a block of identity and a block of anti-diagonal matrix with one as entries. This matrix is shown in (3.29).

$$P_{\max} = \begin{pmatrix} 1 & 0 & 0 & 0 & 0 & 0 & 0 & 0 & 0 & 0 & 0 \\ 0 & 1 & 0 & 0 & 0 & 0 & 0 & 0 & 0 & 0 & 0 \\ 0 & 0 & 0 & 0 & 0 & 0 & 0 & 0 & 0 & 0 & 1 \\ 0 & 0 & 0 & 0 & 0 & 0 & 0 & 0 & 0 & 1 & 0 \\ 0 & 0 & 0 & 0 & 0 & 0 & 0 & 0 & 1 & 0 & 0 \\ 0 & 0 & 0 & 0 & 0 & 0 & 0 & 1 & 0 & 0 & 0 \\ 0 & 0 & 0 & 0 & 0 & 0 & 1 & 0 & 0 & 0 & 0 \\ 0 & 0 & 0 & 0 & 0 & 1 & 0 & 0 & 0 & 0 & 0 \\ 0 & 0 & 0 & 0 & 1 & 0 & 0 & 0 & 0 & 0 & 0 \\ 0 & 0 & 0 & 1 & 0 & 0 & 0 & 0 & 0 & 0 & 0 \\ 0 & 0 & 1 & 0 & 0 & 0 & 0 & 0 & 0 & 0 & 0 \end{pmatrix}. \tag{3.29}$$

When $q = 0.1\%$, we find the optimal matrix $P_{\max}$ as an anti-diagonal matrix with one as entries. For all three cases, P_+ is an anti-diagonal matrix with one as entries. Note that among all the previous matrices, some of them are easier to achieve in real life application than others, for instance the anti-diagonal matrix or the identity/anti-diagonal two-block matrices (3.29).

3.3.4 Further numerical tests

As shown in previous section, Problem (3.6) admits non trivial optimal permutation strategies which may significantly change according to the parameter settings. In this section, we study and compare the true and the approximated solutions as well as their efficiency with respect to the average net specific (3.23).

We start by investigating some properties of the items defined in the previous sections. Recall that the two sequences u, v used in Section 3.2.2 correspond in our application to Γ, V respectively. We consider $N = 20$ layers and two parameters triplets, namely $(I_s, q, T) = (2000, 5\%, 1000)$ and (800,0.5%,1). Figure 3.2 shows the evolution of these two quantities as a function of I. Note that in both cases, V is positive with sorted entries, as it can be seen in (3.3). On the contrary, the discretized Γ is negative and not necessarily sorted. We refer to Appendix 3.A for more details about V and Γ.

We then study the behaviour of the sequences F_m^+, F_m^-, s_m and $\phi(m_1)$ defined in Section 3.2.4 for the same two parameters triplets. Note that since Γ is negative, F_m^- and F_m^+ are defined as

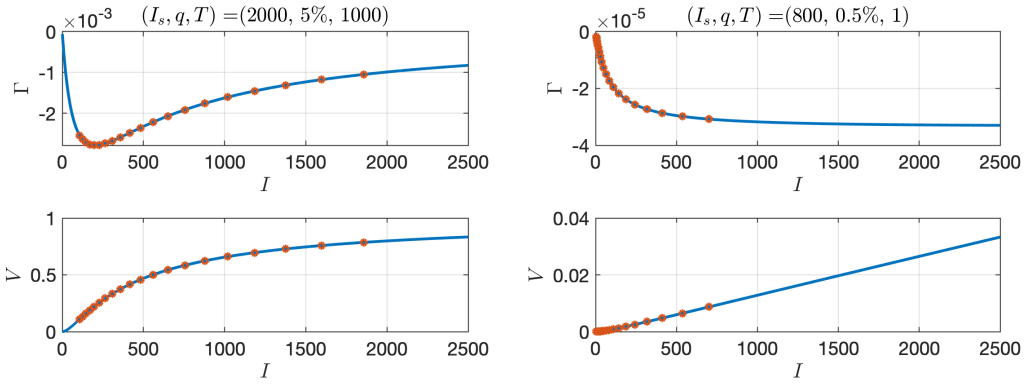

Figure 3.2: Γ and V with respect to the light intensity I (Blue curve). Discretisation points (Red point) chosen for $(I_s, q, T) = (2000, 5\%, 1000)$ (Left) and (800,0.5%,1) (Right).

in Appendix 3.C (and not as in (3.13)). We choose $N = 7$ and $N = 20$ to check the performance for two different discretisation numbers of layers. The two figures at the top in Figure 3.3 show the values of the two sequences F_m^+, F_m^- (see (3.13)), whereas the two bottom figures show the values of s_m (see (3.12)). As mentioned in the previous section, one can see that F_m^+ is always greater than F_m^- for all m. Figure 3.4 shows the values of the function $\phi(m_1)$ (see (3.14)) with respect to m_1. One can see in Figure 3.4 that the maximal value of $\phi(m_1)$ is always obtained for $m_1 = 2$, and that the maximal value $\phi(m_1)$ appears to be an increasing function of N. This makes the criterion given in Section 3.2.4 less efficient for a large number of layers N. Further analysis is required to obtain a criterion that does not depend on N.

The next test is devoted to the convergence of the average growth rate $\bar{\mu}_N$ with respect to the number of layers N. We keep the two triplets of parameters of the previous test. Due to the limit of the computer memory, the computation of $\bar{\mu}_N(P_{\max})$ is tractable for small values of N, in our case lower than or equal to $N = 11$. Such an issue does not occur in the case of $\bar{\mu}_N(P_+)$. Figure 3.5 presents the behaviour of $\bar{\mu}_N$. For the parameter triplet (2000,5%,1000), the criterion is satisfied until $N = 7$ (green circle), which is confirmed in Figure 3.4 (Left) where the maximal value of $\phi(m_1)$ is already close to 1. Though the criterion is not satisfied for $N > 7$, we observe that $P_+ = P_{\max}$ from $N = 2$ to $N = 11$. As for the triplet (800,0.5%,1), one can see that $P_+ = P_{\max}$ until $N = 3$. Figure 3.6 shows the optimal matrices for these two different parameter triplets in the case $N = 11$ and $N = 100$. It can be observed that for the parameter triplet (2000,5%,1000), the two matrices $P_+, P_{\max}$ have the same form for $N = 11$ and $N = 100$ (Figure 3.6 Top). Hence, one can expect $P_{\max} = P_+$ for larger N. However, this may not be the case for (800,0.5%,1) since $P_+, P_{\max}$ have already different forms for $N = 11$ (Figure 3.6 Bottom).

In the following tests, we focus only on two special cases: large lap duration time ($T = 1000\,\mathrm{s}$) and small lap duration time ($T = 1\,\mathrm{s}$). In practise, the former corresponds to typical time required to complete one lap in a raceway pond system, whereas the latter rather corresponds to the optimal case in a photobioreactor, for instance see [77]. In the small lap duration time case, we observe the so-called *flashing effect*. This phenomenon corresponds to the fact that the higher the light exposition frequency is, the larger the growth rate is. In other words, algae exposed to high frequency flashing, in our case, a small time duration for one lap, have a better growth. It can be observed in Figure 3.7, where $\bar{\mu}_N(P_{\max})$ decreases with respect to T for all considered light intensities. This phenomenon has already been reported in literature, see, e.g. [62, 77].

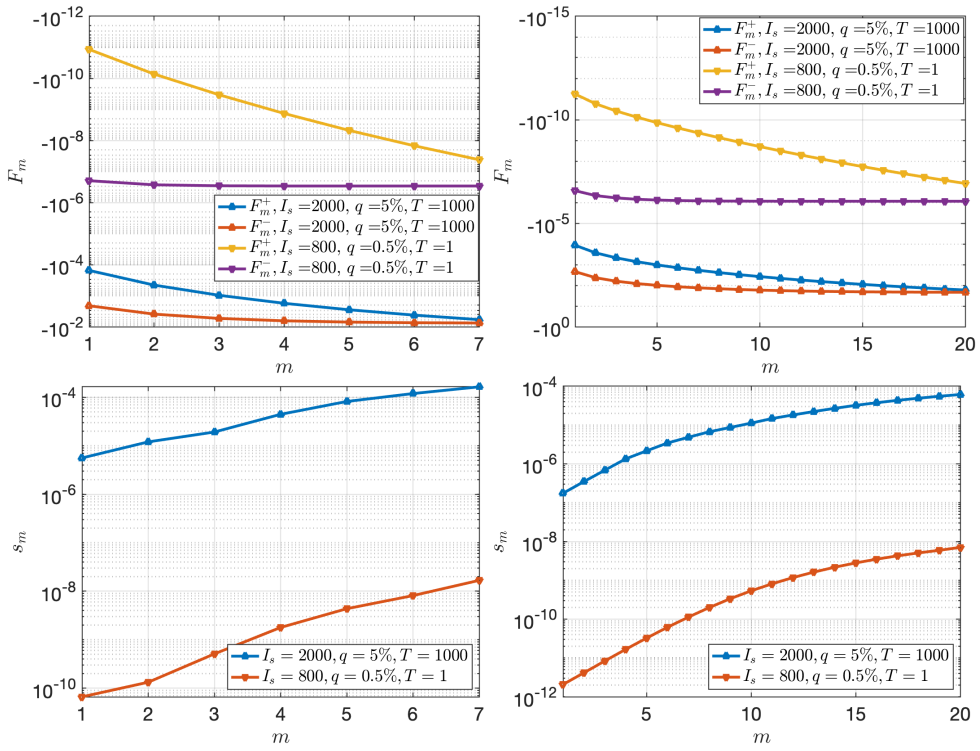

Figure 3.3: Example of sequences F_m^+, F_m^- (Top) and s_m (Bottom) with respect to m for the two parameters triplets. Left: $N = 7$. Right: $N = 20$.

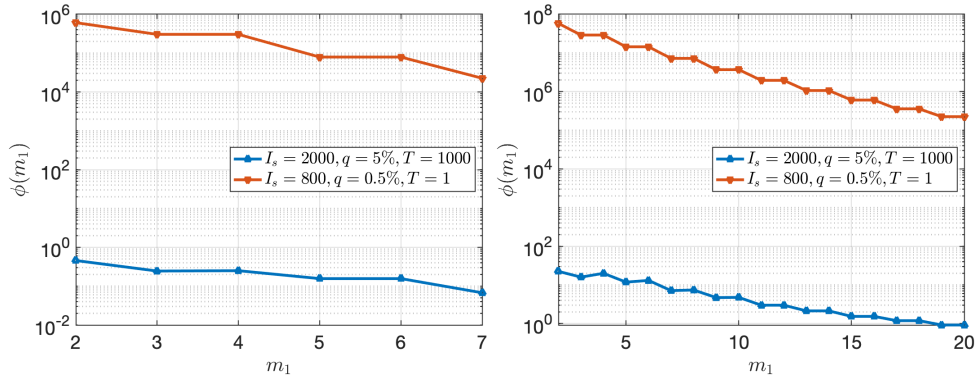

Figure 3.4: Example of behaviour of $\phi(m_1)$ with respect to m_1 for two parameters triplets and two different N. Left: $N = 7$. Right: $N = 20$.

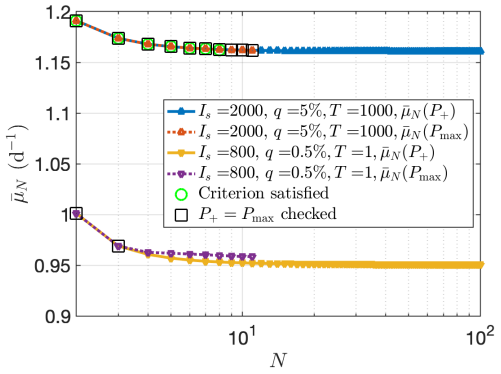

Figure 3.5: Average growth rate $\bar{\mu}_N$ obtained with $P_{\max}$ and P_+ as a function of N for the two parameters triplets. The green circles mark the case when the criterion is satisfied. The black squares mark the case when $P_{\max} = P_+$ is observed.

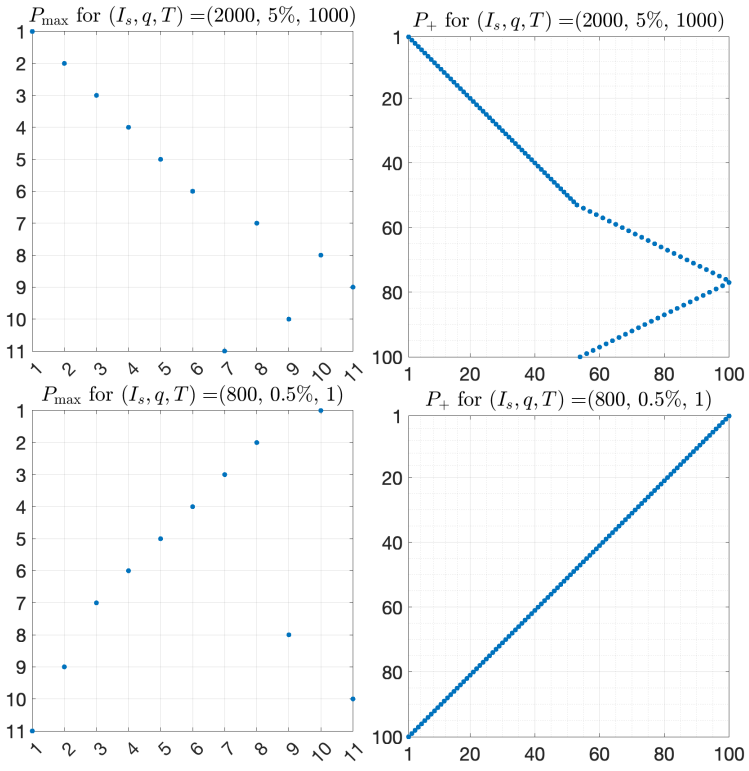

Figure 3.6: Optimal matrix $P_{\max}$ for Problem (3.6) and $N = 11$ (Left) and P_+ for Problem (3.7) and $N = 100$ (Right) for the two parameters triplets. The blue points represent non-zero entries, i.e., entries equal to 1.

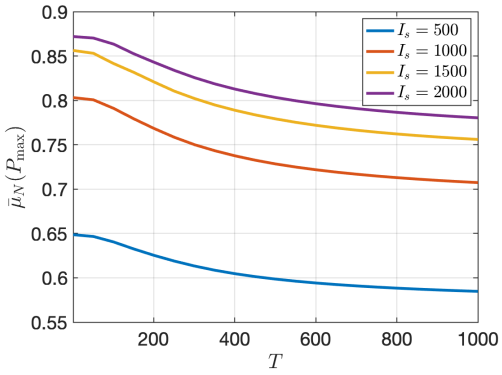

Figure 3.7: Average specific growth rate in the case $q = 0.1\%$ and $N = 7$ for four different light intensities I_s.

To assess the influence of the light intensity at the free surface I_s and the light attenuation ratio q, we compute $\bar{\mu}_N$ for the optimal strategy associated with $P_{\max}$. We consider again $N = 7$ layers, $I_s \in [0, 2500]$, $q \in [0.1\%, 10\%]$ and $T \in [1, 1000]$. The results are shown in Figure 3.8. We observe that for a fixed light intensity at surface (I_s), the influence of the time duration (T)

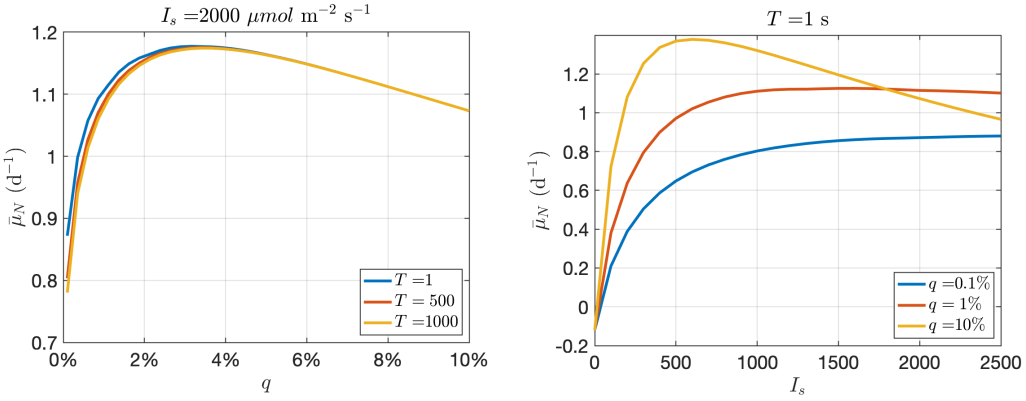

Figure 3.8: Average net specific growth rate $\bar{\mu}_N(P_{\max})$ for $q \in [0.1\%, 10\%]$ when $I_s = 2000\,\mu\text{mol}\,\text{m}^{-2}\,\text{s}^{-1}$ (Left) and for $I_s \in [0, 2500]$ when $T = 1\,\text{s}$ (Right).

is very weak. Moreover, there exists an optimal value for % of the transmitted light (q) which is around 3%. We also find that for small values of q, there exists a non-trivial optimal light intensity at surface, e.g., $I_s \approx 500\,\mu\text{mol}\,\text{m}^{-2}\,\text{s}^{-1}$ for $q = 0.1\%$.

We aim at now studying the influence of permutation strategies on the average of net specific growth rate $\bar{\mu}_N$. More precisely, we compute $\bar{\mu}_N$ for the next four strategies: the optimal matrix $P_{\max}$ that solves Problem (3.6), the worst matrix $P_{\min}$ which minimizes (3.6), the no permutation case where $P = I$ and the matrix P_+ which solves the approximate Problem (3.7). In our test, we consider $N = 7$ layers, $I_s \in [0, 2500]$, and $q \in [0.1\%, 10\%]$. Figure 3.9 presents the results for $T = 1\,\text{s}$, $T = 500\,\text{s}$ and $T = 1000\,\text{s}$.

We see that the original problem (3.6) and the approximated problem (3.7) coincide much more often for large values of the lap duration time T. In fact, the four surfaces become closer one to the others for large values of T.

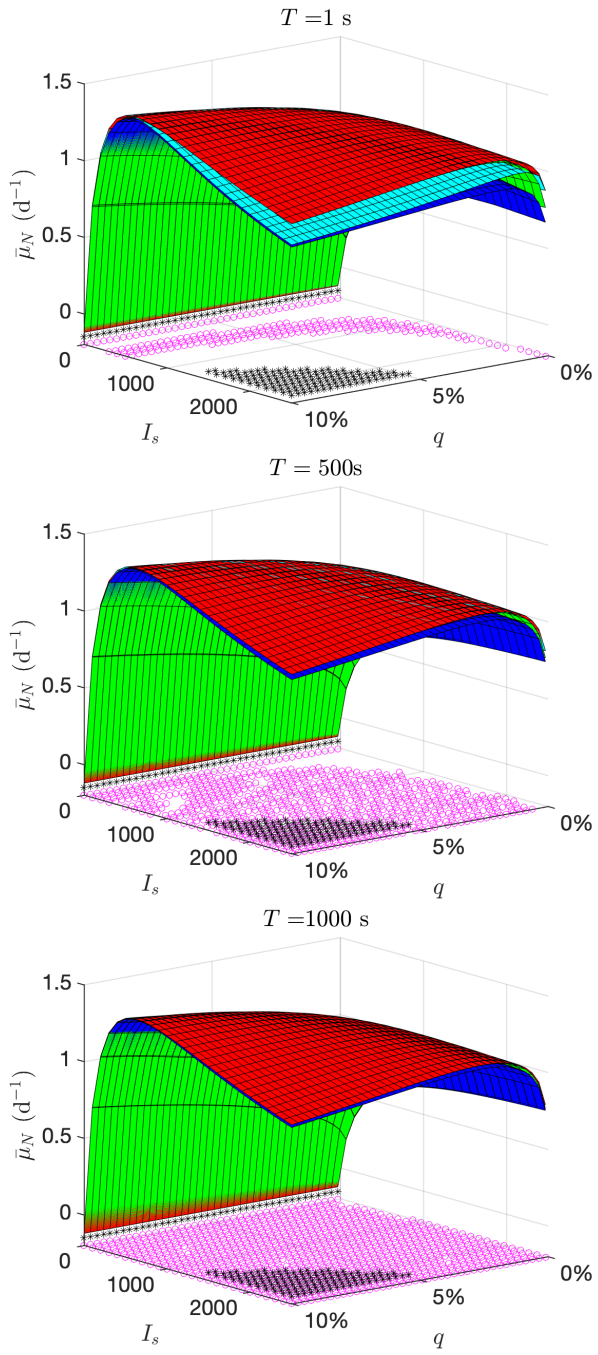

Figure 3.9: Average net specific growth rate $\bar{\mu}_N$ for $I_s \in [0, 2500]$ and $q \in [0.1\%, 10\%]$. In each figure, the red surface is obtained with $P_{\max}$, the dark blue surface is obtained with $P_{\min}$, the green surface is obtained with I and the light blue surface is obtained with P_+. The black stars represent the cases where $P_{\max} = I$ and the purple circles represent the cases where $P_{\max} = P_+$. Top: for $T = 1\,\mathrm{s}$. Middle: for $T = 500\,\mathrm{s}$. Bottom: for $T = 1000\,\mathrm{s}$.

The next test is dedicated to the efficiency of the criterion (3.15). More precisely, we evaluate the function $\bar{\mu}_N$ defined by (3.25) for the optimal matrix $P_{\max}$ which solves Problem (3.6) and for the matrix P_+ which solves the approximated Problem (3.7). We consider two different discretisation values $N = 5$ and $N = 9$. Figure 3.10 shows the results for $T = 1\,\mathrm{s}$ and $T = 1000\,\mathrm{s}$. We see that for large values of T, the optimum approximation almost always coincides to the true

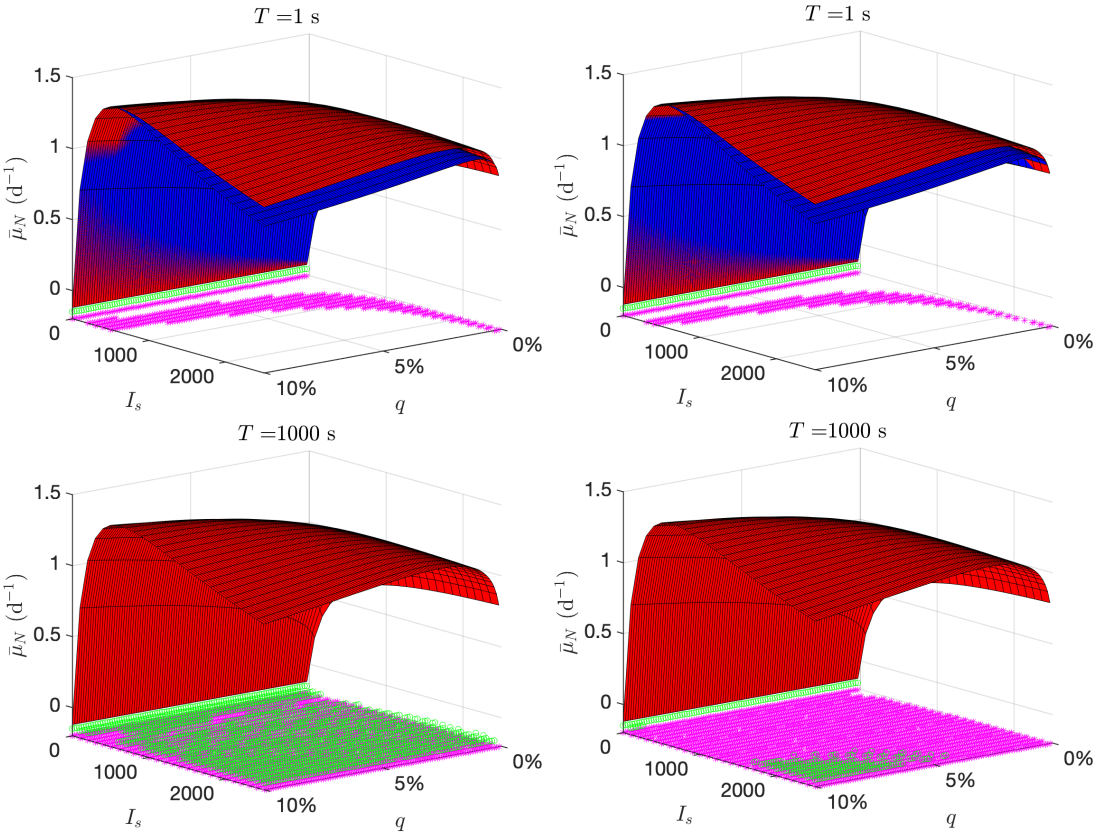

Figure 3.10: Average net specific growth rate $\bar{\mu}_N$ for $T = 1\,\mathrm{s}$ (Top) and for $T = 1000\,\mathrm{s}$ (Bottom). Left: $N = 5$. Right: $N = 9$. The red surface is obtained with $P_{\max}$ and the blue surface is obtained with P_+. The purple stars represent the cases where $P_{\max} = P_+$ or, in case of multiple solution, $\bar{\mu}_N(P_{\max}) = \bar{\mu}_N(P_+)$. The green circle represent the cases where the criterion (3.15) is satisfied.

optimum. Nevertheless, we observe that the criterion (3.15) becomes less efficient for larger N. Note that the case corresponding to $I_s = 0\,\mu\mathrm{mol\,m^{-2}\,s^{-1}}$ is particular since no light is available in the system, implying that Γ, V equal to zero. In this case the value of the functionals do not depend on P. Hence $\bar{\mu}_N(P_{\max}) = \bar{\mu}_N(P_+)$ when $I_s = 0\,\mu\mathrm{mol\,m^{-2}\,s^{-1}}$.

We finally evaluate the efficiency of various mixing strategies. Define

$$r_1 := \frac{\bar{\mu}_N(P_{\max}) - \bar{\mu}_N(I)}{\bar{\mu}_N(I)}, \tag{3.30}$$

$$r_2 := \frac{\bar{\mu}_N(P_{\max}) - \bar{\mu}_N(P_{\min})}{\bar{\mu}_N(P_{\min})}, \tag{3.31}$$

$$r_3 := \frac{\bar{\mu}_N(I) - \bar{\mu}_N(P_{\min})}{\bar{\mu}_N(I)}, \tag{3.32}$$

where $P_{\min} \in \mathcal{P}_N$ is the matrix that minimizes J, (see (3.6)), i.e., that corresponds to the worse strategy. We consider $N = 9$ layers. Figure 3.11 presents the results for $T = 1\,\mathrm{s}$ and $T = 1000\,\mathrm{s}$. Better performance is in most cases obtained for a small time duration $T = 1\,\mathrm{s}$. In this way, we

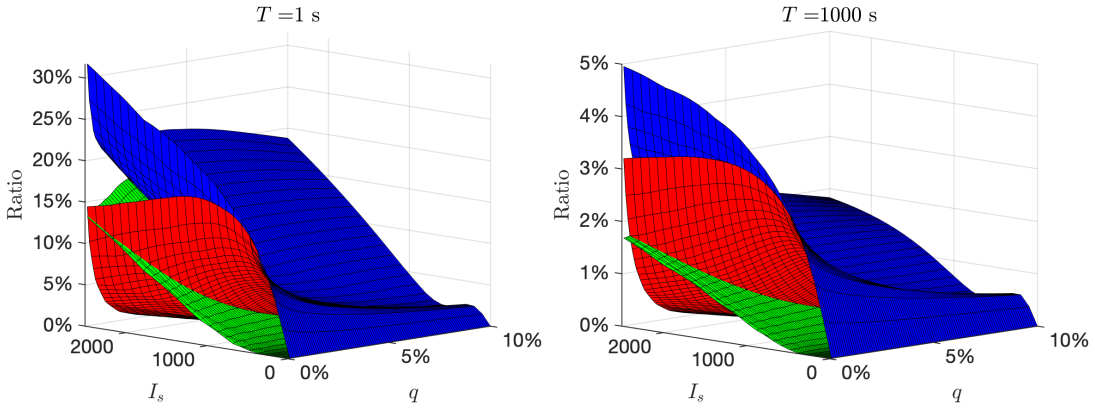

Figure 3.11: Three ratios (3.30)- (3.32) for $T = 1\,\mathrm{s}$ (Left) and for $T = 1000\,\mathrm{s}$ (Right). In each figure, the red surface represents r_1, the blue surface represents r_2 and the green surface represents r_3.

observe that the relative improvement between the best and the no mixing strategy may reach 15%, whereas the relative improvement between the worst and the best strategy may reach 30%. In both two cases, a better improvement can be obtained with high values of I_s and low values of q.

To compare the efficiency of the approximation P_+ with respect the true optimal mixing strategy $P_{\max}$, we define two extra ratios:

$$\tilde{r}_1 := \frac{\bar{\mu}_N(P_+) - \bar{\mu}_N(I)}{\bar{\mu}_N(I)}, \tag{3.33}$$

$$\tilde{r}_2 := \frac{\bar{\mu}_N(P_+) - \bar{\mu}_N(P_{\min})}{\bar{\mu}_N(P_{\min})}. \tag{3.34}$$

Figure 3.12 presents the results for $T = 1\,\mathrm{s}$ and $T = 1000\,\mathrm{s}$. As already mentioned, for a large lap duration time, the optimization problem (3.7) provides a good approximation.

This can be observed with the blue and red surface in Figure 3.11 (Right) and in Figure 3.12 (Right), both surfaces have the same behaviours. As expected, the approximation becomes less efficient in the case of short lap duration time. This can be observed in Figure 3.11 (Left) and in Figure 3.12 (Left). However, the maximal values of r_1, r_2 are still preserved by their approximations $\tilde{r}_1, \tilde{r}_2$. This is due to the fact that the maximal value is obtained at the extreme

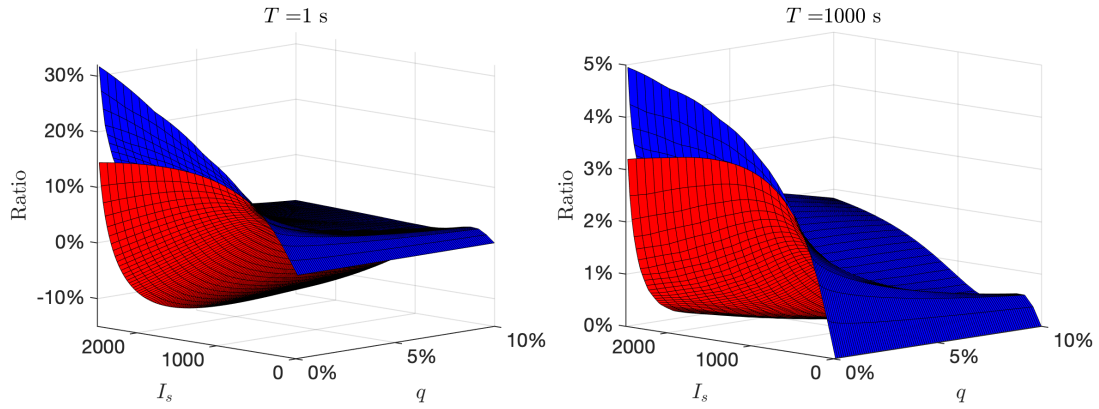

Figure 3.12: Two ratios (3.33)- (3.34) for $T = 1\,\mathrm{s}$ (Left) and for $T = 1000\,\mathrm{s}$ (Right). In each figure, the red surface represents $\tilde{r}_1$, the blue surface represents $\tilde{r}_2$.

case (i.e. $I_s = 2500\,\mu\mathrm{mol\,m^{-2}\,s^{-1}}$ and $q = 0.1\%$) where $\bar{\mu}_N(P_{\max}) = \bar{\mu}_N(P_+)$ as shown in Figure 3.10 (Top).

3.4 Conclusion

We have presented a periodic resource allocation problem combined with a linear dynamical system. The periodicity of the problem enables us to reduce the computation to one assignment process. A significant computational effort is still required when dealing with larger number of N. We overcome this difficulty by defining a second optimization problem which has an explicit solution that coincide with the true solution when a given criterion is satisfied.

This developed theory is then applied to a microalgal production system with a mixing device. Non-trivial optimal mixing strategies can be obtained and the proposed second optimization problem provides a reliable approximation for large time duration T. Meanwhile, our experimental results show the significance of the choice of the mixing strategy: the relative ratio between the best and the worst case reaches 30% in some cases. We also observe a flashing effect meaning that better results are obtained when T goes to zero.

Further works will be devoted to the improvement of the function ϕ used in Theorem 3.2.2 in order to improve our approach for large number of N. More complicated dynamical system can also be considered including nonlinearities.

3.A Explicit Computations

In this appendix, we provide the computational details to solve (3.1) and (3.25) for an arbitrary number $n \in \{1, \dots, N\}$. Given two points $t_1, t_2 \in [0, T]$. Since I_n is constant, Equation (3.1) can be integrated and becomes

$$x_n(t_2) = e^{\alpha(I_n)(t_1-t_2)} x_n(t_1) + \frac{\beta(I_n)}{\alpha(I_n)}(1 - e^{\alpha(I_n)(t_1-t_2)}). \tag{3.35}$$

The time integral in (3.25) can be computed by

$$\int_0^T \mu(C_n(t), I_n)\mathrm{d}t = \int_0^T -\gamma(I_n)C_n(t) + \zeta(I_n)\mathrm{d}t = -\gamma(I_n)\int_0^T C_n(t)\mathrm{d}t + \zeta(I_n)T.$$

Replacing x_n by C_n, t_2 by t and t_1 by 0 in (3.35) and integrating t from 0 to T gives

$$\begin{aligned}\int_0^T C_n(t)\mathrm{d}t =& \int_0^T \Big(e^{-\alpha(I_n)t}C_n(0) + \frac{\beta(I_n)}{\alpha(I_n)}(1-e^{-\alpha(I_n)t})\Big)\mathrm{d}t \\ =& \frac{C_n(0)}{\alpha(I_n)}(1-e^{-\alpha(I_n)T}) + \frac{\beta(I_n)}{\alpha(I_n)}T - \frac{\beta(I_n)}{\alpha^2(I_n)}(1-e^{-\alpha(I_n)T}).\end{aligned}$$

Using notations given in Section 3.3.1, we have

$$\Gamma = \frac{\gamma(I)}{\alpha(I)}(e^{-\alpha(I)T}-1), \quad V = \frac{\beta(I)}{\alpha(I)}(1-e^{-\alpha(I)T}).$$

From the definition of $\alpha(I), \beta(I), \gamma(I)$, we find

$$\begin{aligned}\frac{\beta(I)}{\alpha(I)} &= \frac{\beta(I)}{\beta(I)+k_r} = \frac{k_d\tau(\sigma_H I)^2}{k_d\tau(\sigma_H I)^2 + k_r\tau\sigma_H I + k_r}, \\ \frac{\gamma(I)}{\alpha(I)} &= \frac{k_H\sigma_H I}{k_d\tau(\sigma_H I)^2 + k_r\tau\sigma_H I + k_r}.\end{aligned}$$

Remark that Γ and V always have the opposite sign. Note also that $I \mapsto \frac{\beta(I)}{\alpha(I)}$ is increasing on $[0,+\infty)$, which is not the case for $I \mapsto \frac{\gamma(I)}{\alpha(I)}$. It follows that V increases on $\mathbb{R}^+$ and Γ is not monotonic on $\mathbb{R}^+$ (see Figure 3.2).

3.B Optimization problem with arbitrary vectors

Let $\tilde{u}, v \in \mathbb{R}^N$ two arbitrary vectors. Let $Q \in \mathcal{P}_N$ such that $u := Q\tilde{u}$ has entries sorted in an ascending order. Since Q is a permutation matrix, we have $Q^T = Q^{-1}$. For any $P \in \mathcal{P}_N$, let us denote by $\tilde{P} := Q^{-1}PQ$, we have $\tilde{P} \in \mathcal{P}_N$ a permutation matrix. Let us denote by $\tilde{v} := Q^{-1}v$ and by $\tilde{D} = Q^{-1}DQ$. Note that $\tilde{D}$ is still a diagonal matrix with a different order of the diagonal coefficients. Using this notation, we find for the objective function (3.6) satisfies

$$\begin{aligned}J(P) := \langle u, (\mathcal{I}_N - PD)^{-1}Pv\rangle &= \langle \tilde{u}, Q^{-1}(\mathcal{I}_N - PD)^{-1}QQ^{-1}PQQ^{-1}v\rangle \\ &= \langle \tilde{u}, \big(Q^{-1}(\mathcal{I}_N - PD)Q\big)^{-1}\tilde{P}\tilde{v}\rangle \\ &= \langle \tilde{u}, (Q^{-1}Q - Q^{-1}PQQ^{-1}DQ)^{-1}\tilde{P}\tilde{v}\rangle \\ &= \langle \tilde{u}, (\mathcal{I}_N - \tilde{P}\tilde{D})^{-1}\tilde{P}\tilde{v}\rangle.\end{aligned}$$

For the objective function (3.7), we get

$$J^{\text{approx}}(P) := \langle u, Pv\rangle = \langle \tilde{u}, Q^{-1}PQQ^{-1}v\rangle = \langle \tilde{u}, \tilde{P}\tilde{v}\rangle.$$

Therefore, these problems can still be treated similarly in the general case.

3.C Remark on F_m^+, F_m^-

Let $u, v \in \mathbb{R}^N$ such that the entries of u are sorted in an ascending order. One should be careful when defining the two sequences F_m^+ and F_m^- in Section 3.2.4, since the sign of u and v plays an important role in the definition of these two sequences. For instance, assume that u is now negative and v is positive. Let $\tilde{u} := -u$, since u is assumed to be sorted in an ascending order, $\tilde{u}$ is positive and sorted in a descending order. Using the definition in (3.13), one has

$$\tilde{F}_m^+ := \sum_{n=1}^{\min(m,N)} \tilde{u}_n v_{\tilde{\sigma}_+(n)}, \quad \tilde{F}_m^- := \sum_{n=\max(1,N-m+1)}^{N} \tilde{u}_n v_{\tilde{\sigma}_-(2N-m-n+1)},$$

where $v_{\tilde{\sigma}_+(1)} \geq v_{\tilde{\sigma}_+(2)} \geq, \ldots, \geq v_{\tilde{\sigma}_+(N)}$ and $v_{\tilde{\sigma}_-(1)} \leq v_{\tilde{\sigma}_-(2)} \leq, \ldots, \leq v_{\tilde{\sigma}_-(N)}$. Let us define by $\sigma_+ := \tilde{\sigma}_-$ and $\sigma_- := \tilde{\sigma}_+$. One has

$$\tilde{F}_m^+ = -\sum_{n=1}^{\min(m,N)} u_n v_{\sigma_-(n)}, \quad \tilde{F}_m^- = -\sum_{n=\max(1,N-m+1)}^{N} u_n v_{\sigma_+(2N-m-n+1)}.$$

Therefore, in this case we can define F_m^+ and F_m^- by

$$F_m^- := \sum_{n=1}^{\min(m,N)} u_n v_{\sigma_-(n)}, \quad F_m^+ := \sum_{n=\max(1,N-m+1)}^{N} u_n v_{\sigma_+(2N-m-n+1)}.$$

The case where u is positive and v is negative, or both u, v are negative can be treated in a similar way.

Chapter 4

Shape optimization of a microalgal raceway to enhance productivity

4.1 Introduction

Studies on the shape of the topography (or the bathymetry) have always been a challenging problem, since this problem usually involves the free-surface incompressible Navier-Stokes system, for instance see [23, 30, 118, 97]. In particular, explicit computation some time may be difficult to provide due to the complexity of the chosen model, meanwhile large computational resources are needed to provide numerical simulations and experimental results. The goal of this chapter is to investigate the influence of the topography in the raceway ponds. More precisely, we base on a common belief that some specific topographies can bring more light to the algae (at the lower part of the raceway), since they are closer to the surface when reaching the peak of these topographies.

In order to study this complex system, we develop a coupled model to describe the growth of algae in a raceway pond, accounting for the light that they receive. More precisely, this coupled model consists in combining the Han photosynthesis equations with an hydrodynamic law based on the Saint-Venant equations. This approach enables us to formulate an optimization problem where the raceway topography is designed to maximize the productivity. For this problem, we present an adjoint-based optimization scheme which includes the constraints associated with the Saint-Venant regime. On the contrary to a widespread belief, we prove that the flat topography is optimal in a periodic case for productivity in laminar regime. However, non-trivial topographies can be obtained in other contexts, e.g., when the periodic assumption is removed or an extra mixing strategy is included in the model. Note that in the examples considered in our numerical tests, such topographies only slightly improved the biomass production. Furthermore, some well chosen mixing strategies can boost this production.

The outline of this chapter is as follows. In Section 4.2, we present the biological and hydrodynamic models underlying our coupled model. Section 4.3 is devoted to the optimization problem and a corresponding numerical optimization procedure in different cases. We then provide some numerical results obtained with our approach in Section 4.4 and conclude in Section 4.5 with some perspectives opened by this work.

4.2 Coupling hydrodynamic and biological models

Our approach is based on a coupling between the hydrodynamic behavior of the particles and the evolution of the photosystems driven by the light intensity they received when traveling across the raceway pond.

4.2.1 Modeling the photosystems dynamics

We consider the Han model [59] which describes the dynamics of the reaction centres. These subunits of the photosynthetic process harvest photons and transfer their energy to the cell to fix CO_2. In this compartmental model, the photosystems can be described by three different states: open and ready to harvest a photon A, closed while processing the absorbed photon energy B, or inhibited if several photons have been absorbed simultaneously C. Their evolution satisfies the following dynamical system

$$\begin{cases} \dot{A} = -\sigma I A + \frac{B}{\tau}, \\ \dot{B} = \sigma I A - \frac{B}{\tau} + k_r C - k_d \sigma I B, \\ \dot{C} = -k_r C + k_d \sigma I B. \end{cases}$$

Here A, B and C are the relative frequencies of the three possible states with $A + B + C = 1$, and I is the photon flux density, a continuous time-varying signal. The other parameters are σ, that stands for the specific photon absorption, τ which is the turnover rate, k_r which represents the photosystem repair rate and k_d which is the damage rate. As shown in Subsection 1.2.1, one can reduce this system to a single evolution equation:

$$\dot{C} = -\alpha(I)C + \beta(I), \tag{4.1}$$

where $\alpha(I) = \beta(I) + k_r$ with $\beta(I) = k_d \tau \frac{(\sigma I)^2}{\tau \sigma I + 1}$. The net specific growth rate is obtained by balancing photosynthesis and respiration, which gives

$$\mu(C, I) = -\gamma(I)C + \zeta(I), \tag{4.2}$$

where $\zeta(I) = \gamma(I) - R$ with $\gamma(I) = \frac{k\sigma I}{\tau\sigma I + 1}$. Here, k is a factor that relates received energy with growth rate and the term R represents the respiration rate. In particular for a constant light intensity I, the growth rate μ associated with the steady state of (4.1) is given by

$$\mu(I) = -\gamma(I)C^*(I) + \zeta(I),$$

where

$$C^*(I) = \frac{\beta(I)}{\alpha(I)}. \tag{4.3}$$

In this framework, the dynamics of the biomass concentration X in an open system where a fraction of the biomass is continuously sampled and is derived from the growth rate μ:

$$\dot{X} = (\bar{\mu} - D)X, \tag{4.4}$$

where D is the dilution rate and $\bar{\mu}$ is the average net growth rate which will be defined later.

4.2.2 Steady 1D Saint-Venant equations

The Saint-Venant system is one of the most popular model for describing geophysical flows, which is derived from the free surface incompressible Navier-Stokes equations (see for instance [52]). In the current study, we focus on the smooth steady state solutions of the Saint-Venant equations in a laminar regime. Such steady states are governed by the following partial differential equations:

$$\partial_x(hu) = 0, \tag{4.5}$$

$$\partial_x(hu^2 + g\frac{h^2}{2}) = -gh\partial_x z_b, \tag{4.6}$$

where h is the water elevation, u is the horizontal averaged velocity of the water, the constant g stands for the gravitational acceleration, and z_b defines the topography. The free surface η is given by $\eta = h + z_b$ and the averaged discharge $Q = hu$. This system is presented in Figure 4.1. The z axis represents the vertical direction and the x axis represents the horizontal direction.

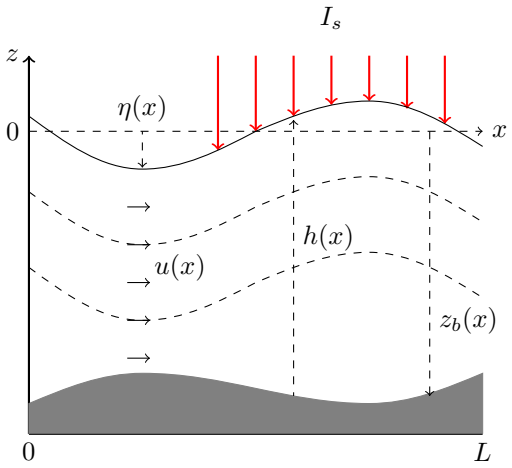

Figure 4.1: Representation of the hydrodynamic model.

Furthermore, I_s represents the light intensity at the free surface (assumed to be constant).

Integrating (4.5), we get

$$hu = Q_0, \tag{4.7}$$

for a fixed positive constant Q_0, which implies a constant discharge in space. Then (4.6) can be rewritten as

$$hu\partial_x u + h\partial_x gh + h\partial_x g z_b = 0. \tag{4.8}$$

Let us assume that h is strictly positive. Dividing (4.8) by h and using (4.7) to eliminate u, we get

$$\partial_x\Big(\frac{Q_0^2}{2h^2} + g(h + z_b)\Big) = 0.$$

This equation corresponds to the Bernoulli's principle. Now let us consider two fixed constants

$h(0), z_b(0) \in \mathbb{R}$. For all $x \in [0, L]$, we obtain

$$\frac{Q_0^2}{2h^2} + g(h + z_b) = \frac{Q_0^2}{2h^2(0)} + g(h(0) + z_b(0)) =: M_0,$$

meaning that the topography z_b satisfies

$$z_b = \frac{M_0}{g} - \frac{Q_0^2}{2gh^2} - h. \tag{4.9}$$

Remark

Define the Froude number for the steady state by $Fr = u/\sqrt{gh}$. The situation $Fr < 1$ corresponds to the subcritical case (i.e. the flow regime is fluvial) while $Fr > 1$ is to the supercritical case (i.e. the flow regime is torrential). In particular, the threshold value of h for $Fr = 1$ is given by

$$h_c := (\frac{Q_0^2}{g})^{\frac{1}{3}}.$$

Because of (4.9), the water depth h is the solution of a third order polynomial equation. Given a smooth topography z_b, if

$$h_c + z_b + \frac{Q_0^2}{2gh_c^2} - \frac{M_0}{g} < 0.$$

there exists a unique positive smooth solution of (4.9) which satisfies the subcritical flow condition (see [96, Lemma 1]). The velocity u can then be obtained thanks to (4.7).

4.2.3 Lagrangian trajectories of the algae and captured light intensity

Let $z(t)$ be the depth of a particle at time t in the raceway pond. We first determine the Lagrangian trajectory of an algal cell that starts at a given position $z(0)$ at time 0.

From the incompressibility of the flow, we have $\nabla \cdot \underline{\mathbf{u}} = 0$ with $\underline{\mathbf{u}} = (u(x), w(x, z))$. Here, $w(x, z)$ is the vertical velocity. This implies that

$$\partial_x u + \partial_z w = 0. \tag{4.10}$$

Integrating (4.10) from z_b to z gives:

$$\begin{aligned} 0 &= \int_{z_b}^{z} \big(\partial_x u(x) + \partial_z w(x, z)\big) \mathrm{d}z \\ &= \partial_x \int_{z_b}^{z} u(x) \mathrm{d}z + \int_{z_b}^{z} \partial_z w(x, z) \mathrm{d}z \\ &= \partial_x \big((z - z_b)u(x)\big) + w(x, z) - w(x, z_b) \\ &= (z - z_b)\partial_x u(x) - u(x)\partial_x z_b + w(x, z), \end{aligned}$$

where we have used the kinematic condition at the bottom (i.e. $w(x, z_b) = u(x)\partial_x z_b$). It then follows from (4.9) that

$$w(x, z) = (\frac{M_0}{g} - \frac{3u^2(x)}{2g} - z)u'(x).$$

The Lagrangian trajectory is characterized by the system

$$\begin{pmatrix} \dot{x}(t) \\ \dot{z}(t) \end{pmatrix} = \begin{pmatrix} u(x(t)) \\ w(x(t), z(t)) \end{pmatrix}. \tag{4.11}$$

Remark

The geometry of the raceway pond with small dissipation and shear effects (reduced wall friction and viscosity) justifies a laminar flow modelled by a shallow water model, such as the Saint-Venant system. This regime also minimizes the mixing energy, hence is favoured at industrial scale.
A higher mixing energy would lead to a turbulent regime. A possible way to enrich the representation of the Lagrangian trajectories in this case would consists in adding a Brownian motion to the definition (4.11). However, getting time-free expressions of the trajectories (as in Equations (4.12) and (4.16)) in this case is much more challenging so that such a strategy optimisation procedure would require a large set of simulations together with an averaging strategy.

The previous expression of the Lagrangian trajectory (4.11) is the general formulation which is still available even if we change the hydrodynamical model. However based on the special form of the Saint-Venant system that we have chosen, we can find a simpler formulation of the Lagrangian trajectory. More precisely, we denote by $z(x)$ the depth of a particle at the position x. From (4.11), we get

$$z' := \frac{\dot{z}}{\dot{x}} = (\frac{M_0}{g} - \frac{3u^2}{2g} - z)\frac{u'}{u}. \tag{4.12}$$

Note that from (4.7) and (4.9), we have $\eta = h + z_b = \frac{M_0}{g} - \frac{u^2}{2g}$, which implies $\eta' = -uu'/g$. Multiplying (4.12) both sides by u and using the formulation of η, η' gives

$$z'u + zu' = (\eta - \frac{u^2}{g})u' = \eta u' + \eta' u,$$

which implies that $\big(u(z-\eta)\big)' = 0$. We then obtain

$$z(x) = \eta(x) + \frac{u(0)}{u(x)}(z(0) - \eta(0)).$$

Using (4.7), then the equation above can be re-written as

$$z(x) = \eta(x) + \frac{h(x)}{h(0)}(z(0) - \eta(0)). \tag{4.13}$$

The computation of trajectories in the Saint-Venant system can be carried out with this formula, where $h(0)$, $z(0)$ and $\eta(0) = h(0) + z_b(0)$ are given as data of the system. On the contrary, $h(x), \eta(x)$ will depend on the parameterization of the system. Indeed, if we choose to parameterize the topography $z_b(x)$, then the water depth $h(x)$ can be found naturally by (4.9) and it will then be used to compute the free surface $\eta(x) = h(x) + z_b(x)$.

Remark

Since Q_0 is chosen to be positive, h is necessarily positive and so does u from (4.7). Moreover, from (4.13), if $z(0)$ belongs to $[z_b(0), \eta(0)]$, then $z(x)$ belongs to $[z_b(x), \eta(x)]$. In particular, choosing $z(0) = z_b(0)$ in (4.13) and using (4.7) gives $z(x) = z_b(x)$. In the same way, we find that $z(x) = \eta(x)$ when $z(0) = \eta(0)$.

We assume that the system is perfectly mixed such that the biomass concentration X in (4.4) is homogeneous. Furthermore, it is often assumed that the photosynthetic units grow slowly so that the variations of biomass concentration X and background turbidity α_1 are negligible over one lap of the raceway. As a consequence, the turbidity α_1 and the biomass concentration X are supposed to be constant over the considered time scale. In this framework, we use the Beer-Lambert law to describe the light intensity observed on the trajectory z:

$$I(x, z) = I_s \exp\Big(- \varepsilon(\eta(x) - z)\Big). \tag{4.14}$$

Here ε is the light extinction coefficient. Combining (4.14) with (4.13), we get the following expression for the captured light intensity along the trajectory z

$$I(x, z(x)) = I_s \exp\Big(- \varepsilon \frac{h(x)}{h(0)}(\eta(0) - z(0))\Big). \tag{4.15}$$

It follows that in this approach, the light intensity I couples the hydrodynamic model and Han model: the hydrodynamical movement provides the trajectories of the algae and then define the received light intensity, which is used in the photosystem dynamics.

We can then derive the equation satisfied by C. Indeed, repeating the reasoning done to get (4.12) with (4.1), we find a time-free reformulation, namely

$$C' := \frac{\dot{C}}{\dot{x}} = -\frac{\alpha(I)}{Q_0} hC + \frac{\beta(I)}{Q_0} h, \tag{4.16}$$

where all functions on the right-hand side only depend on x.

4.3 Optimization problem

In this section, we define the optimization problem associated with the biological-hydrodynamical model. We first introduce our procedure in the case of one single layer, and then extend this to a multiple layers system. The volume of our 1D system V [m^2] is defined by

$$V = \int_0^L h(x) \mathrm{d}x. \tag{4.17}$$

And as we have mentioned in Subsection 4.2.2, a given topography z_b corresponds to a unique water depth h in the subcritical case. Therefore, we choose to parameterize h by a vector $a \in \mathbb{R}^N$, which will be the variable to be optimized, in order to handle the volume of our system. In this way, we assume the volume is constant with respect to the parameter a. Given a vector a and the associated h, the optimal topography can be obtained by means of (4.9).

Remark

In usual Saint-Venant solver, equations of type (4.9) are usually consider to compute water depth h for a given topography z_b in the simulations. Here, we use this equation in the opposite way, i.e., to recover the topography z_b from water depth h.

4.3.1 Optimization problem for non periodic case with time dependent description

In this section, we study the optimization problem for the time dependent description. Note that in this case the Lagrangian trajectory is defined by (4.11) and the photoinhibition state is defined by (4.1). For sake of clarity, we first present the formulation of the optimization problem for a single trajectory, then we generalize it for multiple trajectories. For simplicity, we omit t in the notations.

One single trajectory

Our goal here is to optimize the topography to maximize the average net growth rate for one trajectory $\bar{\mu}_1$ which is defined by

$$\bar{\mu}_1(a) = \frac{1}{T}\int_0^T -\gamma(I(x,z;a))C + \zeta(I(x,z;a))\mathrm{d}t,$$

where C, x, z satisfy

$$\begin{cases} \dot{C} = -\alpha(I(x,z;a))C + \beta(I(x,z;a)) \\ \dot{x} = u(x;a) \\ \dot{z} = w(x,z;a). \end{cases} \tag{4.18}$$

The optimal control problem then reads:

Find $a^\star$ solving the maximization problem:

$$\max_{a\in\mathbb{R}^N} \bar{\mu}_1(a). \tag{4.19}$$

In order to solve this optimization problem, we apply the technique presented in Subsection 1.4. More precisely, define the Lagrangian of Problem (4.19) by

$$\begin{aligned} \mathcal{L}(C,z,x,p_1,p_2,p_3,a) := \frac{1}{T}\int_0^T \big(-\gamma(I(x,z;a))C + \zeta(I(x,z;a))\big)\mathrm{d}t \\ - \int_0^T p_1\big(\dot{C} + \alpha(I(x,z;a))C - \beta(I(x,z;a))\big)\mathrm{d}t \\ - \int_0^T p_2\big(\dot{z} - w(x,z;a)\big)\mathrm{d}t - \int_0^T p_3\big(\dot{x} - u(x;a)\big)\mathrm{d}t. \end{aligned}$$

where p_1, p_2 and p_3 are the Lagrange multipliers associated with the constraints (4.18).

The optimality system is obtained by cancelling all the partial derivatives of $\mathcal{L}$. Differentiating $\mathcal{L}$ with respect to p_1, p_2, p_3 and equating the resulting terms to zero gives the corrected model equations (4.18). Integrating the terms $\int p_1\dot{C}\mathrm{d}t$, $\int p_2\dot{z}\mathrm{d}t$ and $\int p_3\dot{x}\mathrm{d}t$ on the interval $[0,T]$ by

parts and differentiating $\mathcal{L}$ with respect to $C, z, x, C(T), z(T), x(T)$ gives rise to

$$\begin{cases} \partial_C \mathcal{L} = -\frac{1}{T}\gamma(I) + \dot{p}_1 - \alpha(I)p_1 \\ \partial_z \mathcal{L} = \Big(\frac{1}{T}\big(-\gamma'(I)C + \zeta'(I)\big) + p_1\big(-\alpha'(I)C + \beta'(I)\big)\Big)\partial_z I + \dot{p}_2 + p_2\partial_z w \\ \partial_x \mathcal{L} = \Big(\frac{1}{T}\big(-\gamma'(I)C + \zeta'(I)\big) + p_1\big(-\alpha'(I)C + \beta'(I)\big)\Big)\partial_x I + p_2\partial_x w + \dot{p}_3 + p_3\partial_x u \\ \partial_{C(T)}\mathcal{L} = p_1(T) \\ \partial_{z(T)}\mathcal{L} = p_2(T) \\ \partial_{x(T)}\mathcal{L} = p_3(T). \end{cases} \tag{4.20}$$

Given a vector a, let us still denote by C, x, z, p_1, p_2, p_3 the corresponding solutions of (4.18) and (4.20). The gradient $\nabla\bar{\mu}_1(a)$ is obtained by

$$\nabla\bar{\mu}_1(a) = \partial_a \mathcal{L},$$

where

$$\partial_a \mathcal{L} = \int_0^T \Big(\frac{1}{T}\big(-\gamma'(I)C + \zeta'(I)\big) + p_1\big(-\alpha'(I)C + \beta'(I)\big)\Big)\partial_a I + p_2\partial_a w + p_3\partial_a u \mathrm{d}t. \tag{4.21}$$

Remark

Note that in one trajectory case, all the formulations above are presented in continuous form which may not be the case for multiple trajectories.

Multiple trajectories Problem

We now extend the previous procedure to deal with multiple layers. Let us denote by N_z the number of layers and C_i the photoinhibition state associated with the trajectory z_i. We consider the semi-discrete average net growth rate over the domain as the objective function, namely:

$$\bar{\mu}_{N_z}(a) = \frac{1}{N_z}\sum_{i=1}^{N_z}\frac{1}{T}\int_0^T \mu(C_i, I_i(a))\mathrm{d}t, \tag{4.22}$$

where C_i, x, z_i verify the constraints (4.18) for $i = 1, \ldots, N_z$.

Remark

Note that the average net growth rate over the domain is defined by:

$$\bar{\mu}_\infty := \frac{1}{T}\int_0^T \frac{1}{h\left(x(t)\right)}\int_{z_b(x(t))}^{\eta(x(t))} \mu\big(C\left(x(t), z(t)\right), I\left(x(t), z(t)\right)\big)\mathrm{d}z\mathrm{d}t. \tag{4.23}$$

Our approach consequently consists in considering a vertical discretization of $\bar{\mu}_\infty$, which gives (4.22). This discretization should not give rise to any problem and is left to Subsection 4.3.2 for further details.

The Lagrangian of the problem is defined by

$$\begin{aligned}\mathcal{L}(C_i, z_i, x, p_{1,i}, p_{2,i}, p_3, a) := \frac{1}{TN_z}\sum_{i=1}^{N_z}\int_0^T -\gamma(I(x,z_i;a))C_i + \zeta(I(x,z_i;a))\mathrm{d}t \\ -\sum_{i=1}^{N_z}\int_0^T p_{1,i}\big(\dot{C}_i + \alpha(I(x,z_i;a))C_i - \beta(I(x,z_i;a))\big)\mathrm{d}t \\ -\sum_{i=1}^{N_z}\int_0^T p_{2,i}\big(\dot{z}_i - w(x,z_i;a)\big)\mathrm{d}t - \int_0^T p_3\big(\dot{x} - u(x;a)\big)\mathrm{d}t.\end{aligned}$$

where $p_{1,i}, p_{2,i}, p_3$ the associated Lagrange multipliers with C_i, z_i, x respectively. Similar computations as in the previous section give rise to the following systems

$$\begin{cases}\partial_{C_i}\mathcal{L} = -\frac{1}{TN_z}\gamma(I_i) + \dot{p}_{1,i} - \alpha(I_i)p_{1,i} \\ \partial_{z_i}\mathcal{L} = \Big(\frac{1}{TN_z}\big(-\gamma'(I_i)C_i + \zeta'(I_i)\big) + p_{1,i}\big(-\alpha'(I_i)C_i + \beta'(I_i)\big)\Big)\partial_{z_i}I_i + \dot{p}_{2,i} + p_{2,i}\partial_z w \\ \partial_x\mathcal{L} = \displaystyle\sum_{i=1}^{N_z}\Big(\frac{1}{TN_z}\big(-\gamma'(I_i)C_i + \zeta'(I_i)\big) + p_{1,i}\big(-\alpha'(I_i)C_i + \beta'(I_i)\big)\Big)\partial_x I_i \\ \qquad + \displaystyle\sum_{i=1}^{N_z} p_{2,i}\partial_x w_i + \dot{p}_3 + p_3\partial_x u \\ \partial_{C_i(T)}\mathcal{L} = p_{1,i}(T) \\ \partial_{z_i(T)}\mathcal{L} = p_{2,i}(T) \\ \partial_{x(T)}\mathcal{L} = p_3(T)\end{cases}$$

where $I_i := I(x, z_i; a)$ and $w_i := w(x, z_i; a)$. Finally, the gradient $\nabla\bar{\mu}_{N_z}(a)$ is given by

$$\begin{aligned}\partial_a\mathcal{L} = &\sum_{i=1}^{N_z}\int_0^T \Big(\frac{1}{TN_z}\big(-\gamma'(I_i)C_i + \zeta'(I_i)\big) + p_{1,i}\big(-\alpha'(I_i)C_i + \beta'(I_i)\big)\Big)\partial_a I_i\mathrm{d}t \\ &+\sum_{i=1}^{N_z}\int_0^T p_{2,i}\partial_a w_i\mathrm{d}t + \int_0^T p_3\partial_a u\mathrm{d}t.\end{aligned}$$

4.3.2 Optimization problem for periodic case with time independent description

In this section, we study the optimization problem for the time independent description. Note that in this case the Lagrangian trajectory is defined by (4.13) and the photoinhibition state is defined by (4.16). We first present the formulation of the optimization problem then we add periodic assumption to investigate the optimal topography in this case.

Optimality system

The parameter-dependent average net growth rate over the domain is defined by

$$\bar{\mu}_\infty(a) := \frac{1}{V}\int_0^L \int_{z_b(x;a)}^{\eta(x;a)} \mu\big(C(x,z), I(x,z;a)\big)\mathrm{d}z\mathrm{d}x, \tag{4.24}$$

Note that this formulation is actually the same as (4.23) (see Appendix 4.B). In order to tackle numerically this optimization problem, let us consider a vertical discretization. Let us keep N_z as the number of particles, and consider a uniform vertical discretization of their initial position:

$$z_i(0) = \eta(0) - \frac{i - \frac{1}{2}}{N_z} h(0), \quad i = 1, \dots, N_z.$$

From (4.13), we obtain

$$z_i(x) - z_{i+1}(x) = \frac{1}{N_z} h(x), \quad i = 1, \dots, N_z,$$

meaning that the distribution of particles remains uniform along the trajectories. To simplify notations, we write $I_i(a)$ instead of $I(x, z_i(x); a)$ hereafter. Then the semi-discrete average net specific growth rate in the raceway pond can be defined from (4.24) by

$$\bar{\mu}_{N_z}(a) := \frac{1}{V} \int_0^L \sum_{i=1}^{N_z} \frac{1}{N_z} h(a) \mu(C_i, I_i(a)) \mathrm{d}x = \frac{1}{V N_z} \sum_{i=1}^{N_z} \int_0^L \mu(C_i, I_i(a)) h(a) \mathrm{d}x. \tag{4.25}$$

where C_i satisfies the following parameterized version of (4.16)

$$C_i' = \left(-\alpha\left(I_i(a)\right) C_i + \beta\left(I_i(a)\right)\right) \frac{h(x;a)}{Q_0}. \tag{4.26}$$

Remark

One of the advantages of the time free formulation is that this expression helps us to reduce the computational cost. Indeed, in this case the optimization constraint (4.26) reduces to one single constraint comparing to the constraints (4.18) in time dependent formulation.

In this case, the optimization problem reads:

Find a^* solving the maximization problem:

$$\max_{a \in \mathbb{R}^N} \bar{\mu}_{N_z}(a). \tag{4.27}$$

The Lagrangian of the problem is then defined by

$$\mathcal{L}(C_i, a, p_i) = \sum_{i=1}^{N_z} \int_0^L \Big(\frac{1}{V N_z} \big(-\gamma(I_i(a)) C_i + \zeta(I_i(a)) \big) h(a) - p_i \big(C_i' + \frac{\alpha(I_i(a)) - \beta(I_i(a))}{Q_0} h(a) \big) \Big) \mathrm{d}x$$

where p_i the associated Lagrange multipliers. Similar computations as in the previous section give rise to the following systems

$$\begin{cases} \partial_{C_i} \mathcal{L} = -\frac{1}{V N_z} \gamma(I_i) h + p_i' - \frac{\alpha(I_i)}{Q_0} h p_i, \\ \partial_{C_i(T)} \mathcal{L} = p_i(T). \end{cases} \tag{4.28}$$

As we have mentioned above, one can also see that the optimality system has been much simplified comparing to (4.20).

Finally, the partial derivative $\partial_a \mathcal{L}$ (hence the gradient $\nabla \bar{\mu}_{N_z}(a)$) is then given by

$$\begin{aligned}\partial_a \mathcal{L} =& \sum_{i=1}^{N_z} \int_0^L \Big(\frac{1}{VN_z} \big(-\gamma'(I_i) C_i + \zeta'(I_i) \big) + p_i \frac{-\alpha'(I_i) C_i + \beta'(I_i)}{Q_0} \Big) h \partial_a I_i \mathrm{d}x \\ &+ \sum_{i=1}^{N_z} \int_0^L \Big(\frac{1}{VN_z} \big(-\gamma(I_i) C_i + \zeta(I_i) \big) + p_i \frac{-\alpha(I_i) C_i + \beta(I_i)}{Q_0} \Big) \partial_a h \mathrm{d}x.\end{aligned} \tag{4.29}$$

Periodic problem

We now consider a variant of our problem, where the photoinhibition state C is periodic, with a period corresponding to a raceway lap. This situation occurs, e.g., when an appropriate harvest is performed after each lap. To describe the corresponding model, let us first consider a variant of the usual Cauchy problem for (4.16):

Given $I \in L^2(0, L; \mathbb{R})$, find $(C_0, C) \in [0,1] \times \mathcal{C}(0, L; [0,1])$ such that

$$\begin{cases} C'(x) = \frac{-\alpha(I(x))C(x) + \beta(I(x))}{Q_0} h(x), \quad x \in [0, L] \\ C(L) = C(0) = C_0. \end{cases} \tag{4.30}$$

A similar theorem as Theorem 1.3.2 gives the existence and uniqueness of a (weak) solution of the problem (4.30).

Theorem 4.3.1. *Given $I \in L^2(0, L; \mathbb{R})$, there exists a unique couple $(C_0, C) \in [0,1] \times \mathcal{C}(0, L; [0,1])$ satisfying*

$$\begin{cases} C(x) = C_0 + \int_0^x \frac{-\alpha(I(s))C(s) + \beta(I(s))}{Q_0} h(s) \mathrm{d}s \quad , \\ C(L) = C_0 \end{cases} \tag{4.31}$$

for all $x \in [0, L]$.

The proof follows the same technique given in Subsection 1.3. The optimality system in this case is obtained as shown in the previous sections.

Remark

Note that the periodicity of C_i implies that p_i is also periodic. Indeed, since $C_i(L) = C_i(0)$, then by differentiating $\mathcal{L}$ with respect to $C_i(L)$, we have

$$\partial_{C_i(L)} \mathcal{L} = p_i(L) - p_i(0),$$

so that equating the above equation to zero gives the periodicity for p_i.

Next, we state a result in the case $(C_i)_{i=1,\dots,N_z}$ are periodic.

Theorem 4.3.2. *Assume the volume of the system V is constant. Then $\nabla \bar{\mu}_{N_z}(0) = 0$.*

Proof. Replacing the formulation for z_i (4.13) in (4.14) gives

$$I_i(a) = I_s \exp(-\varepsilon \frac{i - \frac{1}{2}}{N_z} h(a)). \tag{4.32}$$

The partial derivative of I with respect to a gives

$$\partial_a I_i = -\varepsilon \frac{i - \frac{1}{2}}{N_z} I_i \partial_a h.$$

Consider now the vector a_f for representing the parameter in the case where the topography is flat. In this way, the water depth $h(a_f)$ hence the light intensity $I_i(a_f)$ are all constant with respect to x that denote by h_f and I_i^f respectively. For a given $C(0)$, (4.26) gives

$$C_i(x) = e^{-\frac{\alpha(I_i(a_f))}{Q_0}h(a_f)x}C_i(0) + \frac{\beta(I_i(a_f))}{\alpha(I_i(a_f))}(1 - e^{-\frac{\alpha(I_i(a_f))}{Q_0}h(a_f)x}). \tag{4.33}$$

Since C_i are periodic (i.e. $C_i(L) = C_i(0)$), we get from the previous equation that $C_i(0) = \frac{\beta(I_i(a_f))}{\alpha(I_i(a_f))}$. Inserting this value in (4.33), we find

$$C_i(x) = \frac{\beta(I_i(a_f))}{\alpha(I_i(a_f))}, \quad \forall x \in [0, L],$$

which corresponds to the steady state (4.3), that we denote by C_i^f hereafter. Similar operations applying on the dynamics of p_i

$$p_i' = \frac{1}{VN_z}\gamma(I_i)h + \frac{\alpha(I_i)}{Q_0}hp_i,$$

gives

$$p_i(x) = -\frac{Q_0\gamma(I_i(a_f))}{VN_z\alpha(I_i(a_f))}, \quad \forall x \in [0, L],$$

that denote by p_i^f hereafter.

On the other hand, since the volume of the system is assumed to be constant with respect to a, one has

$$0 = \partial_a V = \partial_a \int_0^L h(x; a)\mathrm{d}x = \int_0^L \partial_a h \mathrm{d}x.$$

Replacing a by a_f in (4.29) gives

$$\begin{aligned}
\nabla\bar{\mu}_{N_z}(a_f) =& \sum_{i=1}^{N_z}\int_0^L \Big(\frac{1}{VN_z}\big(-\gamma'\left(I_i^f\right)C_i^f + \zeta'\left(I_i^f\right)\big) + p_i^f\frac{-\alpha'(I_i^f)C_i^f + \beta'(I_i^f)}{Q_0}\Big)h_f\big(-\varepsilon\frac{i-\frac{1}{2}}{N_z}I_i^f\big)\partial_a h\mathrm{d}x \\
&+ \sum_{i=1}^{N_z}\int_0^L \Big(\frac{1}{VN_z}\big(-\gamma\left(I_i^f\right)C_i^f + \zeta\left(I_i^f\right)\big) + p_i^f\frac{-\alpha(I_i^f)C_i^f + \beta(I_i^f)}{Q_0}\Big)\partial_a h\mathrm{d}x \\
=& \sum_{i=1}^{N_z}\Big[\Big(\frac{1}{VN_z}\big(-\gamma'\left(I_i^f\right)C_i^f + \zeta'\left(I_i^f\right)\big) + p_i^f\frac{-\alpha'(I_i^f)C_i^f + \beta'(I_i^f)}{Q_0}\Big)h_f\big(-\varepsilon\frac{i-\frac{1}{2}}{N_z}I_i^f\big) \\
&+ \Big(\frac{1}{VN_z}\big(-\gamma\left(I_i^f\right)C_i^f + \zeta\left(I_i^f\right)\big) + p_i^f\frac{-\alpha(I_i^f)C_i^f + \beta(I_i^f)}{Q_0}\Big)\Big]\int_0^L \partial_a h\mathrm{d}x \\
=& 0.
\end{aligned}$$

This concludes the proof. □

Remark

This theorem consequently shows that in the case C periodic, the flat topography is a critical point for Problem (4.27). On the contrary, in the case C non periodic, (4.33) implies that C depends also on the space variable x, hence the computations above will no longer hold. In other words, the flat topography is not an optimum for the case C non periodic, These has been confirmed by our numerical tests. In particular, we have observed that the flat topography is actually optimal in the periodic case (see Subsection 4.4.3).

4.3.3 Optimization for non-constant volume problem

In this section, we focus on the case where the volume of the system also changes hence can be optimized. Let us define a volume related parameter a_0 as the average depth of the raceway system:

$$a_0 := \frac{1}{L}\int_0^L h(x)\mathrm{d}x = \frac{V}{L}. \tag{4.34}$$

In this way, the biomass concentration changes with the system volume, therefore the light extinction ε can no longer be assumed as a constant. Hence, we consider the general form of ε as shown in (1.17). As mentioned in Chapter 2, one of the solution to find the relation between the biomass concentration X with the system volume V is to use the optimal optical depth Y_{opt} defined by (2.9). This consists in regulating the biomass concentration X to a value such that the steady state value of the net growth rate μ at the average depth a_0 is 0, i.e.

$$\mu(I_{a_0}) = 0. \tag{4.35}$$

This gives us the following relation:

$$Y_{\text{opt}} = \varepsilon(X)a_0 = (\alpha_0 X + \alpha_1)a_0,$$

or in other words

$$X = \frac{\frac{Y_{\text{opt}}}{a_0} - \alpha_1}{\alpha_0}.$$

Optimize areal productivity

In this framework, maximizing areal productivity is a relevant target. Productivity per unit of surface for a given biomass concentration X is given by:

$$\Pi := \bar{\mu} X \frac{V}{S},$$

where S is the ground surface of the raceway pond and $\bar{\mu}$ is defined in (4.24). Note that this is a general form of the surface biomass productivity defined in (2.6).

Note that the water depth h now depends both on the parameter a and a_0, which we will denote by the extended parameter vector $\tilde{a} = [a_0, a] \in \mathbb{R}^{N+1}$ hereafter. Moreover, since we consider a 1D framework, we have $S = L$. Let us consider the parameter-dependent objective function:

$$\Pi(\tilde{a}) = \frac{Y_{\text{opt}} - \alpha_1 a_0}{\alpha_0}\frac{1}{VN_z}\sum_{i=1}^{N_z}\int_0^L \mu(C_i, I_i(\tilde{a}))h(\tilde{a})\mathrm{d}x,$$

where C_i satisfies (4.26) with a replacing by $\tilde{a}$.

The corresponding optimization problem reads:

Find $\tilde{a}^*$ solving the maximization problem:

$$\max_{\tilde{a}\in\mathbb{R}^{N+1}} \Pi(\tilde{a}).$$

The Lagrangian associated with this problem reads as

$$\begin{aligned}\mathcal{L}(C_i,p_i,\tilde{a}) = \frac{Y_{\text{opt}}-\alpha_1 a_0}{VN_z\alpha_0}\sum_{i=1}^{N_z}\int_0^L \big(-\gamma(I_i(\tilde{a}))C_i+\zeta(I_i(\tilde{a}))\big)h(\tilde{a})\mathrm{d}x\\ -\sum_{i=1}^{N_z}\int_0^L p_i\big(C_i'+\frac{\alpha(I_i(\tilde{a}))C_i-\beta(I_i(\tilde{a}))}{Q_0}h(\tilde{a})\big)\mathrm{d}x,\end{aligned}$$

where p_i is the Lagrangian multiplier associated with the constraint (4.26) for C_i. By computations similar to that of the previous section, we find the optimality system as

$$\begin{cases}\partial_{C_i}\tilde{\mathcal{L}} = p_i' - p_i\frac{\alpha(I)}{Q_0}h-\gamma(I)h\frac{Y_{\text{opt}}-\alpha_1 a_0}{VN_z\alpha_0}\\ \partial_{C_i(L)}\tilde{\mathcal{L}} = p_i(L).\end{cases}$$

However, there is an extra element in the gradient $\Pi(\tilde{a})$, namely the derivative with respect to a_0, meaning that $\nabla\Pi(\tilde{a}) := [\partial_{a_0}\mathcal{L},\partial_a\mathcal{L}]$, where

$$\begin{aligned}\partial_{a_0}\mathcal{L} =&\sum_{i=1}^{N_z}\int_0^L\Big(\frac{Y_{\text{opt}}/a_0-\alpha_1}{LN_z\alpha_0}\big(-\gamma'(I_i)C_i+\zeta'(I_i)\big)+p_i\frac{-\alpha'(I_i)C_i+\beta'(I_i)}{Q_0}\Big)h\partial_{a_0}I_i\mathrm{d}x\\ &+\sum_{i=1}^{N_z}\int_0^L\Big(\frac{Y_{\text{opt}}/a_0-\alpha_1}{LN_z\alpha_0}\big(-\gamma(I_i)C_i+\zeta(I_i)\big)+p_i\frac{-\alpha(I_i)C_i+\beta(I_i)}{Q_0}\Big)\partial_{a_0}h\mathrm{d}x\\ &-\sum_{i=1}^{N_z}\int_0^L\frac{Y_{\text{opt}}/a_0^2}{LN_z\alpha_0}\big(-\gamma(I_i)C_i+\zeta(I_i)\big)h\mathrm{d}x.\end{aligned}\tag{4.36}$$

$$\begin{aligned}\partial_{a}\mathcal{L} =&\sum_{i=1}^{N_z}\int_0^L\Big(\frac{Y_{\text{opt}}-\alpha_1 a_0}{VN_z\alpha_0}\big(-\gamma'(I_i)C_i+\zeta'(I_i)\big)+p_i\frac{-\alpha'(I_i)C_i+\beta'(I_i)}{Q_0}\Big)h\partial_{a}I_i\mathrm{d}x\\ &+\sum_{i=1}^{N_z}\int_0^L\Big(\frac{Y_{\text{opt}}-\alpha_1 a_0}{VN_z\alpha_0}\big(-\gamma(I_i)C_i+\zeta(I_i)\big)+p_i\frac{-\alpha(I_i)C_i+\beta(I_i)}{Q_0}\Big)\partial_{a}h\mathrm{d}x..\end{aligned}\tag{4.37}$$

Periodic problem

Note that the water depth h for a flat topography is a constant (meaning that vector $a=\mathbf{0}$). From the definition of a_0 (4.34), one has in particular

$$h(x;[a_0,\mathbf{0}]) = a_0,\quad \forall x\in[0,L],$$

which means that there exists a function h_1 such that

$$h(x;\tilde{a}) := a_0 + h_1(x;a),\quad \int_0^L h_1(x;a)\mathrm{d}x = 0,\quad \forall a\in\mathbb{R}^N.\tag{4.38}$$

Unlike Theorem 4.3.2, the flat topography does not cancel the gradient $\nabla\Pi$.

Theorem 4.3.3. *Assume that the net growth rate at the surface satisfies $\mu(I_s) > 0$ and that I_{a_0} solves (4.35). Let $\tilde{a}_f = [a_0, a_f]$ the flat topography with an average depth a_0, then $\nabla\Pi(\tilde{a}_f) \neq 0$.*

Proof. Computations similar to that in the proof of Theorem 4.3.2 gives $\partial_a \mathcal{L}(\tilde{a}_f) = 0$. It follows from (4.34), that $\partial_{a_0} h = 1$, $h(\tilde{a}_f) = a_0$. Consider $i \in \{1, \cdots, N_z\}$. Since

$$I_i(\tilde{a}) = I_s \exp\Big(- \frac{Y_{\text{opt}}}{a_0} \frac{i - \frac{1}{2}}{N_z} h(\tilde{a})\Big),$$

we find that

$$\partial_{a_0} I_i(\tilde{a}_f) = -(-\frac{Y_{\text{opt}}}{a_0} + \frac{Y_{\text{opt}}}{a_0}) \frac{i - \frac{1}{2}}{N_z} I_i(\tilde{a}_f) = 0.$$

Hence the first sum in (4.36) is zero. Keeping the notation of Theorem 4.3.2, and using that $I_i(\tilde{a}_f) = I_i^f$, we obtain that $C_i := C_i^f$. In particular $-\alpha(I_i^f)C_i^f + \beta(I_i^f) = 0$, so that (4.36) gives

$$\partial_{a_0} \mathcal{L}(\tilde{a}_f) = -\sum_{i=1}^{N_z} \int_0^L \Big(\frac{\alpha_1}{L N_z \alpha_0} \big(- \gamma \left(I_i^f \right) C_i^f + \zeta \left(I_i^f \right) \big) \Big) \mathrm{d}x.$$

Since $\mu(I_s) > 0$, $\mu(I_{a_0}) = 0$ and μ is concave with respect to I, one has $\mu(I_i^f) = -\gamma \left(I_i^f \right) C_i^f + \zeta \left(I_i^f \right) > 0$. In other words, $\partial_{a_0} \mathcal{L}(\tilde{a}_f) \neq 0$. This concludes the proof. □

Remark

Note that the coefficient a_0 considered in the previous theorem needs to satisfy $h_c \leq a_0$ to guarantee that the system remains in a subcritical regime (see Remark 4.2.2).

4.3.4 Optimization problem in periodic case for topographies combining with mixing strategies

In this section, we present the optimization problem by combining the topography with the mixing strategy $P \in \mathcal{P}_N$. As shown in Chapter 3 in a periodic case, the period is actually one for whatever the permutation matrix is. Therefore, we only focus on the periodic case with period one in the following. In particular, we cannot keep the proof of the critical topography in Theorem 4.3.1 since an extra matrix P is added into the system so that the solution of the state C_i and p_i in periodic case can no longer be constant.

Constant reactor volume

In this way, we first define the objective function which is similar as (4.25) for the constant volume case:

$$\bar{\mu}_{N_z}^P(a) := \frac{1}{V N_z} \sum_{i=1}^{N_z} \int_0^L \mu(C_i^P, I_i(a)) h(a) \mathrm{d}x, \tag{4.39}$$

where C_i^P satisfies the following parameterized version of (4.16) with a periodic condition

$$\begin{cases} (C_i^P)' = \big(-\alpha(I_i(a))C_i + \beta(I_i(a))\big)\frac{h(a)}{Q_0}, \\ PC_i^P(L) = C_i^P(0). \end{cases} \tag{4.40}$$

Our optimization problem then reads:

Find a permutation matrix $P_{\max}$ and a parameter vector a^* solving the maximization problem:

$$\max_{P\in\mathcal{P}_N}\max_{a\in\mathbb{R}^N} \bar{\mu}_\Delta^P(a).$$

For a given permutation matrix $P \in \mathcal{P}_N$, the Lagrangian of (4.39) can then be written by

$$\begin{aligned}\mathcal{L}(C_i, p_i, a) = \frac{1}{VN_z}\sum_{i=1}^{N_z}\int_0^L \big(-\gamma(I_i(a))C_i^P + \zeta(I_i(a))\big)h(a)\mathrm{d}x \\ -\sum_{i=1}^{N_z}\int_0^L p_i^P\Big((C_i^P)' + \big(\alpha(I_i(a))C_i^P - \beta(I_i(a))\big)\frac{h(a)}{Q_0}\Big)\mathrm{d}x,\end{aligned}$$

where p_i^P is the Lagrange multiplier associated with the constraint (4.40).

The optimality system is obtained by cancelling all the partial derivatives of $\mathcal{L}$. Differentiating $\mathcal{L}$ with respect to p_i^P and equating the resulting expression to zero gives (4.40). Integrating the terms $\int p_i^P(C_i^P)'\mathrm{d}x$ on the interval $[0, L]$ by parts enables to differentiate $\mathcal{L}$ with respect to C_i^P and $C_i^P(L)$. Equating the result to zeros gives rise to

$$\begin{cases} (p_i^P)' - p_i^P\alpha(I_i(a))\frac{h(a)}{Q_0} - \frac{h(a)}{VN_z}\gamma(I_i(a)) & = 0, \\ p_i^P(L) - p_i^P(0)P & = 0. \end{cases} \tag{4.41}$$

Given a vector a, let us still denote by C_i^P, p_i^P the corresponding solutions of (4.40) and (4.41). The gradient $\nabla\bar{\mu}_{N_z}^P(a)$ is obtained by $\nabla\bar{\mu}_{N_z}^P(a) = \partial_a\mathcal{L}$, where

$$\begin{aligned}\partial_a\mathcal{L} = \sum_{i=1}^{N_z}\int_0^L \Big(\frac{1}{VN_z}\big(-\gamma'(I_i)C_i^P + \zeta'(I_i)\big) + p_i^P\frac{-\alpha'(I_i)C_i^P + \beta'(I_i)}{Q_0}\Big)h\partial_a I_i\mathrm{d}x \\ + \sum_{i=1}^{N_z}\int_0^L \Big(\frac{1}{VN_z}\big(-\gamma(I_i)C_i^P + \zeta(I_i)\big) + p_i^P\frac{-\alpha(I_i)C_i^P + \beta(I_i)}{Q_0}\Big)\partial_a h\mathrm{d}x.\end{aligned}$$

4.3.5 Variable reactor volume

In this section, we focus on the case where the reactor volume can also vary. Consider the extend parameter vector $\tilde{a} := [a_0, a] \in \mathbb{R}^{N+1}$. From (4.39), the objective function is given by

$$\Pi^P(\tilde{a}) := \frac{Y_{\text{opt}} - \alpha_1 a_0}{VN_z\alpha_0}\sum_{i=1}^{N_z}\int_0^L \mu(C_i^P, I_i(a))h(a)\mathrm{d}x. \tag{4.42}$$

The corresponding optimization problem reads:

Find a permutation matrix $P_{\max}$ and a parameter vector $\tilde{a}^*$ solving the maximization problem:

$$\max_{P\in\mathcal{P}_N}\max_{\tilde{a}\in\mathbb{R}^{N+1}} \Pi^P(\tilde{a}).$$

Let us denote by $\mathcal{L}$ the Lagrangian associated to (4.42). We follow the same optimization procedure presented in previous sections. Note that an extra element appears in this gradient, which is the partial derivative of $\mathcal{L}$ with respect to the variable a_0. More precisely, we have $\nabla \Pi^P(\tilde{a}) = [\partial_{a_0}\mathcal{L}, \partial_a \mathcal{L}]$ where

$$\begin{aligned}\partial_{a_0}\mathcal{L} =& \sum_{i=1}^{N_z}\int_0^L \Big(\frac{Y_{\text{opt}}/a_0 - \alpha_1}{LN_z\alpha_0}\big(-\gamma'(I_i)C_i^P + \zeta'(I_i)\big) + p_i^P\frac{-\alpha'(I_i)C_i^P + \beta'(I_i)}{Q_0}\Big)h\partial_{a_0}I_i \mathrm{d}x\\ &+\sum_{i=1}^{N_z}\int_0^L \Big(\frac{Y_{\text{opt}}/a_0 - \alpha_1}{LN_z\alpha_0}\big(-\gamma(I_i)C_i^P + \zeta(I_i)\big) + p_i^P\frac{-\alpha(I_i)C_i^P + \beta(I_i)}{Q_0}\Big)\partial_{a_0}h \mathrm{d}x\\ &-\sum_{i=1}^{N_z}\int_0^L \frac{Y_{\text{opt}}/a_0^2}{LN_z\alpha_0}\Big(-\gamma(I_i)C_i^P + \zeta(I_i)\Big)h\mathrm{d}x\end{aligned}$$

and $\partial_a\mathcal{L}$ is similar to the constant volume case.

4.4 Numerical Experiments

In this section, we will illustrate some optimal topographies obtained in various frameworks as presented in Section 4.3.

4.4.1 Numerical Methods

We start with an algorithm to solve the optimization problem and the numerical solver that we use for our numerical tests.

Gradient Algorithm

We detail now a gradient-based optimization procedure and apply it to Problem (4.27). The procedure is given in Algorithm 2.

Algorithm 2 Gradient-based optimization algorithm

Input: Tol> 0, $\rho > 0$.
Initial guess: a.
Output: a
Set $err :=$ Tol$+1$ and define h by (4.43) using the input data.
while $err >$Tol and $\min_{x\in[0,L]} h(x) > h_c$ **do**
    Compute I_i by (4.15).
    Set C_i as the solution of (4.26).
    Set p_i as the solution of (4.28).
    Compute the gradient ∇J by (4.29).
    $a = a + \rho\nabla J$,
    Set $err := \|\nabla J\|$.
end while

In addition to a numerical tolerance criterion on the magnitude of the gradient, we need to take into account a constraint on the water depth h to guarantee that the simulated flow remains in a subcritical regime ($\min_{x\in[0,L]} h(x) > h_c$), see Remark 4.2.2 (and in the range of industrial

constraints, see [29]). Remark that since no interaction between trajectories is considered, the gradient computation can be partially parallelized when computing I_i (hence C_i) and p_i.

Numerical Solvers

To solve our optimization problem numerically, we introduce a supplementary space discretization with respect to x. In this way, let us take a space increment Δx, set $N_x = [L/\Delta x]$ and $x^{n_x} = n_x \Delta x$ for $n_x = 0, \dots, N_x$. We choose to use the Heun's method for computing C_i via (4.26). Following a first-discretize-then-optimize strategy, we get that the Lagrange multiplier p_i is also computed by a Heun's type scheme. Note that this scheme is still explicit since it solves a backward dynamics starting from $p_i(L) = 0$.

4.4.2 Parameter settings

In this section, we provide the parameter used in the numerical test and the parameterization of the water depth h.

Parameter for the models

The spatial increment is set to $\Delta x = 0.01\,\mathrm{m}$ so that the convergence of the numerical scheme has been ensured and the numerical tolerance is set to Tol$= 10^{-10}$. We set the averaged discharge $Q_0 = 0.04\,\mathrm{m}^2\,\mathrm{s}^{-1}$ and $z_b(0) = -0.4\,\mathrm{m}$ to stay in standard ranges for a raceway. The free-fall acceleration $g = 9.81\,\mathrm{m\,s}^{-2}$. We choose $I_s = 2000\,\mu\mathrm{mol\,m}^{-2}\,\mathrm{s}^{-1}$ which approximates the maximum light intensity, e.g., at summer in the south of France. All the numerical parameters values for Han's model are taken from [54] and recalled in Table 4.1.

Table 4.1: Parameter values for Han Model.

k_r	$6.8\ 10^{-3}$	s^{-1}
k_d	$2.99\ 10^{-4}$	-
τ	0.25	s
σ	0.047	$\mathrm{m}^2 \cdot (\mu\mathrm{mol})^{-1}$
k	$8.7\ 10^{-6}$	-
R	$1.389\ 10^{-7}$	s^{-1}

In order to determinate the light extinction coefficient ε, two cases must be considered:

- constant volume: let us assume that only 1% of light can be captured by the cells at the bottom of the raceway, i.e. for $z = z_b$, meaning that $I_b = 0.01 I_s$. Then ε can be computed by
$$\varepsilon = (1/h(0;a)) \ln(I_s/I_b).$$
- non-constant volume: in this case, the volume related parameter a_0 is also to be optimized and one needs to use (1.17) to take into account of the variation of the volume. We take from [93] the specific light extinction coefficient of the microalgae specie $\alpha_0 = 0.2\,\mathrm{m}^2 \cdot \mathrm{g}$ and the background turbidity $\alpha_1 = 10\,\mathrm{m}^{-1}$.

Parameterization

In order to describe the bottom of an optimal raceway pond, we choose to parameterize h by a truncated Fourier series for our numerical tests. More precisely, h reads:

$$h(x) = a_0 + \sum_{i=1}^{N} a_i \sin(2n\pi \frac{x}{L}). \tag{4.43}$$

The parameter to be optimized is then the Fourier coefficients $a := [a_1, \ldots, a_N]$. Although other parameterizations can also be considered, in this chapter, we focus only on this parameterization based on the following reasons :

- We consider a hydrodynamic regime where the solutions of the Saint-Venant equations are smooth and hence the water depth can be approximated by (4.43). Hence, the truncated Fourier number N is set to be small and limit situations where $N \to +\infty$ are not considered in what follows.
- One has naturally $h(0) = h(L)$ under this parameterization, which means that we have accomplished one lap of the raceway pond.
- We assume a constant volume of the system V, which can be achieved by fixing a_0. Indeed, under this parameterization and using (4.17), one finds $V = a_0 L$.

From (4.7) and (4.9), the velocity u and the topography z_b read also as functions of a. Once we find the vector a maximizing the functional $\bar{\mu}_{N_z}$, we then find the optimal topography of our system. Note that in constant volume case, a_0 is fixed to be 0.4, and in non constant volume case, we keep $a_0 = 0.4$ as the initial guess.

4.4.3 Numerical results

In this section, we provide the numerical support for the optimization problems presented in Section 4.3.

Convergence of the vertical discretization

The first test consists in studying the influence of the vertical discretization number N_z. For this purpose, let us set the length $L = 10\,\mathrm{m}$ and the truncated Fourier number $N = 5$. We take 100 random initial guesses of a. Note that the choice of a should respect the subcritical condition. For N_z varies from 1 to 80, we compute the average value of $\bar{\mu}_{N_z}$ for each N_z. The results are shown in Figure 4.2. We observe numerical convergence when N_z grows, showing the convergence towards continuous model. In view of these results, we take $N_z = 40$ for the successive studies.

Influence of the truncated Fourier value

The second test is given to study the influence of the truncated Fourier value N on the optimal average growth rate $\bar{\mu}_{N_z}$. Let us set $N = [0, 5, 10, 15, 20]$ and set flat topography as the initial guess, meaning that a is set to 0. Meanwhile, we keep the length $L = 10\,\mathrm{m}$ as in previous test. Table 4.2 shows the optimal value of our objective function $\bar{\mu}_{N_z}$ for different values of N. There is a slight increase of the optimal value of the average growth rate $\bar{\mu}_{N_z}$ when N becomes larger. However, the corresponding values of $\bar{\mu}_{N_z}$ remain close to the one associated with a flat topography.

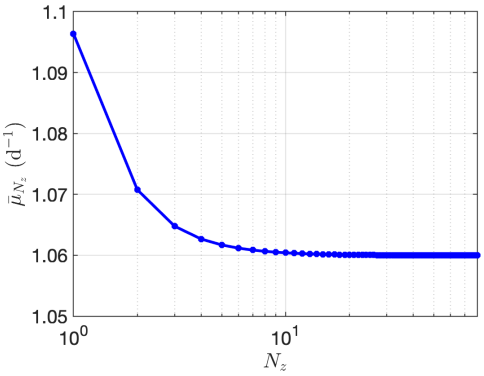

Figure 4.2: The value of $\bar{\mu}_{N_z}$ for $N_z = [1, 80]$.

Table 4.2: The value of $\bar{\mu}_{N_z}$ for different N

N	$\bar{\mu}_{N_z}$ (unit d^{-1})	$\log_{10}(\|\nabla\bar{\mu}_{N_z}\|)$
0	1.061	–
5	1.0754	-10.0161
10	1.0763	-10.0248
15	1.0766	-10.0282
20	1.0768	-10.0297

Optimal topography shape in non periodic case

We focus now on the shape of the optimal topography in the case C non periodic. We choose $N = 5$ the truncated Fourier series and keep the length $L = 10\,\mathrm{m}$ as an example to show the shape of the optimal topography. We consider the flat topography as the initial guess. The optimal shape of the topography is shown in Figure 4.3. In particular, the resulting optimal topography is not flat and the a^* for the final iteration reads $a^* = [0.1043, 0.0503, 0.0333, 0.0250, 0.0201]$.

Optimal topography shape in periodic case

In this test, we focus on the optimization problem in the case C periodic. We keep the same parameter settings as in previous case and consider a random topography as initial guess. The optimal shape of the topography is shown in Figure 4.4. As shown in this figure, the resulting optimal topography is flat in this case, meaning that the flat topography, proved to be a critical topography in Theorem 4.3.1, is actually the optimal topography.

Example with a mixing device

The next test aims to simulate a more realistic raceway pond situation where a mixing device is considered in the system. More precisely, we simulate several laps, with a mixing device that mix up the algae after each laps. The mixing device is modelled by a permutation matrix P that rearrange the trajectories at each lap. In our test, P is an anti-diagonal matrix with the entries one. This choice actually corresponds to an optimum in some parameter settings and has been

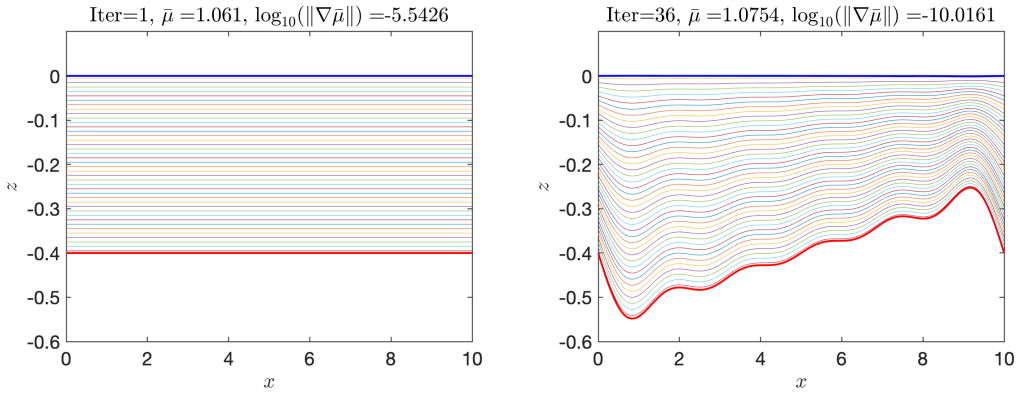

Figure 4.3: The optimal topography at the first iteration (Left) and the final iteration (Right) for the truncated Fourier number $N = 5$. The red thick curve represents the topography (z_b), the blue thick curve represents the free surface (η), and all the other curves between represent the trajectories for different layers.

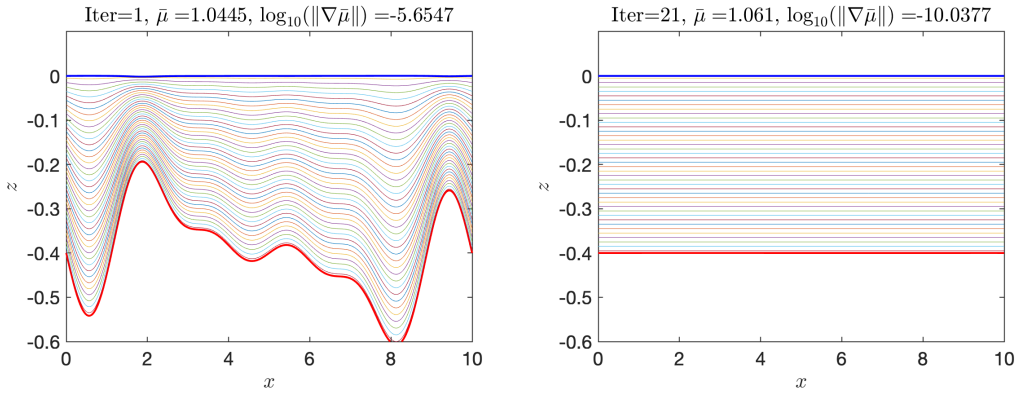

Figure 4.4: The optimization process at the first iteration (Left) and the final iteration (Right) for the truncated Fourier number $N = 5$. The red thick curve represents the topography (z_b), the blue thick curve represents the free surface (η), and all the other curves between represent the trajectories for different layers.

shown in [16], where other choices will be investigated. Meanwhile, this permutation matrix P corresponds to the permutation π which is given by

$$\pi = (1\ N_z)(2\ N_z - 1)(3\ N_z - 2)\cdots,$$

where we use the standard notation of cycles in the symmetric group. Note that π is of order two. The photo-inhibition state C is then set to be 2-periodic (i.e $C^1(0) = PC^2(L)$). The details about the optimization procedure are given in Appendix 4.C.

We keep the truncated Fourier number $N = 5$ and set the length $L = 100\,\mathrm{m}$. The initial guess a is still zero. Figure 4.5 presents the shape of the optimal topography and the evolution of the photoinhibition state C for two laps. Note that here we are still in a periodic regime,

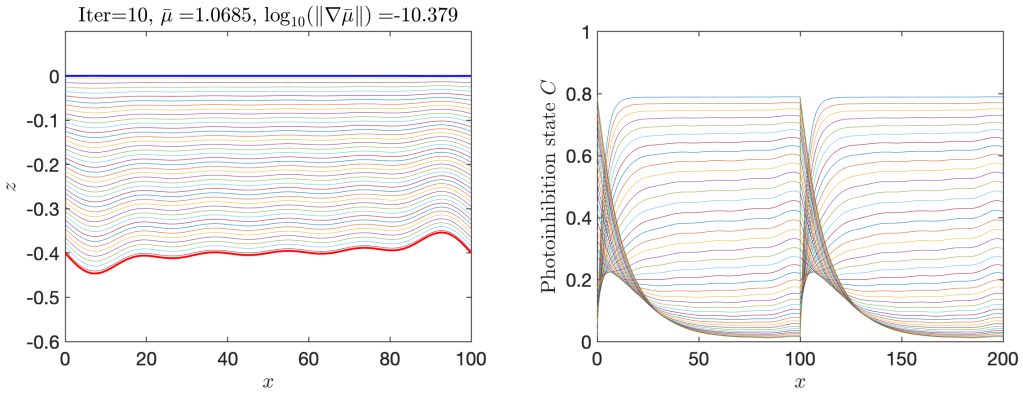

Figure 4.5: The optimal topography (Left) and the evolution of the photoinhibition state C (Right) for two laps.

unlike the previous test the resulting optimal topography in this case is not flat. However, the increase in the optimal value of the objective function $\bar{\mu}_{N_z}$ compared to a flat topography is around 0.216%, and compare to a flat topography with non permutation (i.e. $P = \mathcal{I}_{N_z}$) case is around 0.263%, in both cases, the increase remains small. On the other hand, we observe that the state C is actually 1-periodic for each laps. This result is actually proved in [16] in the case of a flat topography. In particular, this result enables us to perform the computation for any permutation matrix by doing one lap of the raceway. In this way, we provide the next test.

Constant volume with mixing device

The current test is dedicated to study the optimal permutation matrix and the associated shape of the topography for constant volume. To evaluate the efficiency of the corresponding mixing strategy, define:

$$r_1 := \frac{\bar{\mu}_{N_z}^{P_{\max}}(a^*) - \bar{\mu}_{N_z}^{P_{\max}}(0)}{\bar{\mu}_{N_z}^{P_{\max}}(0)}, r_2 := \frac{\bar{\mu}_{N_z}^{P_{\max}}(a^*) - \bar{\mu}_{N_z}^{\mathcal{I}_{N_z}}(0)}{\bar{\mu}_{N_z}^{\mathcal{I}_{N_z}}(0)}. \tag{4.44}$$

Here r_1 defines the gain of the optimal permutation strategy with the optimal topography compare to the optimal permutation strategy with a flat topography, and r_2 defines the gain of the optimal permutation strategy with the optimal topography compare to no permutation strategy with a flat topography. Let us consider two raceway pond length $L = 100\,\mathrm{m}$ and $L = 1\,\mathrm{m}$ re-

spectively. The optimal matrices $P_{\max}$ for different L are denoted by $P_{\max}^{L}$ and given in (4.45) with the associated optimal topographies presented in Figure 4.6.

$$P_{\max}^{100} = \begin{pmatrix} 0 & 1 & 0 & 0 & 0 & 0 & 0 \\ 0 & 0 & 0 & 1 & 0 & 0 & 0 \\ 0 & 0 & 0 & 0 & 0 & 1 & 0 \\ 0 & 0 & 0 & 0 & 0 & 0 & 1 \\ 0 & 0 & 0 & 0 & 1 & 0 & 0 \\ 0 & 0 & 1 & 0 & 0 & 0 & 0 \\ 1 & 0 & 0 & 0 & 0 & 0 & 0 \end{pmatrix}, \quad P_{\max}^{1} = \begin{pmatrix} 1 & 0 & 0 & 0 & 0 & 0 & 0 \\ 0 & 0 & 0 & 0 & 0 & 0 & 1 \\ 0 & 0 & 0 & 0 & 0 & 1 & 0 \\ 0 & 0 & 0 & 0 & 1 & 0 & 0 \\ 0 & 0 & 0 & 1 & 0 & 0 & 0 \\ 0 & 0 & 1 & 0 & 0 & 0 & 0 \\ 0 & 1 & 0 & 0 & 0 & 0 & 0 \end{pmatrix} \tag{4.45}$$

A non flat topography associated with a non trivial permutation matrix has been observed.

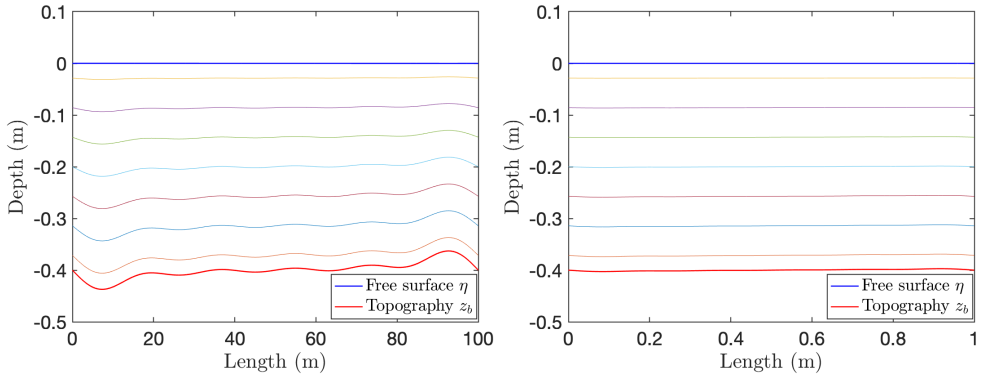

Figure 4.6: The optimal topographies and the associated trajectories for the permutation matrices (4.45). Left: $L = 100\,\text{m}$. Right: $L = 1\,\text{m}$.

In particular, these optimal matrices corresponds to the optimal matrices obtained with a flat topography under the same parameter settings in Chapter 3. More precisely, the left hand side matrix of (4.45) is the same type as (3.27) and the right hand side matrix of (4.45) is the same type as (3.29). The two ratios defined in (4.44) are $r_1 = 0.148\%$, $r_2 = 1.070\%$ and $r_1 = 0.001\%$ $r_2 = 3.453\%$ respectively.

As we observed in the test above, the length of raceway has a potential influence on the objective function and the gain, we then provide a test for different values of the length L. Figure (4.7) shows the objective function $\bar{\mu}_{N_z}$ and the two ratios r_1, r_2 as a function of the length L. Note that the objective function decreases when L increases except in the neighbourhood of $L = 12.5\,\text{m}$, on the same time, we observe that the influence of topography is very limited comparing to the influence of the permutation strategies.

Varying volume with mixing device

We consider now that the volume of the system (V) can also vary, meaning that the volume related coefficient a_0 is also a parameter to be optimized. Let us define two ratios similar

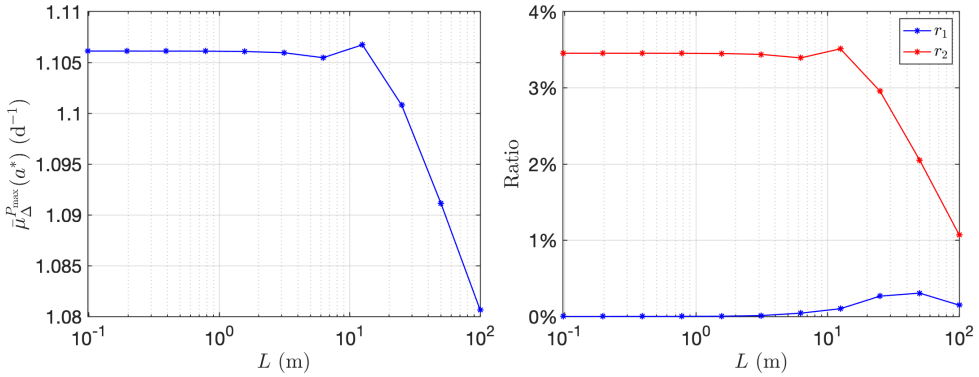

Figure 4.7: The optimal value of the objective function $\bar{\mu}_{N_z}$ (Left) and the two ratios r_1, r_2 (Right) for $L = 100/2^{\{0,\dots,10\}}$.

as (4.44) to evaluate the efficiency of the permutation strategies,

$$\begin{aligned} \tilde{r}_1 :=& \frac{\Pi^{P_{\max}}(\tilde{a}^*) - \Pi^{P_{\max}}(\tilde{a}_f)}{\Pi^{P_{\max}}(\tilde{a}_f)}, \\ \tilde{r}_2 :=& \frac{\Pi^{P_{\max}}(\tilde{a}^*) - \Pi^{\mathcal{I}_{N_z}}(\tilde{a}_f)}{\Pi^{\mathcal{I}_{N_z}}(\tilde{a}_f)}, \end{aligned} \tag{4.46}$$

where $\tilde{a}_f := [\tilde{a}_0^*, 0, \cdots, 0]$ and $\tilde{a}_0^*$ is the optimal volume related value. We keep the same length setting as in the previous test, the optimal matrices $P_{\max}^L$ are given in (4.47) and the associated optimal topographies are presented in Figure 4.8.

$$P_{\max}^{100} = \begin{pmatrix} 0 & 0 & 0 & 1 & 0 & 0 & 0 \\ 0 & 0 & 0 & 0 & 0 & 1 & 0 \\ 0 & 0 & 0 & 0 & 0 & 0 & 1 \\ 0 & 0 & 0 & 0 & 1 & 0 & 0 \\ 0 & 0 & 1 & 0 & 0 & 0 & 0 \\ 0 & 1 & 0 & 0 & 0 & 0 & 0 \\ 1 & 0 & 0 & 0 & 0 & 0 & 0 \end{pmatrix}, \quad P_{\max}^{1} = \begin{pmatrix} 0 & 0 & 0 & 0 & 0 & 0 & 1 \\ 0 & 0 & 0 & 0 & 0 & 1 & 0 \\ 0 & 0 & 0 & 0 & 1 & 0 & 0 \\ 0 & 0 & 0 & 1 & 0 & 0 & 0 \\ 0 & 0 & 1 & 0 & 0 & 0 & 0 \\ 0 & 1 & 0 & 0 & 0 & 0 & 0 \\ 1 & 0 & 0 & 0 & 0 & 0 & 0 \end{pmatrix} \tag{4.47}$$

The optimization algorithm stops before finding an optimum since it is limited by the constraint subcritical flow, one can see that the water depth becomes very small. This corresponds to the result that we have mentioned in Chapter 2 where smaller water depths provide better biomass surface productivity. The two ratios defined in (4.46) are $\tilde{r}_1 = 0.918\%$, $\tilde{r}_2 = 9.284\%$ and $\tilde{r}_1 = 0.00003\%$, $\tilde{r}_2 = 12.714\%$ respectively.

As shown experimentally in the previous test, the influence of the topographies remain limited, at the same time, non trivial permutation strategies $P_{\max}^L$ are obtained for different raceway length L, in particular these strategies are also different from the case with a fixed volume. Moreover, these strategies have a better improvement when the volume is also optimized. Figure 4.9 shows the objective function Π^P and the two ratios $\tilde{r}_1, \tilde{r}_2$ as a function of the length L. Note that the average growth rate Π^P increase when L goes to 0. This *flashing effect* corresponds to the fact that the algae exposed to high frequency flashing have a better growth. This phenomenon has already been reported in literature e.g. [16, 77].

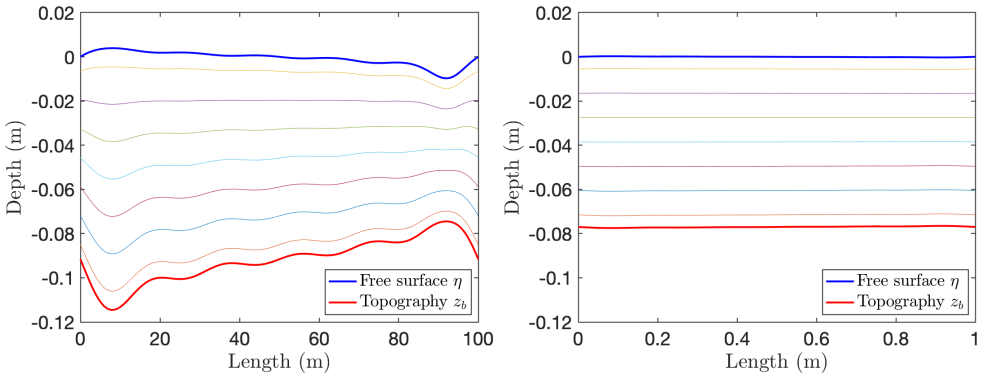

Figure 4.8: The optimal topographies and the associated trajectories for the permutation matrices (4.47). Left: $L = 100\,\mathrm{m}$. Right: $L = 1\,\mathrm{m}$.

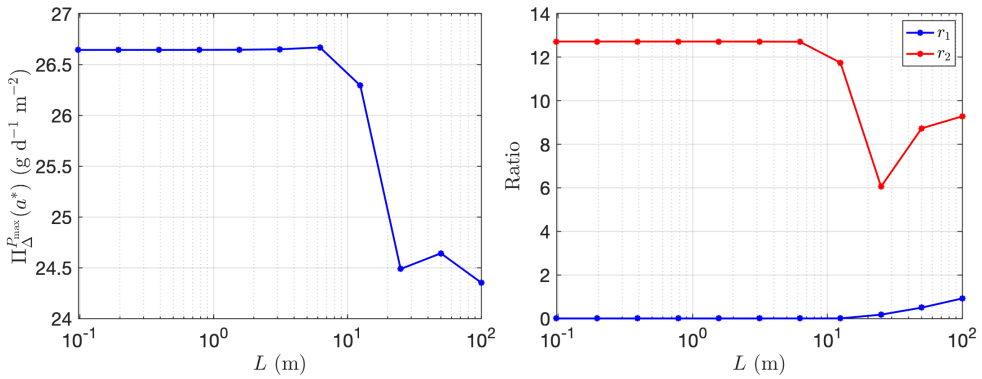

Figure 4.9: The optimal value of the objective function Π^P (Left) and the two ratios $\tilde{r}_1, \tilde{r}_2$ (Right) for $L = 100/2^{\{0,\dots,10\}}$.

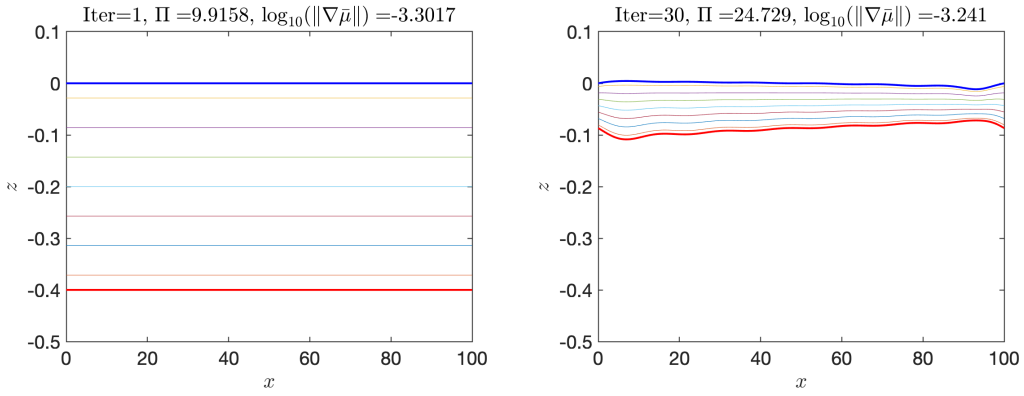

Figure 4.10: The optimization process for length $L = 100\,\mathrm{m}$ and $P = P_{\max}^{100}$ in (4.45).

On the other hand, if we just focus on the increase provided by the optimization of the volume as shown in Figure 4.10. One can see that comparing with the initial state which is a flat topography with 0.4 m water depth, the value of the objective function Π at its final state is doubled. Therefore a shallow raceway may provide a more considerable gain comparing a non flat topography or a mixing strategy.

4.5 Conclusion and future works

A non flat topography slightly enhances the average growth rate. However the gain remains very limited and it is not clear if the difficulty to design such a pattern could be compensated by the increase in the process productivity.

A flat topography cancels the gradient of the objective functional in many situations where C is assumed to be periodic. However, including a mixing device gives rise to an optimal non flat topography with a slight gain of the average growth rate. Adapting the shape of the raceway to an original mixing system is an innovative strategy to boost the algal process productivity. To realize in practice the ideal mixing a system more elaborated than a paddle wheel is required.

If the condition is allowed, a shallow raceway pond may then provide considerable gain comparing with the topography or mixing strategy design.

4.A Proof of Theorem 4.3.1

Let us give the details about the proof of Theorem 4.3.1. To prove the existence and uniqueness of a (weak) solution of this problem, we need the following result.

Lemma 4.A.1. *Given $Z_0 \in \mathbb{R}$, let $Z \in \mathcal{C}(0, L; \mathbb{R})$ be the weak solution of*

$$\begin{cases} Z'(x) = -\frac{\alpha(I(x))h(x)}{Q_0} Z(x), \quad x \in [0, L] \\ Z(L) = Z_0 \end{cases} \tag{4.48}$$

For $x \in [0, L]$:

$$\|Z(x)\|_2 \leq e^{-\frac{k_T h_c}{Q_0} x} \|Z_0\|_2 . \tag{4.49}$$

Proof. Let $x \in [0, L]$, as a weak solution of (4.48), the function Z is almost everywhere differentiable and a direct calculation gives

$$\frac{\mathrm{d}\left\|Z(x)\right\|_2^2}{\mathrm{d}x} = 2\langle Z(x), -\frac{\alpha(I(x))h(x)}{Q_0} Z(x)\rangle \leq -2\frac{k_r h_c}{Q_0}\left\|Z(x)\right\|_2^2, \tag{4.50}$$

where we have used the fact that $\alpha(I) = \beta(I) + k_r$, $\beta(I) \geq 0$ and $h > h_c$ (in subcritical case). Defining $f(x) := \frac{\mathrm{d}\left\|Z(x)\right\|_2^2}{\mathrm{d}x} + 2\frac{k_r h_c}{Q_0}\left\|Z(x)\right\|_2^2$ and multiplying both sides by $e^{2\frac{k_r h_c}{Q_0}x}$, we obtain:

$$\frac{\mathrm{d}e^{2\frac{k_r h_c}{Q_0}x}\left\|Z(x)\right\|_2^2}{\mathrm{d}x} = e^{2\frac{k_r h_c}{Q_0}x} f(x),$$

which gives by integration over $[0, x]$

$$\left\|Z(x)\right\|_2^2 = e^{-2\frac{k_r h_c}{Q_0}x}\left\|Z_0\right\|_2^2 + \int_0^x e^{2\frac{k_r h_c}{Q_0}(s-x)} f(s)\mathrm{d}s.$$

Because of (4.50), $f(x) \leq 0$, this concludes the proof. □

Let us now give the proof of Theorem 4.3.1.

Proof. Introduce the mapping $\Phi : \mathbb{R} \to \mathbb{R}$ defined by

$$\Phi(C_0) := C(L),$$

where C is the weak solution of (4.16). Given $\bar{C}_0^1 \in \mathbb{R}$ and $\bar{C}_0^2 \in \mathbb{R}$, define $Z_0 = \bar{C}_0^2 - \bar{C}_0^1$ and $Z(x) = \bar{C}^2(x) - \bar{C}^1(x)$, where $\bar{C}^1$ and $\bar{C}^2$ are the weak solutions of (4.16) with initial conditions $\bar{C}_0^1$ and $\bar{C}_0^2$, respectively. Subtracting the corresponding weak representations, we obtain that Z satisfies the assumptions of Lemma 4.A.1 so that (4.49) holds. As a consequence,

$$\left\|\bar{C}^2(L) - \bar{C}^1(L)\right\|_2 \leq e^{-\frac{k_r h_c}{Q_0}L}\left\|\bar{C}_0^2 - \bar{C}_0^1\right\|_2,$$

which implies that Φ is a contraction. Applying Banach fixed-point theorem, it follows that there exists a unique $C_0 \in \mathbb{R}$ such that $\Phi(C_0) = C_0$. The corresponding weak solution C of (4.16) satisfies (4.31). □

4.B Relation between two growth rate definitions

Let us start with the definition of the average growth rate in time (4.23). Note that the time duration of one lap of the raceway pond $T = \int_0^L \frac{1}{u}\mathrm{d}x$ and $hu = Q_0$ because of (4.7). By doing a

change of variable $x = x(t)$ and using the fact that $\mathrm{d}x = u\mathrm{d}t$, one has

$$\begin{aligned}\bar{\mu}_\infty =& \frac{1}{T}\int_0^T \frac{1}{h\left(x(t)\right)}\int_{z_b(x(t))}^{\eta(x(t))} \mu\big(C\left(x(t),z(t)\right), I\left(x(t),z(t)\right)\big)\mathrm{d}z\mathrm{d}t \\ =& \frac{1}{\int_0^L \frac{1}{u}\mathrm{d}x}\int_0^L \frac{1}{h\left(x\right)}\int_{z_b(x)}^{\eta(x)} \mu\big(C\left(x,z\right), I\left(x,z\right)\big)\frac{1}{u\left(x\right)}\mathrm{d}z\mathrm{d}x \\ =& \frac{Q_0}{\int_0^L h\mathrm{d}x}\int_0^L \frac{1}{h\left(x\right)u\left(x\right)}\int_{z_b(x)}^{\eta(x)} \mu\big(C\left(x,z\right), I\left(x,z\right)\big)\mathrm{d}z\mathrm{d}x \\ =& \frac{1}{V}\int_0^L \int_{z_b(x)}^{\eta(x)} \mu\big(C\left(x,z\right), I\left(x,z\right)\big)\mathrm{d}z\mathrm{d}x.\end{aligned}$$

Therefore we find the expression (4.24).

4.C System with a paddle-wheel

Let us denote by P the permutation matrix associated with π i.e., 1 as entries on the anti-diagonal. Let us denote by C^1 (resp. C^2) the photo-inhibition state for the first (resp. second) lap of the raceway. We then assume that the state C is 2-periodic, meaning that $C^1(0) = PC^2(L)$. From (4.25), we define the objective function by

$$\frac{1}{2}\sum_{j=1}^{2}\bar{\mu}^j_{N_z}(a) = \frac{1}{2VN_z}\sum_{j=1}^{2}\sum_{i=1}^{N_z}\int_0^L \frac{-\gamma(I_i(a))C_i^j + \zeta(I_i(a))}{Q_0}h(a)\mathrm{d}x. \tag{4.51}$$

Let us still denote by $\mathcal{L}$ the Lagrangian associated with this optimization problem. It can be written as

$$\mathcal{L}(C,p,a) = \sum_{j=1}^{2}\sum_{i=1}^{N_z}\int_0^L \frac{-\gamma(I_i(a))C_i^j + \zeta(I_i(a))}{2VN_z}h(a) - p_i^j\big(C_i^{j\prime} + \frac{\alpha(I_i(a))C_i^j - \beta(I_i(a))}{Q_0}h(a)\big)\mathrm{d}x,$$

where p_i^j is the Lagrangian multiplier associated with the constraint (4.26) for C_i^j. Integrating the terms $\int p_i^j C_i^{j\prime}\mathrm{d}x$ on the interval $[0, L]$ by parts, we get

$$\int_0^L p_i^j C_i^{j\prime}\mathrm{d}x = -\int_0^L p_i^{j\prime} C_i^j\mathrm{d}x + p_i^j(L)C_i^j(L) - p_i^j(0)C_i^j(0).$$

By definition of our paddle wheel model, $C^2(0) = PC^1(L)$. Differentiating $\mathcal{L}$ with respect to $C^1(L)$ and $C^2(L)$, we find

$$\begin{cases} \partial_{C^1(L)}\mathcal{L} = p^1(L) - p^2(0)P, \\ \partial_{C^2(L)}\mathcal{L} = p^2(L) - p^1(0)P. \end{cases}$$

Then differentiating $\mathcal{L}$ with respect to C_i^j gives the evolution of p_i^j by

$$\partial_{C_i^j(L)}\mathcal{L} = p_i^{j\prime} - p_i^j\frac{\alpha(I_i(a))}{Q_0}h(a) - \frac{1}{2VN_z}\gamma(I_i(a))h(a).$$

Finally, the partial derivative $\partial_a \mathcal{L}$ (hence the gradient) is given by

$$\begin{aligned}\partial_a \mathcal{L} =& \sum_{j=1}^{2}\sum_{i=1}^{N_z}\int_0^L \Big(\frac{-\gamma'(I_i(a))C_i^j + \zeta'(I_i(a))}{2VN_z} + p_i^j \frac{-\alpha'(I_i(a))C_i^j + \beta'(I_i(a))}{Q_0}\Big) h(a)\partial_a I_i(a)\mathrm{d}x \\ &+ \sum_{j=1}^{2}\sum_{i=1}^{N_z}\int_0^L \Big(\frac{-\gamma(I_i(a))C_i^j + \zeta(I_i(a))}{2VN_z} + p_i^j \frac{-\alpha(I_i(a))C_i^j + \beta(I_i(a))}{Q_0}\Big) \partial_a h(a)\mathrm{d}x.\end{aligned}$$

In general, the average growth rate for multiple laps is defined by replacing 2 in (4.51) with the number of the laps and follow the same computation as above. As one may have noticed, this computation becomes fastidious especially when the number of the laps increase. Therefore the periodic result like one presented in Theorem 3.2.1 is very necessary to reduce the computational cost.

Conclusion

Main contributions

In this thesis, we provide a deeper insight into different aspects on dynamics of microalgae growth with three main contributions.

Optimal optical conditions

In Chapter 2, we have extended the results of [94] and [55] where the authors have identified an optimal strategy for biomass productivity maximization in photobioreactors. This so-called compensation condition consists in canceling the net growth rate at the bottom of the photobioreactors to maximize the surface biomass productivity. Based on their works, we investigate the influence of the optical condition for microalgal production. More precisely, we consider a general light attenuation function relying on biomass concentration and the background turbidity of the system. We introduce the notion of optical depth productivity which is much more convenient to study the optimal condition of the optical depth of the light intensity. A global optimal condition for the optical depth is determined which depends only on the parameter of the model. This optimal condition also coincides with the compensation condition found in literature in other contexts. Then, we study the classical areal biomass productivity maximization problem. For a given biomass concentration, it is shown that an optimal water depth exists and can be determined explicitly using the optimal optical depth. However, optimizing biomass concentration for a given reactor depth is more tricky, since the biomass concentration determined by the compensation condition is not always an optimum. In this case, we find an asymptotic behaviour both for areal biomass productivity and net growth rate at the bottom of the reactors. A nonlinear controller is designed to stabilize the evolution of the biomass concentration to its desired value. In practise, this optimal optical depth helps in establishing a relation between the biomass concentration and the reactor depth as shown in variable volume case in Chapter 4.

Optimal mixing strategies

In Chapter 3, we identify a class of problem where N resources are distributed to N activities, each activity then uses the assigned resource to evolve during a given time $T > 0$ after which the resources are redistributed. In light of a bibliographic review, this type of allocation problem is not much documented, especially when dealing with a dynamical system. However, this type of problem often arises in real life applications. In this way, we develop a complete theory that can be apply to various applications. As classical resource allocation problems, we study the allocation strategies which optimize the cost or the benefit generated by the system. For this purpose, we introduce an objective function related to the average benefit or cost which, in addition, takes into account a periodic condition associated with the dynamics. We show that the

periodicity of the resulting problem does not depend on the order of the permutation associated with the assignment. We then propose a suboptimal problem whose solution can be determined explicitly a priori and provide a criterion to compare it with the original non linear problem. We apply finally this theory to the raceway microalgal production where a mixing device, such as a paddle wheel, is considered to control the rearrangement of the depth of the algae cultures hence the light perceived at each lap. Non trivial permutation strategies are observed and the approximation quality of the suboptimal problem has also been examined.

Optimal topographies

In Chapter 4, we study the influence of the shape of the topography on algal growth in raceway ponds. An intuitive idea is that non-flat topographies could ensure a better distribution of the light intensity, in particular at the lower part of the pond, by bringing up the algae closer to the surface. The optimization of this complex system is challenging since it contains both a hydrodynamical movement and biological evolution. For this purpose, we consider a coupled biological-hydrodynamical model which enables us to describe this complex dynamical system, and use it to optimize the topography. We then apply an adjoint-based optimization scheme which includes the constraints associated with the shallow water regime. On the contrary to a widespread belief, the flat topography is proved to be the optimal topography in a periodic regime, whereas non-trivial topographies can be obtained in other contexts, e.g., when we remove the periodic assumption or when an extra mixing strategy is included in the model. Note that in the examples considered in our numerical tests, such topographies only slightly improved the biomass production.

Discussion and Perspectives

Microalgal industrial production is still challenging, especially in full-scale systems subjected to permanent fluctuations of light intensity. In order to obtain an optimal productivity in the reactors, an appropriate light intensity must be supplied to guarantee a continuous growth. Note that low light intensity will limit the growth, especially in dense algal cultures case due to self-shading. On the other hand, too high levels may lead to photoinhibition of the algal cell which will also limit their growth. In our work, we mainly focus on the light condition aspect and provide an optimal condition. The co-limitation problem could be considered in future work to account for both light and nutrients limitation and test this optimal condition. On the other hand, other controllers can be investigated for instance by using the extremum seeking strategy in order to find automatic controller without identifying it in advance.

As for the raceway ponds design, we work on a simplified coupling model to provide some optimization results in Chapter 3 and Chapter 4. One of the advantages of our coupling system is that this allows us to provide some explicit computations on this complex system as well as some theoretical proofs about optimal topographies and mixing strategies. A second order study on the optimization problem could be investigated to prove that the flat topography is the local optimal solution in the periodic case. Other investigations could consists of numerical tests dealing with coupled models closer to real life situations, e.g., in [8], where a coupled multilayer model (2D multilayer Saint-Venant and Droop) is considered. One can also use the optimal control strategies (for instance Bocop code) to investigate this coupling optimization problem.

From a hydrodynamical point of view, our study is based on the laminar flow assumption, therefore future work may account for the turbulent flow where particles can change their vertical positions. Such a dynamic play the role of a mixing device acting continuously along the

trajectories. Since our work in Chapter 3 shows that a mixing device could enhance the algal growth, this working direction may provide another insight on the industrial raceway ponds design. As a preliminary test, one could include a Brownian motion component into the Lagrangian trajectories to simulate this turbulence as mentioned in Remark 1.2.2.

As for the periodic dynamical resource allocation problem that we present in Chapter 3, we provide an application to the algal production. Other applications would also be interesting by applying our theory in other contexts, as mentioned in Remark 3.2. As an example, we could consider the case where the dynamical system is associated with the growth of different trees species, as done in [32]. Meanwhile, one can also consider other strategies of solving the resource allocation problems presented in this chapter, for instance by using the mixed-integer optimization techniques.

From a theoretical point of view, although our suboptimal problem provides a faithful approximation for real life simulation cases, the proposed criterion can still be improved. For instance, other strategies to regroup the permutations can be used to establish a new criteria, or an improvement on the two bounds provided in the proof of Theorem 3.2.2. Meanwhile, providing an approximation for small time duration problem is also an interesting working direction. Although this may be difficult to accomplish in real life algal production, the productivity in this limit case is still attractive, and this corresponds to the flashing effect observed for other types of photobioreactors. The main challenge in this case is that the diagonal matrix D in (3.6) tends to the identity matrix for which $(\mathcal{I}_N - PD)^{-1}$ is no longer invertible, therefore it is much more difficult to identify it and propose an approximation for it. Numerically, we have tested it with some algorithms which can not always find the optimal permutation matrices. Therefore, this could be a challenging working direction.

Bibliography

[1] Borowitzka M. A. Limits to growth. *Wastewater Treatment with Algae*, pages 203–226, 1998.

[2] A. Abdelrazec, J. Bélair, C. Shan, and H. Zhu. Modeling the spread and control of dengue with limited public health resources. *Mathematical Biosciences*, 271:136–145, 2016.

[3] A. R. Akhmetzhanov, F. Grognard, and L. Mailleret. Optimal life-history strategies in seasonal consumer-resource dynamics. *Evolution*, 65(11):3113–3125, 2011.

[4] R. Amos. Principles for attaining maximal microalgal productivity in photobioreactors: an overview. *Hydrobiologia*, 512(1):33–37, 2004.

[5] J. Barber and B. Andersson. Too much of a good thing: light can be bad for photosynthesis. *Trends in Biochemical Sciences*, 17(2):61–66, 1992.

[6] S. K. Baruah, N. K. Cohen, C. G. Plaxton, and D. A. Varvel. Proportionate progress: A notion of fairness in resource allocation. *Algorithmica*, 15:600–625, 1996.

[7] A. Bensoussan and J.-L. Lions. *Contrôle impulsionnel et inéquations quasi variationnelles*, volume 11 of *Méthodes Mathématiques de l'Informatique [Mathematical Methods of Information Science]*. Gauthier-Villars, Paris, 1982.

[8] O. Bernard, A.-C. Boulanger, M.-O. Bristeau, and J. Sainte-Marie. A 2d model for hydrodynamics and biology coupling applied to algae growth simulations. *ESAIM: Mathematical Modelling and Numerical Analysis*, 47(5):1387–1412, September 2013.

[9] O. Bernard and J.-L. Gouzé. Transient behavior of biological loop models with application to the droop model. *Mathematical Biosciences*, 127(1):19–43, 1995.

[10] O. Bernard and J.-L. Gouzé. Non-linear qualitative signal processing for biological systems: application to the algal growth in bioreactors. *Mathematical Biosciences*, 157(1):357–372, 1999.

[11] O. Bernard and L.-D. Lu. Optimal optical conditions for Microalgal production in photobioreactors. Submitted paper, August 2021.

[12] O. Bernard, L.-D. Lu, J. Sainte-Marie, and J. Salomon. Controlling the bottom topography of a microalgal pond to optimize productivity. In *2021 American Control Conference (ACC)*, pages 634–639, 2021.

[13] O. Bernard, L.-D. Lu, J. Sainte-Marie, and J. Salomon. Shape optimization of a microalgal raceway to enhance productivity. Submitted paper, November 2021.

[14] O. Bernard, L.-D. Lu, and J. Salomon. Mixing strategies combined with shape design to enhance productivity of a raceway pond. To appear in the Proceedings of the 11th IFAC SYMPOSIUM on Advanced Control of Chemical Processes(ADCHEM2021), 2021.

[15] O. Bernard, L.-D. Lu, and J. Salomon. Optimization of mixing strategy in microalgal raceway ponds. Submitted paper, March 2021.

[16] O. Bernard, L.-D. Lu, and J. Salomon. Optimizing microalgal productivity in raceway ponds through a controlled mixing device. In *2021 American Control Conference (ACC)*, pages 640–645, 2021.

[17] O. Bernard, F. Mairet, and B. Chachuat. Modelling of microalgae culture systems with applications to control and optimization. *Microalgae Biotechnology*, 153(59-87), 2015.

[18] O. Bernard, P. Masci, and A. Sciandra. A photobioreactor model in nitrogen limited conditions. In *Proceedings of the Mathmod 09 conference*, Vienna, Austria, January 2009.

[19] D. Bertsimas and J. N. Tsitsiklis. *Introduction to Linear Optimization.* Athena Scientific, 1997.

[20] L. Bittner. L. s. pontryagin, v. g. boltyanskii, r. v. gamkrelidze, e. f. mishechenko, the mathematical theory of optimal processes. viii + 360 s. new york/london 1962. john wiley & sons. preis 90/–. *ZAMM - Journal of Applied Mathematics and Mechanics / Zeitschrift für Angewandte Mathematik und Mechanik*, 43(10-11):514–515, 1963.

[21] F. Bouchut and M. Westdickenberg. Gravity driven shallow water models for arbitrary topography. In *Communications in Mathematical Sciences*, volume 2, pages 359–389. International Press of Boston, 2004.

[22] G. Bougaran, O. Bernard, and A. Sciandra. Modeling continuous cultures of microalgae colimited by nitrogen and phosphorus. *Journal of Theoretical Biology*, 265(3):443–454, 2010.

[23] A. Bouharguane and B. Mohammadi. Minimization principles for the evolution of a soft sea bed interacting with a shallow. *International Journal of Computational Fluid Dynamics*, 26(3):163–172, May 2012.

[24] L. Brennan and P. Owende. Biofuels from microalgae—a review of technologies for production, processing, and extractions of biofuels and co-products. *Renewable and Sustainable Energy Reviews*, 14(2):557–577, 2010.

[25] P. G. Brewer. Productivity of the ocean. present and past. w. h. berger, v. s. smetacek, and g. wefer, eds. wiley-interscience, new york, 1989. xviii, 470 pp., illus. $146. life sciences research reports, vol. 44. from a workshop, berlin, f.r.g., april 1988. *Science*, 247(4944):865–865, 1990.

[26] R. Burkard, M. Dell'Amico, and S. Martello. *Assignment Problems.* SIAM, 2008.

[27] Q. Béchet, A. Shilton, and B. Guieysse. Modeling the effects of light and temperature on algae growth: State of the art and critical assessment for productivity prediction during outdoor cultivation. *Biotechnology Advances*, 31(8):1648–1663, 2013.

[28] J. Caperon and J. Meyer. Nitrogen-limited growth of marine phytoplankton—ii. uptake kinetics and their role in nutrient limited growth of phytoplankton. *Deep Sea Research and Oceanographic Abstracts*, 19(9):619–632, 1972.

[29] D. Chiaramonti, M. Prussi, D. Casini, M. R. Tredici, L. Rodolfi, N. Bassi, G. Chini Zittelli, and P. Bondioli. Review of energy balance in raceway ponds for microalgae cultivation: Re-thinking a traditional system is possible. *Applied Energy*, 102:101–111, Feburary 2013.

[30] P.-H. Cocquet, S. Riffo, and J. Salomon. Optimization of bathymetry for long waves with small amplitude. Submitted, 2020.

[31] F. Colonius. *Optimal periodic control*, volume 1313 of *Lecture Notes in Mathematics*. Springer-Verlag, Berlin, 1988.

[32] R. Cominetti and A. Piazza. Asymptotic convergence of optimal policies for resource management with application to harvesting of multiple species forest. *Mathematics of Operations Research*, 34(3):576–593, 2009.

[33] J.-F. Cornet. Calculation of optimal design and ideal productivities of volumetrically lightened photobioreactors using the constructal approach. *Chemical Engineering Science*, 65(2):985–998, 2010.

[34] J.-F. Cornet and C.-G. Dussap. A simple and reliable formula for assessment of maximum volumetric productivities in photobioreactors. *Biotechnology Progress*, 25(2):424–435, 2009.

[35] J. A. V. Costa, G. A. Linde, D. I. P. Atala, G. M. Mibielli, and R. T. Krüger. Modelling of growth conditions for cyanobacterium spirulina platensis in microcosms. *World Journal of Microbiology and Biotechnology*, 16(1):15–18, 2000.

[36] M. Cuaresma, M. Janssen, E. Jan van den End, C. Vílchez, and R. H. Wijffels. Luminostat operation: A tool to maximize microalgae photosynthetic efficiency in photobioreactors during the daily light cycle? *Bioresource Technology*, 102(17):7871–7878, 2011.

[37] M. C. Cuello, J. J. Cosgrove, A. Randhir, A. Vadiveloo, and N. R. Moheimani. Comparison of continuous and day time only mixing on tetraselmis suecica (chlorophyta) in outdoor raceway ponds. *Journal of Applied Phycology*, 27(5):1783–1791, 2015.

[38] H. De la Hoz Siegler, W. C. McCaffrey, R. E. Burrell, and A. Ben-Zvi. Optimization of microalgal productivity using an adaptive, non-linear model based strategy. *Bioresource Technology*, 104:537–546, 2012.

[39] A.-J.-C. Barré de Saint-Venant. Théorie du mouvement non permanent des eaux avec applica- tions aux crues des rivières et à l'introduction des marées dans leur lit. *Comptes rendus hebdomadaires des séances de l'Académie des sciences*, 73:147–154, 1871.

[40] D. Demory, C. Combe, P. Hartmann, A. Talec, E. Pruvost, R. Hamouda, F. Souillé, P.-O. Lamare, M.-O. Bristeau, J. Sainte-Marie, S. Rabouille, F. Mairet, A. Sciandra, and O. Bernard. How do microalgae perceive light in a high-rate pond? towards more realistic lagrangian experiments. *The Royal Society*, May 2018.

[41] M. R. Droop. Vitamin b12 and marine ecology. iv. the kinetics of uptake, growth and inhibition in monochrysis lutheri. *Journal of the Marine Biological Association of the United Kingdom*, 48(3):689–733, 1968.

[42] M. R. Droop. 25 years of algal growth kinetics a personal view. *Botanica Marina*, 26(3):99–112, 1983.

[43] P. Duarte. A mechanistic model of the effects of light and temperature on algal primary productivity. *Ecological Modelling*, 82(2):151–160, 1995.

[44] P. Duarte and J. G. Ferreira. Dynamic modelling of photosynthesis in marine and estuarine ecosystems. *Environmental Modeling & Assessment*, 2(1):83–93, 1997.

[45] P. H. C. Eilers and J. C. H. Peeters. Dynamic behaviour of a model for photosynthesis and photoinhibition. *Ecological Modelling*, 69(1):113 – 133, 1993.

[46] I. Ekeland and R. Témam. *Convex Analysis and Variational Problems*. Society for Industrial and Applied Mathematics, 1999.

[47] M. H. M. Eppink, G. Olivieri, H. Reith, C. van den Berg, M. J. Barbosa, and R. H. Wijffels. From current algae products to future biorefinery practices: a review. In *Biorefineries*, pages 99–123. Springer, 2017.

[48] P. G. Falkowski. The role of phytoplankton photosynthesis in global biogeochemical cycles. *Photosynthesis Research*, 39(3):235–258, 1994.

[49] P. G. Falkowski and A. D. Woodhead, editors. *Primary Productivity and Biogeochemical Cycles in the Sea*, volume 43 of *Environmental Science Research*. Springer, Boston, MA, 1 edition, 1992.

[50] F. G. A. Fernández, F. G. Camacho, J. A. S. Pérez, J. M. F. Sevilla, and E. M. Grima. A model for light distribution and average solar irradiance inside outdoor tubular photobioreactors for the microalgal mass culture. *Biotechnology and Bioengineering*, 55(5):701–714, 1997.

[51] S. Ferrari and F. Saleri. A new two-dimensional shallow water model including pressure effects and slow varying bottom topography. *ESAIM: Mathematical Modelling and Numerical Analysis*, 38(2):211–234, 2004.

[52] J.-F. Gerbeau and B. Perthame. Derivation of viscous saint-venant system for laminar shallow water; numerical validation. *Discrete and Continuous Dynamical Systems - B*, 1(1):89–102, Feburary 2001.

[53] J. H. Golbeck. Structure, function and organization of the photosystem i reaction center complex. *Biochimica et Biophysica Acta (BBA) - Reviews on Bioenergetics*, 895(3):167–204, 1987.

[54] J. Grenier, F. Lopes, H. Bonnefond, and O. Bernard. Worldwide perspectives of rotating algal biofilm up-scaling. Submitted, 2020.

[55] F. Grognard, A. R. Akhmetzhanov, and O. Bernard. Optimal strategies for biomass productivity maximization in a photobioreactor using natural light. *Automatica*, 50(2):359–368, 2014.

[56] M. Guay, D. Dochain, and M. Perrier. Adaptive extremum seeking control of continuous stirred tank bioreactors with unknown growth kinetics. *Automatica*, 40(5):881–888, 2004.

[57] H. Haario, L. Kalachev, and M. Laine. Reduced models of algae growth. *Bulletin of Mathematical Biology*, 71(7):1626–1648, 2009.

[58] B.-P. HAN. Photosynthesis–irradiance response at physiological level: a mechanistic model. *Journal of Theoretical Biology*, 213(2):121–127, 2001.

[59] B.-P. Han. A mechanistic model of algal photoinhibition induced by photodamage to photosystem-ii. *Journal of theoretical biology*, 214(4):519–527, February 2002.

[60] B.-P. Han, M. Virtanen, J. Koponen, and M. Straškraba. Effect of photoinhibition on algal photosynthesis: a dynamic model. *Journal of Plankton Research*, 22:865–885, May 2000.

[61] J. Hansen, R. Ruedy, M. Sato, and K. Lo. Global surface temperature change. *Reviews of Geophysics*, 48(4), 2010.

[62] P. Hartmann, Q. Béchet, and O. Bernard. The effect of photosynthesis time scales on microalgae productivity. *Bioprocess and Biosystems Engineering*, 37(1):17–25, August 2014.

[63] D. Hennessy and H. Lapan. The use of archimedean copulas to model portfolio allocations. *Mathematical Finance*, 12:143–154, 02 2002.

[64] J. P. Hespanha and A. S. Morse. Switching between stabilizing controllers. *Automatica*, 38(11):1905–1917, NOV 2002.

[65] S.-H. Ho, C.-Y. Chen, D.-J. Lee, and J.-S. Chang. Perspectives on microalgal co2-emission mitigation systems — a review. *Biotechnology Advances*, 29(2):189–198, 2011.

[66] D. L. Huggins, R. H. Piedrahita, and T. Rumsey. Analysis of sediment transport modeling using computational fluid dynamics (cfd) for aquaculture raceways. *Aquacultural Engineering*, 31(3):277–293, 2004.

[67] D. L. Huggins, R. H. Piedrahita, and T. Rumsey. Use of computational fluid dynamics (cfd) for aquaculture raceway design to increase settling effectiveness. *Aquacultural Engineering*, 33(3):167–180, 2005.

[68] T. Ibaraki and N. Katoh. *Resource allocation problems.* Foundations of Computing Series. MIT Press, Cambridge, MA, 1988. Algorithmic approaches.

[69] M. Iehana. Kinetic analysis of the growth of spirulina sp. in batch culture. *Journal of Fermentation Technology*, 65(3):267–275, 1987.

[70] Y.-C. Jeon, C.-W. Cho, and Y.-S. Yun. Measurement of microalgal photosynthetic activity depending on light intensity and quality. *Biochemical Engineering Journal*, 27(2):127–131, 2005.

[71] L. Kantorovich. On the transfer of masses (in russian). *Doklady Akademii Nauk*, 37(2):227–229, 1942.

[72] H. K. Khalil. *Nonlinear Systems.* Pearson, 3 edition, 2002.

[73] H. H. Khoo, P. N. Sharratt, P. Das, R. K. Balasubramanian, P. K. Naraharisetti, and S. Shaik. Life cycle energy and co2 analysis of microalgae-to-biodiesel: Preliminary results and comparisons. *Bioresource Technology*, 102(10):5800–5807, 2011.

[74] J. T. O. Kirk. *Light and photosynthesis in aquatic ecosystems / John T.O. Kirk.* Cambridge University Press Cambridge [England] ; Melbourne, 2nd ed. edition, 1994.

[75] C. A. Klausmeier, E. Litchman, and S. A. Levin. Phytoplankton growth and stoichiometry under multiple nutrient limitation. *Limnology and Oceanography*, 49(4part2):1463–1470, 2004.

[76] A. Kumar, S. Ergas, X. Yuan, A. Sahu, Q. Zhang, Jo Dewulf, F. Xavier Malcata, and H. van Langenhove. Enhanced co2 fixation and biofuel production via microalgae: recent developments and future directions. *Trends in Biotechnology*, 28(7):371–380, 2010.

[77] P.-O. Lamare, N. Aguillon, J. Sainte-Marie, J. Grenier, H. Bonnefond, and O. Bernard. Gradient-based optimization of a rotating algal biofilm process. *Automatica*, 105:80–88, 2019.

[78] K. Lange and F. J. Oyarzun. The attractiveness of the droop equations. *Mathematical Biosciences*, 111(2):261–278, 1992.

[79] N. M. Langley, S. T. L. Harrison, and R. P. van Hille. A critical evaluation of co2 supplementation to algal systems by direct injection. *Biochemical Engineering Journal*, 68:70–75, 2012.

[80] E. Lee and Q. Zhang. Integrated co-limitation kinetic model for microalgae growth in anaerobically digested municipal sludge centrate. *Algal Research*, 18:15–24, 2016.

[81] Y.-K. Lee and C.-W. Soh. Accumulation of astaxanthin in haematococcus lacustris (chlorophyta)1. *Journal of Phycology*, 27(5):575–577, 1991.

[82] J. T. Lehman, D. B. Botkin, and G. E. Likens. The assumptions and rationales of a computer model of phytoplankton population dynamics1. *Limnology and Oceanography*, 20(3):343–364, 1975.

[83] X. Li, H.-Y. Hu, Gan K., and Sun Y.-X. Effects of different nitrogen and phosphorus concentrations on the growth, nutrient uptake, and lipid accumulation of a freshwater microalga scenedesmus sp. *Bioresource Technology*, 101(14):5494–5500, 2010.

[84] D. Liberzon and A. S. Morse. Basic problems in stability and design of switched systems. *IEEE CONTROL SYSTEMS MAGAZINE*, 19(5):59–70, OCT 1999.

[85] E. H. Lieb. Variational principle for many-fermion systems. *Physical Review Letters*, 46(7):457–459, 1981.

[86] J.-L. Lions. *Optimal Control of Systems Governed by Partial Differential Equations*. 170. Springer-Verlag Berlin Heidelberg, 1 edition, 1971.

[87] C. L. Liu and J. W. Layland. Scheduling algorithms for multiprogramming in a hard-real-time environment. *J. ACM*, 20(1):46–61, January 1973.

[88] S.-J. Liu and M. Krstic. Introduction to extremum seeking. In *Stochastic Averaging and Stochastic Extremum Seeking*, pages 11–20. Springer, 2012.

[89] S. P. Long, S. Humphries, and P. G. Falkowski. Photoinhibition of photosynthesis in nature. *Annual Review of Plant Physiology and Plant Molecular Biology*, 45(1):633–662, 1994.

[90] F. Marche. Derivation of a new two-dimensional viscous shallow water model with varying topography, bottom friction and capillary effects. *European Journal of Mechanics - B/Fluids*, 26(1):49–63, 2007.

[91] H. L. Marshall, R. J. Geider, and K. J. Flynn. A mechanistic model of photoinhibition. *New Phytologist*, 145(2):347–359, 2000.

[92] C. Martínez, O. Bernard, and F. Mairet. Maximizing microalgae productivity in a light-limited chemostat. *IFAC-PapersOnLine*, 51(2):735–740, January 2018.

[93] C. Martínez, F. Mairet, and O. Bernard. Theory of turbid microalgae cultures. *Journal of Theoretical Biology*, 456:190–200, November 2018.

[94] P. Masci, F. Grognard, and O. Bernard. Microalgal biomass surface productivity optimization based on a photobioreactor model. *IFAC 11th International Symposium on Computer Applications in Biotechnology*, pages 180–185, July 2010.

[95] A. Melis. Dynamics of photosynthetic membrane composition and function. *Biochimica et Biophysica Acta (BBA) - Bioenergetics*, 1058(2):87–106, 1991.

[96] V. Michel-Dansac, C. Berthon, S. Clain, and F. Foucher. A well-balanced scheme for the shallow-water equations with topography. *Computers and Mathematics with Applications*, 72(3):586–593, August 2016.

[97] B. Mohammadi and A. Bouharguane. Optimal dynamics of soft shapes in shallow waters. *Computers and Fluids*, 40(1):291–298, January 2011.

[98] E. Molina Grima, J. A. Sánchez Pérez, F. García Camacho, J. M. Fernández Sevilla, and F. G. Acién Fernández. Effect of growth rate on the eicosapentaenoic acid and docosahexaenoic acid content of isochrysis galbana in chemostat culture. *Applied Microbiology and Biotechnology*, 41(1):23–27, 1994.

[99] J. Monod. The growth of bacterial cultures. *Annual Review of Microbiology*, 3(1):371–394, 1949.

[100] J. Monod. La technique de culture continue théorie et applications. In *Selected Papers in Molecular Biology by Jacques Monod*, volume 79, pages 390–410. Elsevier Inc, 1950.

[101] A. Morel. Optical modeling of the upper ocean in relation to its biogenous matter content (case i waters). *Journal of Geophysical Research: Oceans*, 93(C9):10749–10768, 1988.

[102] K. Nagahara, Y. Lou, and E. Yanagida. Maximizing the total population with logistic growth in a patchy environment. *Journal of Mathematical Biology*, 82(1):1–50, 2021.

[103] A. Novick and L. Szilard. Description of the chemostat. *Science*, 112(2920):715–716, 1950.

[104] I. Ohad, N. Adir, H. Koike, D. J. Kyle, and Y. Inoue. Mechanism of photoinhibition in vivo. a reversible light-induced conformational change of reaction center ii is related to an irreversible modification of the d1 protein. *J Biol Chem*, 265(4):1972–1979, Feburary 1990.

[105] W. J. Oswald and C. G. Golueke. Biological transformation of solar energy. In Wayne W. Umbreit, editor, *Advances in Applied Microbiology*, volume 2, pages 223–262. Academic Press, 1960.

[106] C. Pahl-Wostl and D. M. Imboden. Dyphora - a dynamic model for the rate of photosynthesis of algae. *Journal of Plankton Research*, 12(6):1207–1221, 1990.

[107] I. Perner-Nochta and C. Posten. Simulations of light intensity variation in photobioreactors. *Journal of Biotechnology*, 131(3):276–285, 2007.

[108] A. Piazza. About optimal harvesting policies for a multiple species forest without discounting. *JOURNAL OF ECONOMICS*, 100(3):217–233, JUL 2010.

[109] S. Pirt, Y. Lee, A. Richmond, and M. W. Pirt. The photosynthetic efficiency of chlorella biomass growth with reference to solar energy utilisation. *Journal of Chemical Technology & Biotechnology*, 30:25–34, 2007.

[110] S. B. Powles. Photoinhibition of photosynthesis induced by visible light. *Annual Review of Plant Physiology*, 35(1):15–44, 1984.

[111] M. Ras, J.-P. Steyer, and O. Bernard. Temperature effect on microalgae: a crucial factor for outdoor production. *Reviews in Environmental Science and Bio/Technology*, 12(2):153–164, 2013.

[112] A. Sciandra and P. Ramani. The steady states of continuous cultures with low rates of medium renewal per cell. *Journal of Experimental Marine Biology and Ecology*, 178(1):1–15, 1994.

[113] J. Sinclair, Y.-I. Park, W. S. Chow, and J. M. Anderson. Target theory and the photoinactivation of photosystem ii. *Photosynthesis Research*, 50(1):33–40, 1996.

[114] P. Spolaore, C. Joannis-Cassan, E. Duran, and A. Isambert. Commercial applications of microalgae. *Journal of Bioscience and Bioengineering*, 101(2):87–96, 2006.

[115] J. J. Stoker. *Water Waves: The Mathematical Theory with Applications*. A Wiley-Interscience Publication, 1957.

[116] A. Sukenik, J. Bennett, and P. Falkowski. Light-saturated photosynthesis — limitation by electron transport or carbon fixation? *Biochimica et Biophysica Acta (BBA) - Bioenergetics*, 891(3):205–215, 1987.

[117] A. Sukenik, P. G. Falkowski, and J. Bennett. Potential enhancement of photosynthetic energy conversion in algal mass culture. *Biotechnology and Bioengineering*, 30(8):970–977, 1987.

[118] A. van Dongeren, N. Plant, A. Cohen, D. Roelvink, M. C.Haller, and P. Catalán. Beach wizard: Nearshore bathymetry estimation through assimilation of model computations and remote observations. *Coastal Engineering*, 55(12):1016–1027, December 2008.

[119] I. Vatcheva, H. de Jong, O. Bernard, and N. J. I. Mars. Experiment selection for the discrimination of semi-quantitative models of dynamical systems. *Artificial Intelligence*, 170(4):472–506, 2006.

[120] X. Wu and J. C. Merchuk. A model integrating fluid dynamics in photosynthesis and photoinhibition processes. *Chemical Engineering Science*, 56(11):3527–3538, 2001.

[121] Y.-S. Yun, S. B. Lee, J. M. Park, C.-I. Lee, and J.-W. Yang. Carbon dioxide fixation by algal cultivation using wastewater nutrients. *Journal of Chemical Technology & Biotechnology*, 69(4):451–455, 1997.

[122] Y.-S. Yun and J. M. Park. Kinetic modeling of the light-dependent photosynthetic activity of the green microalga chlorella vulgaris. *Biotechnology and Bioengineering*, 83(3):303–311, 2003.

[123] J. Zhang and X. Xia. A model predictive control approach to the periodic implementation of the solutions of the optimal dynamic resource allocation problem. *Automatica*, 47(2):358–362, 2011.

[124] W. Y. Zhang, S. Zhang, M. Cai, and J. X. Huang. A new manufacturing resource allocation method for supply chain optimization using extended genetic algorithm. *The International Journal of Advanced Manufacturing Technology*, 53(9):1247–1260, 2011.

[125] C. Zonneveld. Photoinhibition as affected by photoacclimation in phytoplankton: a model approach. *Journal of Theoretical Biology*, 193(1):115–123, 1998.

Approches Lagrangiennes pour la modélisation et l'optimisation du couplage hydrodynamique-photosynthèse

Abstract

Microalgae are photosynthetic micro-organisms whose potential has been highlighted in the last decade. Applications can be found from to renewable energy production and wastewater treatment to some high added value commercial products e.g., food, pharmaceutical, cosmetics. Nevertheless, finding optimal growth conditions for full-scale cultivation of microalgae remains challenging in practice. Mathematical models are therefore of great help to better manage this complex, nonlinear dynamical system. The aim of this thesis is to better understand how different factors affect microalgal growth.

In a first part, we study the influence of the light attenuation and the optimal condition to maximize the productivity. In this way, we introduce an optical productivity which enables us to determine the optimal condition for general light extinction function. A global optimal optical depth is found which consists in canceling the algal net growth rate at the bottom of the reactors to maximize the optical productivity. It can be used to characterize the optimization of the areal productivity in some specific cases, whereas an asymptotic behaviour has been observed in more general case.

We then limit ourselves to a specific reactor - the raceway pond, which is an outdoor circuit basin combining with a paddle wheel. We start by investigating a resource allocation problem issuing from the re-distribution of the light resource to the algae by the paddle wheel. A generic mixing device is considered to assign at each lap the light resource to the algae layers in the raceway. We determine the optimal allocation strategies to maximize the algal growth.

In a third part, we show how the shape of the topography affects (or not) the algal growth in raceway ponds. In this way, we consider a hydrodynamical-biological coupled model and introduce an optimization problem associated with the topography to maximize the algal growth. We also combine the optimization of the topographies with the previous allocation strategies to investigate their influence on algal production. Non-trivial topographies are obtained numerically to enhance the algal growth.

The mathematical study of these optimization problems leads to new interesting working directions, improves and clarifies the understanding of influence by different factors on algal growth. We conclude with some discussions and perspectives of this work.

Keywords: optimization, mathematical modeling, hydrodynamics, dynamical system, resource allocation, periodic control, nonlinear problem, saint-venant equations, han model, microalgae

---

Laboratoire Jacques-Louis Lions
Sorbonne Université – Campus Pierre et Marie Curie – 4 place Jussieu – 75005 Paris – France

Résumé

Les microalgues sont des micro-organismes photosynthétiques dont le potentiel a été mis en évidence au cours de la dernière décennie. Des applications peuvent être trouvées dans la production d'énergie renouvelable ou dans le traitement des eaux usées par exemple. Elles peuvent être utilisées dans beaucoup de produits commerciaux à haute valeur ajoutée comme par exemple dans l'alimentation, la pharmacie ou les cosmétiques. Néanmoins, trouver des conditions optimales pour la production des microalgues à grande échelle reste un défi en pratique. Les modèles mathématiques sont donc d'une grande aide pour mieux gérer ce système dynamique complexe et non linéaire. L'objectif de cette thèse est de mieux comprendre comment différents facteurs affectent la croissance des microalgues.

Dans un premier temps, nous étudions l'influence de l'atténuation lumineuse et obtenons une condition d'optimalité pour maximiser la productivité. De cette façon, nous introduisons une productivité optique qui nous permet de caractériser la fonction d'extinction de la lumière optimale dans un cadre général. On trouve une profondeur optique optimale globale qui consiste à annuler le taux de croissance net des algues au fond des réacteurs pour maximiser la productivité optique. Cette étude nous permet de caractériser la productivité surfacique optimale dans certains cas particuliers, et de décrire le comportement asymptotique des autres cas dans certains régimes.

On se limite ensuite à un réacteur spécifique, le raceway pond, qui est un bassin de circuit extérieur associé à une roue à aubes. Nous commençons par étudier un problème d'allocation de ressources issu de la redistribution de la ressource lumineuse aux algues par la roue à aubes. Un dispositif de mélange générique est envisagé pour affecter à chaque tour la ressource lumineuse aux algues qui se situent sur differentes couches dans le raceway. Nous déterminons les stratégies d'allocation optimales pour maximiser la croissance des algues.

Dans une troisième partie, nous montrons comment la forme de la topographie affecte (ou non) la croissance des algues dans le raceway. De cette façon, nous considérons un modèle hydrodynamique-biologique couplé et introduisons un problème d'optimisation associé à la topographie pour maximiser la croissance des algues. Nous combinons également l'optimisation des topographies avec les stratégies d'allocation précédentes pour étudier leur influence sur la production d'algues. Des topographies non triviales sont obtenues numériquement pour améliorer la croissance des algues.

L'étude mathématique de ces problèmes d'optimisation conduit à de nouvelles directions de travail, améliore et clarifie la compréhension de l'influence de différents facteurs sur la croissance des algues. Nous concluons par quelques discussions et perspectives de ce travail.

Mots clés : optimisation, modélisation, hydrodynamique, système dynamique, allocation des ressources, contrôle périodique, problème nonlinéaire, équations de saint-venant, modèle de han, microalgues

---